Brief overview on the UVGI disinfection technology

Cătălin I. LUNGU, PhD*, Ilinca NĂSTASE, PhD*

*Bucharest Technical University of Civil Engineering
66 Pache Protopopescu, Bucharest, Romania
catalin.lungu@utcb.ro

Summary

The information in this document is useful for HVAC professionals, facility engineers and specialists like employers and building owners and administrators seeking basic knowledge about ultraviolet germicidal irradiation (UVGI) technology.

This article explains the specific terms used in the UV field, reasons why UVGI is used for virus inactivation and the main features of UV-C lamps. UVGI device typology is presented, and some general rules and limitations for safe usage are provided.

Given the complexity of the UV transmission physics, specific software is needed for sizing UV systems. The sizing guidelines and design examples for different UV-C devices are not included in this document. This annexe scope is general and not limited to any specific building category (e.g., office buildings, educational buildings, shopping areas, sports premises, hospitals, healthcare settings, even residences). However, considering the negative effects on human health and some materials that UV-C radiation could generate when the design is defective, the most important rule is to use only certified products that are properly sized and tested.

Key words: covid-19, coronavirus, uvgi, uv-c, dose, disinfection

1. Short history and terminology

Germicidal lamps with UV-C radiation have been used since the 1950s to inactivate or destroy microorganisms like bacteria, mould, yeast, and viruses that severely affect indoor air quality (IAQ). Niels Ryberg Finsen was the first scientist to discover UV rays for treating diseases and was awarded the Nobel Prize for Medicine in 1903. He invented the Finsen curative lamp, which was used successfully during the 1950s. Westinghouse co-developed the first commercial UV-C germicidal lamps during the 1930s. They were used mainly in hospitals.

The applications for UV-C lamps grew after the Second World War when they were used anywhere microbiological contamination was a concern: for sterilising air and

surfaces in hospitals, pharmaceutical plants and animal labs. Eventually, they were incorporated into air handling equipment.

Many studies run under the Integrative Emergency Services (IES) or the Center for Disease Control and Prevention (CDC) in the United States [1] proved that UV-C irradiation could easily inactivate or kill different pathogens. UV-C became a major component in the control and eradication of tuberculosis in the 1950s [1].

Recently, many researchers have proven that UV-C technology can be safely utilised in many fields of applications [2], and scientific reports [3,4] have shown that UV-C can successfully be used in HVAC and the fight against COVID-19.

A portion of the **electromagnetic spectrum** is shown in Figure 1. Table 1 shows the five types of UV radiation defined according to their wavelength range in nm: vacuum UV, far UV-C, UV-C, UV-B and UV-A. Table 1 gives information regarding the safety of use, the plastic degradation speed (photodegradation) and the practical uses for each UV radiation type. The most powerful germicidal effect is obtained at around 265 nm, as the graph shows. UV-C lamps emit radiation at 253.7 nm.
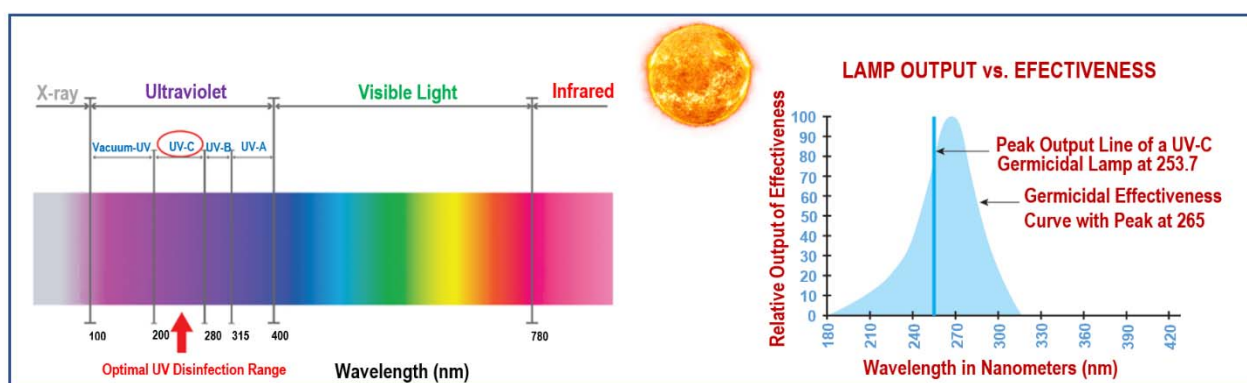
Figure 1 – electromagnetic spectrum and germicidal effectiveness of a UV lamp

Table 1 types of UV radiation

UV type	Wavelength (nm)	Safe for skin&eyes	Degradation of plastic/rubbber	Practical uses
VUV Far-UV	100-200	YES	rapid	Medical equipment
Far-UVC	207-222	YES	rapid	Germicidal desinfection
UV-C	200-280	NO	rapid	Germicidal desinfection
UV-B	280-315	NO	rapid	Tanning, medical treatment
UV-A	315-400	NO	very slow	Curing, printing, lithography, sensing, medical applications

UV-C is a low-penetrating form of UV radiation compared to UV-A or UV-B (Figure 2). Measurements on human skin exposed to a wide range of UV wavelengths, from 250 to 400 nm, showed that a small amount of UV-C is transmitted through the epidermis. Only 4 to 7% of UV-C is absorbed in the first 2 μm of the outer, dead layer of the human skin **[2]**. However, because UV is far more energetic than visible light and invisible to humans, exposure to UV-C may result in inflammation of the cornea (photokeratitis) or inflammation of the conjunctiva, called photo-keratoconjunctivitis. Other symptoms, like the sensation of sand in the eyes, tearing, and even eye pain, can occur 6 to 12 h after UV exposure. Acute overexposure to UV-C radiation leaves no permanent damage to human eyes, and generally, the symptoms fully disappear within 24 to 48 h. Cutaneous damage consists of erythema, a reddening of the skin without tanning. The maximum effect of erythema occurs at a wavelength of 296.7 nm in the UV-B band. Erythema produced by UV-C radiation at a wavelength of 253.7 nm is less likely.

Ultraviolet radiation, in general, is carcinogenic, and even if the radiation from germicidal lamps does not penetrate the eyes and the skin over short time intervals, health and safety measures are compulsory in the case when the exposure to the irradiation is long. Human skin and eyes must be protected against UV-C by using shielded or enclosed UV-C lamps.
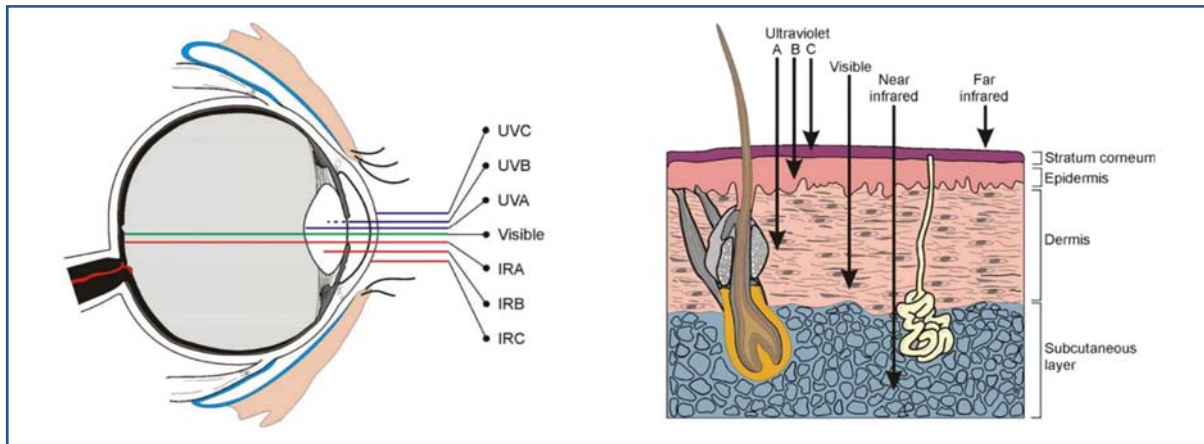
Figure 1 penetration power of different UV types for the human eye or skin [5]

An **exposure dose** in general, or a particular **UV dose**, D, represents the amount of radiant energy absorbed by an organism living in a droplet nucleus; it is calculated as (UV irradiance) times (t – the time of exposure); a UV dose is usually expressed as $\mu W \cdot s/cm^2$ or $\mu J/cm^2$.

$$\mathbf{D} = \mathbf{I} \times \mathbf{t} \ [\mu J/cm^2] \tag{1}$$

The term **fluence** (total radiant energy incident on the outer surface of an infinitesimal sphere) is linked to a UV lamp. It differs slightly from **UV dose** because the latter implies total absorption of UV energy received, whereas fluence represents irradiation energy transmitted over a given duration. Those two are, however, considered to be equal ($\mu J/cm^2$).

The dose-response correlates with the amount of energy received by a population of microorganisms and the resulting effect. For example, the UV-C dose-response of the SARS-COV-2 is the inactivated fraction or the survival fraction among that coronavirus population.

If one exposes a microbial species to an increasing UV irradiation, then the number of inactivated or killed pathogens will increase, or the number of surviving ones will
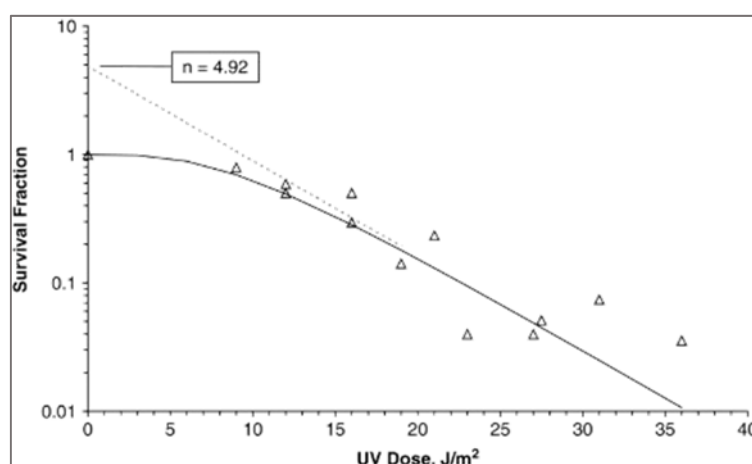
Figure 2 dependence curve of the survival fraction to UV dose [6]

decrease, and the result is a curve whose shape and slope will depend on the microbial species' susceptibility or sensitivity to UV. **The inactivation rate constant (k)** is the slope of this survival curve (Figure 3). k has a unique value for each species (Table 2). k is also called UV rate constant, or decay rate constant and is measured in cm^2/mJ. Its value is used to size UV-C devices.

Table 2 k values for different pathogens [17,18]

UV-C Dose Required	Dose in mWs/cm²		UV-C Dose Required	Dose in mWs/cm²	
	90% (Log 1)	99.9% (Log 3)		90% (Log 1)	99.9% (Log 3)
Bacteria			**Bacteria**		
Bacillus anthracis	4.5	13.5	Streptococcus lactus	6.2	18.5
B. megatherium Veg	11.3	33.9	Streptococcus aureus	5.5	16.5
Bacillus pumilis spores	5.0	15.0	Streptococcus viridans	2.0	6.0
B. subtilis	7.1	21.3			
B. subtilis Sporen	11.2	33.6			
Campylobacter jejuni	1.1	3.3	Yeasts		
Corynebacterium diphteria	3.3	9.9	Sacch. spp	4.4	13.2
Enterobacter cloacae	6.4	19.2	Sacch. ellipsoideus	3.3	9.9
E. coli	5.5	16.5	Sporotrichum schenkii	28.0	84.0
Legionella pneumophila	2.5	7.5			
Listeria Monocytogenes	7.7	23.1			
Micrococcus candidus	6.1	18.2	Virus		
Micrococcus sphaerroides	10.0	30.0	Hepatitis A	4.5	13.5
Mycobacterium tuberculosis	1.1	3.3	Influenza Virus	2.0	6.0
Neisseria catarrhalis	4.4	13.2	Polio Virus	4.4	13.2
Proteus vulgaris	3.0	9.0	Rotavirus	10.5	31.5
Pseudomonas aeruginosa	5.5	16.5			
Pseudomonas fluorescens	3.5	10.5			
Salmonella enteritidis	1.0	3.0	Mould Spores		
Salmonella typhimurium	2.1	6.3	Aspergillus flavus	60.0	180.0
Seratia marcescens	2.2	6.6	Mucor racemosus	17.0	51.0
Shigella sonnei	1.8	5.4	Oospora lactis	2.8	8.4
Spirillum rubrum	4.4	13.2	Penicillium expansum	13.0	39.0
Staphylococcus aureus	5.0	15.0	Penicillium roqueforti	13.0	39.0

There are no standard methods for the determination of k. Furthermore, k values depend, on the one hand, on the conditions under which the UV dose is transmitted, for example, in air, in water, on surfaces; on the other hand, k depends on the measurement methods of the number of the microorganisms surviving.

The survival fraction of a microbial population that was not inactivated after UV-C exposure is determined by one of two similar equations:

$$\ln \left(\frac{N_0}{N}\right) = k \times D \text{ or } \frac{N}{N_0} = e\text{-}k \times I \times t \tag{2}$$

where

N_0 = initial concentration of active microorganisms before disinfection

N   = concentration of active microorganisms after disinfection, for example, after applying an exposure UV-C dose over the virus population
D   = exposure dose or UV irradiation dose (or fluence, mJ/cm^2)
k   = UV inactivation rate constant as explained before
t   = time of the exposure measured in seconds
I   = irradiance measured in $\mu W/cm^2$

These equations are valid only if the shoulder effect and the second stage effect that may affect the disinfection process are neglected. The shoulder appears because there is a delay in response of a microorganism exposed to UV, similar to a threshold dose. This effect could appear when the air velocity is too high and the dose becomes insufficient. Studies **[6]** showed that most microbial species are characterised by two-stage inactivation curves in which each stage has a different rate constant (k_1 and k_2, according to Figure 4).
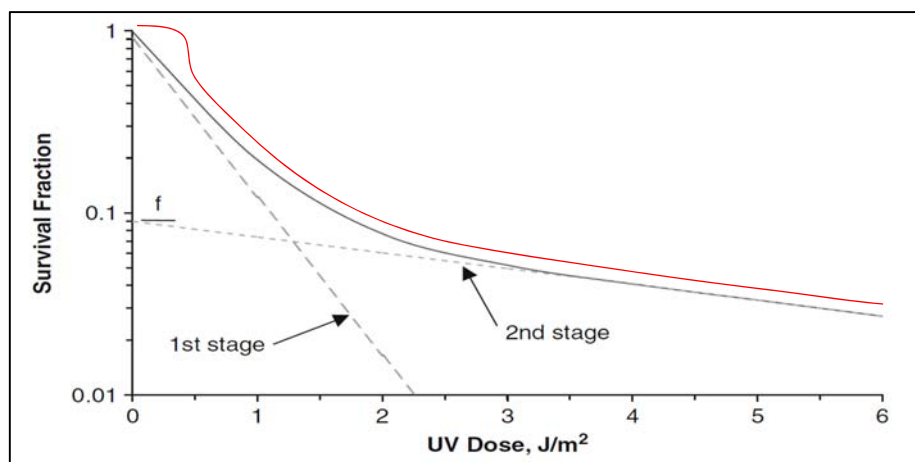
Figure 3   two-stage inactivation curve [adapted by CL from 6]

During the first stage, the decay rate is higher than that of the second stage, when the most resistant fraction will be finally inactivated. For some viruses, this resistant fraction could reach even 10%; for others, it is only 0.01%. The more complex inactivation process can be modelled by the equation below, where F is the fraction of the total initial population subject to fast-decay response:

$$\frac{N}{N_0} = \textbf{F} \times \textbf{e-k1} \times \textbf{I} \times \textbf{t} + \textbf{(1−F)} \times \textbf{e-k2} \times \textbf{I} \times \textbf{t} \tag{3}$$

In 1972, the CDC and the National Institute for Occupational Safety and Health (NIOSH) published the **UV REL value**, which is the recommended exposure limit to UV-C, defined to prevent adverse effects on human eyes and skin. In the United States, this value is 6000 $\mu J/cm^2$ for a wavelength of 254 nm.

According to *Artificial Optical Radiation Directive 2006/25/EC European*, the maintenance operators of the UV-C devices shall not exceed 3000 µJ/cm² for a wavelength equal to 253.7 nm and for a working day of 8 hours, which means that irradiance equals 0.1 µW/cm².

The permissible exposure time PET (sec) for EU workers in healthcare can be calculated with the equation:

$$\textbf{PET(seconds)} = \frac{\textbf{REL} \left(\textbf{3000} \frac{\mu J}{cm^2} \textbf{at 254nm}\right)}{\textbf{Measured irradiance level at 254nm} \left(\frac{\mu W}{cm^2}\right)} \tag{4}$$

The PET values can be then computed if the irradiance values are known (measured). The permissible irradiance level can be determined if the exposure time is limited to a certain level (Table 3).

Permissible exposure time * (seconds)	Effective irradiance (µW/cm2)
28800	0.10
14400	0.21
7200	0.42
3600	0.83
1800	1.67
900	3.33
600	5.00
300	10.00
60	50.00
30	100.00
10	300.00
3	1000.00
1	3000.00
0.5	6000.00
0.3	10000.00
0.1	30000.00

Table 3 PET values for different irradiance (measured) values

In ventilation ducts, for example, due to very short exposure time, UV lamps shall generate between 1000–10,000 µW/cm² to ensure the needed exposure dose for at least a 99.9% inactivation rate, meaning at least 30 mJ/cm², according to the maximum values displayed in Table 2 for viruses. The permissible exposure time is less than 3 s for 1000 µW/cm² or 0.3 s for 10,000 µW/cm².

The average effective life of a UV lamp is measured between the first use (usually after a 100-hour break-in period) and the moment when the UV output is 50% of a specific

level based on testing the lamps from the same production lot. For example, Phillips considers that the effective UV-C lamp life is 9000 h with a 20% decline in the UV output, determined for a specific bulb. Normal values for the average effective lamp life depend on the gas in the glazed balloon and can vary between 5000 and 20,000 h.

2. Types & technical features of UV-C lamps

Modern UV-C lamps (Figure 5) are like fluorescent lamps found in the ceiling or wall fixtures. The similarities of UV-C and fluorescent lamps offer several benefits to producers: the same type of production machine, same shapes, diameters and lengths, the same manner of storage and recycling. UV-C lamps require reduced manufacturing, packing, and shipping costs that compensate for much higher material costs.

Figure 4 UV-C lamps [7]

Both types of lamps operate using identical electrochemical processes: an electric discharge inside the glazed tube strikes argon gas and mercury vapour particles and generates photons in visible and UV-C spectrum (Figure 6).
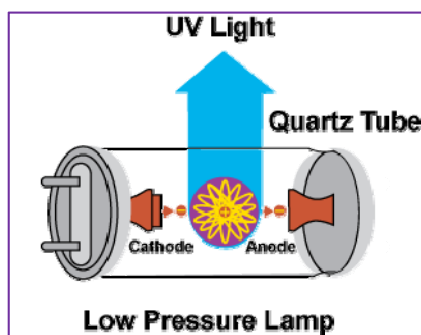
Figure 5 main operating principle of a UV-C lamp [8]

The phosphors that coat the inner surface of the ordinary glass in fluorescent lamps totally absorb UV radiation. The transparent glass envelope of a UV-C lamp is highly

engineered, allowing unfiltered transmission of the 253.7 nm wavelength (UV-C radiation is invisible).

A typical UV-C lamp streams about 90% of its radiative energy in the whole UV-C range, from 200 to 280 nm. About 4–5% of absorbed electric energy is given up as heat, and the rest (approx. 5%) is in the visible light range – mainly blue light.

Low-pressure UV lamps are also called germicidal lamps because UV-C inactivates or destroys microorganisms in both air and water. About 25–35% of their electric energy absorbed is converted directly into UV-C radiation with monochromatic emission at 254 nm for germicidal applications. Approximately 2% of the input power is converted into irradiation at 185 nm, used mainly for ozone generation [20].

UV low-pressure amalgam lamps contain solid amalgam inside the envelope that is an alloy of mercury with titanium, gallium, iron, or lead. The low-pressure amalgam lamps have a very long operating life (up to 20,000 hours) and a UV-C efficiency of up to 45% at 254 nm, compared to the average value of 30% for traditional low-pressure lamps. The efficiency of a UV-C lamp is the ratio between the UV-C power in watts, after 100 hrs burn-in period, and the lamp wattage.

Medium-pressure lamps have the advantage of a much higher power density than traditional low-pressure or amalgam low-pressure lamps.

All lamp technical features are based on measurements performed under laboratory conditions in air, at ambient room temperature, on a high-frequency current, using limited electronic ballast and with average values measured at a 1 m distance from the light source.

The glazed tube of a UV-C lamp is generally made of highly thermal, mechanically stable quartz; quartz glass has high transmission efficiency and is highly transparent to UV radiation. Three different kinds of quartz glass are used, according to the type of ultraviolet lamp to be produced: synthetic quartz, natural quartz and Ti-doped quartz (Figure 7). The latter has the advantage of blocking the 185 nm wavelength radiation that generates ozone, so Ti-doped quartz lamps are ozone-free UV-C lamps. Note that O_3 is at least irritating for occupants if its concentration exceeds the safe level of 120 mg/m^3.
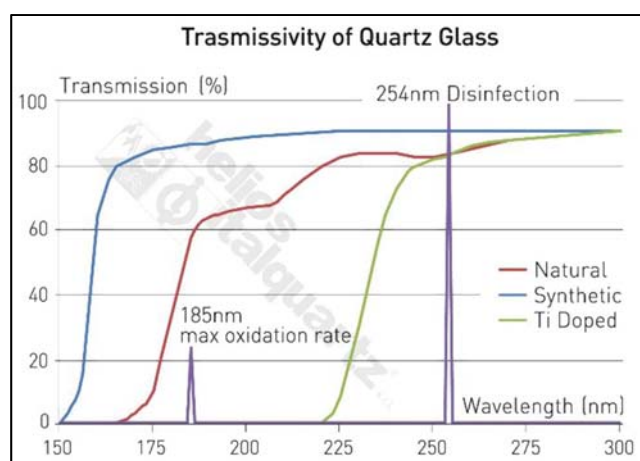
Figure 6 Different quartz glass transmissivity of UV radiation [8]

Generally, UV-C lamps can provide more than 80% of their initial output over a 20,000-hour period (minimum 8000 hours). The average effective life of a UVGI lamp depends on the location temperature, the lamp surface temperature, the number of on-off cycles (or switching rate) and the air velocity. The first three graphs in Figure 8 show the correlations between a UV-C lamp's percentage output and the number of operating hours, the switching rate, and the lamp surface temperature. The fourth graph shows the correlation between three parameters: the air temperature around the UV-C lamp, the airspeed and the UV-C output of the lamp.
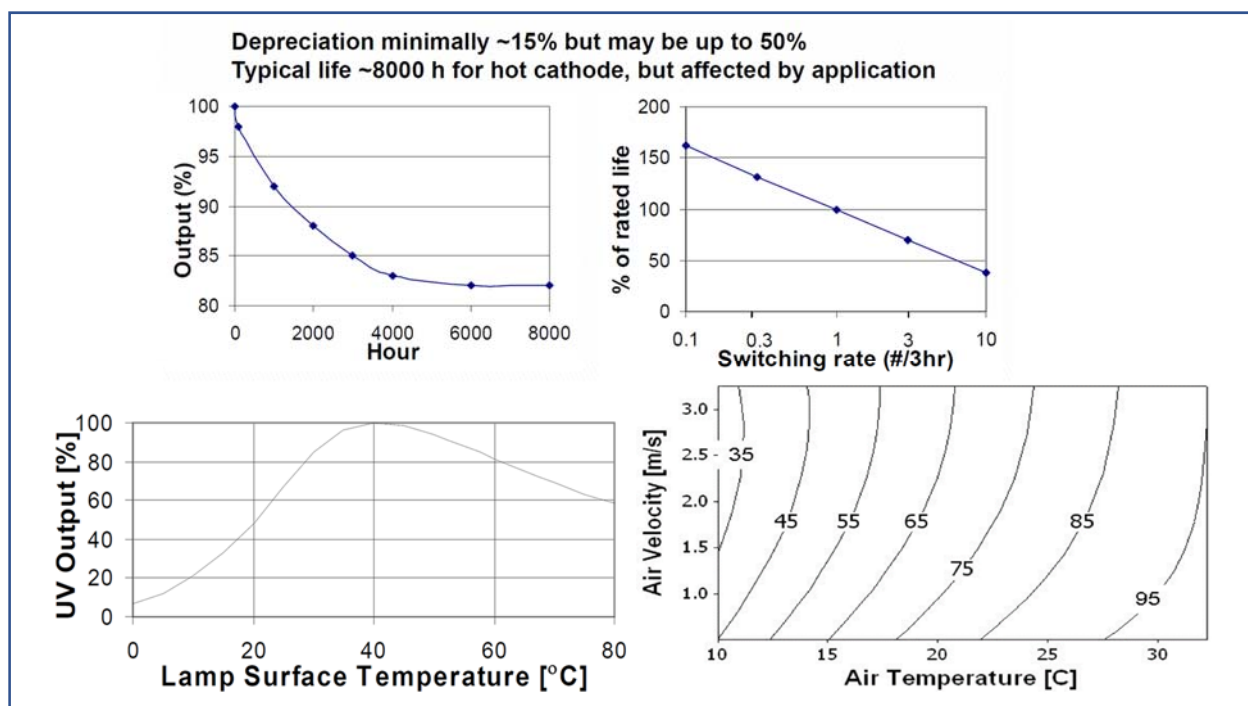
Figure 7 UV output change [%] with different parameters [10,16]

The temperature of the location where a UVGI system is mounted may affect the efficiency of the germicidal effect, depending on the lamp type. Firstly, higher or lower temperatures may decrease the UVGI output of low-pressure mercury lamps or decrease the microorganisms' susceptibility to UVGI. Second, the old (but still commonly used) mechanical/magnetic ballasts may be affected by high or low temperatures. A relationship exists between lamp operating temperature and output in all low-pressure mercury lamps. The UV efficiency of the lamp is directly related to the (saturated) mercury pressure, which, in turn, depends on the spot with the lowest temperature on the lamp. The decrease in UV output will be even greater if there is air movement around the lamp because air flow causes the lamp's mercury vapour to lose heat faster; in addition, low temperatures reduce the lamp's operating life.

One interesting use of a special lamp type using UV-C is the Wood lamp employed in the fight against the counterfeiting of banknotes. It is also used to search for cracks in metal structures coated with materials responsive to UV rays. A Wood lamp produces the so-called 'black light' used to illuminate materials that produce fluorescent and phosphorescent effects when illuminated with this light. Black light is so named because UV-C radiation is not directly visible to the human eye.

3. Why UV-C for air disinfection?

UV-C irradiation inactivates or even kills all viruses, including SARS-COV-2 that produces RNA and DNA mutations (Figure 9).
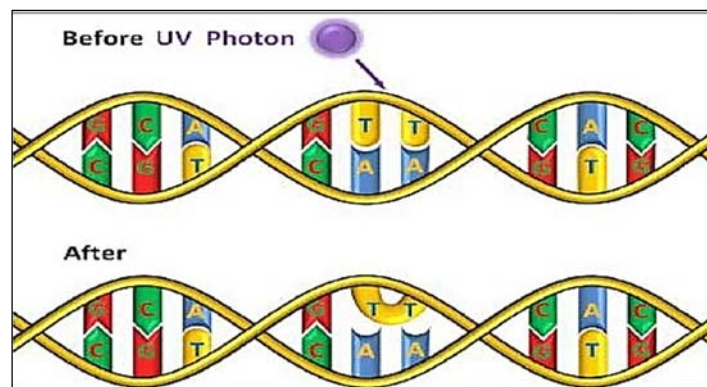
Figure 8 UV-C radiation effect on SARS-COV-2 [11]

The high energy photons of the UV-C radiation are absorbed by the cell proteins' DNA/RNA. The result is that the protein structure is damaged, causing metabolic disruption of the DNA and RNA, so microorganisms, or viruses in our case, can no longer metabolise and replicate.

In conclusion, UV-C is very useful for disinfecting water, building air, transportation, and the surfaces of different objects or products. UV-C is effective for all microorganism species: bacteria, viruses, and fungi. The germicidal effect of UV-C is simple, non-chemical and does not generate toxic by-products. UV-C technology requires low-to-medium investment, and UV-C devices are relatively easy to maintain. UVGI lamps do not affect the environment if they are collected correctly and recycled. If Ti-doped quartz glass is used, a UV-C lamp will not produce ozone.

This disinfection technology can be used practically anywhere infection risk is high: hospitals, retreat houses, sport facilities, in the food or pharmaceutical industry, in HVAC systems, and for transportation safety.

UV-C devices used in ventilation systems have two major advantages: 1) they reduce contamination of AHU elements, especially cooling coils and filters, and 2) they control infection transmission in ventilation systems with recirculation, implying major energy savings.

4. Types of air and surfaces disinfection devices using UV-C

There are three main categories of UV-C devices: in-duct systems, including those installed in AHUs, overhead devices, and stand-alone devices.

i. In-duct UV-C systems

For virus disinfection in AHUs, UV-C lamps shall be installed downstream of the mixing box and filtration section and upstream of the cooling coil in the direction of air
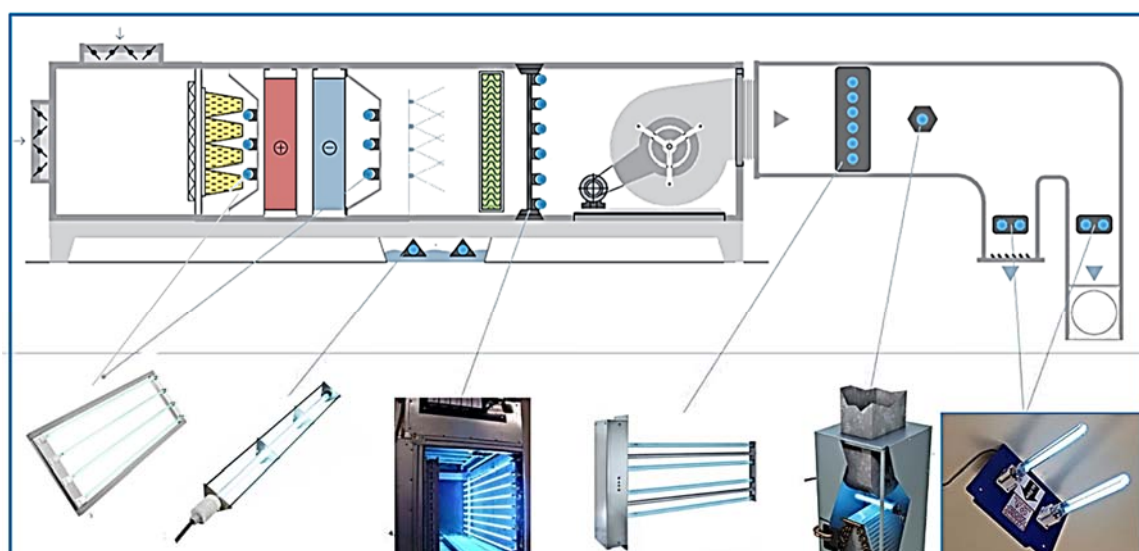
Figure 9 recommended mounting locations for UV-C lamps [adapted by CL from 12]

flow (Figure 10). Here, the low humidity level will not negatively affect lamp irradiation. The mounting position downstream of the cooling coil is preferred for the bacteria disinfection of surfaces because here the air approaches saturation, meaning that within this plenum, there could be raw water, damp insulation, and other conditions that are known to lead to the growth of mould and some forms of bacteria. Also, coil drain pans are often extended in this location to catch raw water carried over from the cooling coil. The lamps used must be resistant to water and or high levels of humidity.

Another mounting position can be even more downstream, between the droplet separator and the fan, or/and in the water collector pan. The in-duct mounting position presents the disadvantage of a higher airspeed that reduces the exposure time. However, the exposure time can be improved by using longer UV-C zones or multi-step exposure. Another countermeasure used to increase the dose is increasing the irradiance with the help of reflective materials or simply increasing the lamp's power. This last measure implies an increase in the electric energy consumed and in the UV-C system acquisition price.

No matter the mounting position of the UV-C lamps, the design engineers must consider at least three additional parameters that affect the lamps' number, size or power. These three parameters are airspeed, air temperature and air humidity.

ii. Overhead UV-C systems (fixtures)

Overhead UV-C devices are shielded units, with a special configuration, generating a band of UV-C radiation above the occupants' heads (Figure 11). Upper-room devices can be safely used when treated spaces are occupied, providing ongoing disinfection if pathogens carried from the occupied lower zone go through the upper irradiated zone near the ceiling. The disinfection effect is not 100% efficient, but it helps to reduce the virus concentration and reduces the transmission risk. Many positive results described in scientific papers were obtained in the past in TB hospitals. Different studies showed that the disinfection effectiveness depends not only on the lamp power but also on the
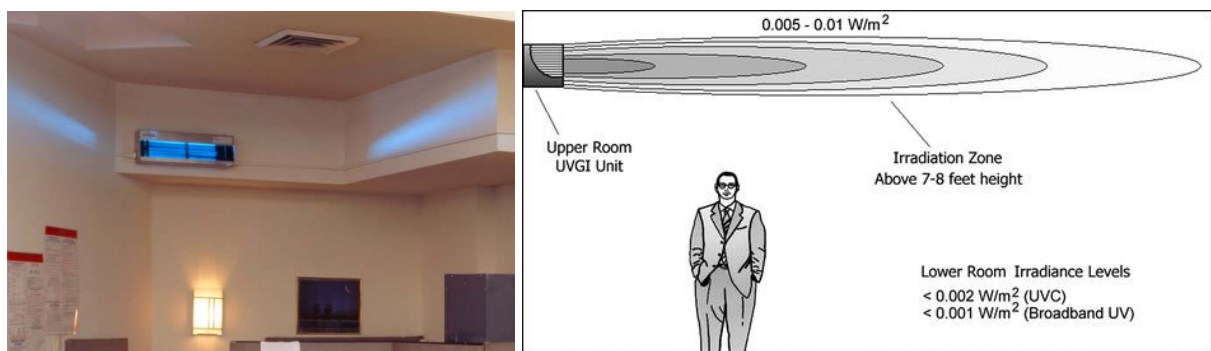
Figure 10 upper room (overhead) UV-C fixture [6]

lamp's position relative to the air flow pattern. The mixing degree of the air in the room can be improved by using mixing additional fans.

A complex model presented in 2015 using the Wells–Riley infection model showed that the impact of an upper-room UVGI device could be comparable to doubling the ventilation rate **[1]**. Other studies found that a UVGI overhead system could be equivalent to a ventilation system providing 2 to 6 ACH **[6]**. However, the infection risk in the 1–2 m range from the infection source will not be reduced substantially.

As displayed in Figure 11, the mounting height is very important related to the value of the UV irradiation at the occupant's eye level, which shall not exceed max 0.1 $\mu W/cm^2$.

iii. Stand-alone UV-C devices

Besides in-duct or overhead devices, other UV systems use enclosed lamps, like air-conditioner types or portable devices. Their disinfection effectiveness depends on the airflow rate they can recirculate, which, in turn, depends on the room size, the infection dose, and similar factors (Figure 12). These systems could be considered the equivalent of personal ventilation systems, and their sizing depends on many variables.

Figure 11 stand-alone UV-C devices [13,14]

5. Basics of UVGI sizing

There are four calculation situations according to each UV-C device type:
(1) UV-C lamps installed in AHUs,
(2) UV-C lamps mounted in ducts,
(3) UV-C fixtures mounted in the upper-room position (overhead type), and
(4) UV-C stand-alone (mobile) devices.

The first two cases cover surface or air stream disinfection, including microbial growth control. The last two refer only to inside rooms air disinfection situations.

The main parameters that must be calculated are:
• the UV-C dose needed to inactivate the microorganisms, in our case SARS-COV-2
• the lamp and ballast characteristics required to meet the individual application's operating conditions
• finally, one must determine how many UV lamps or UV-C devices are necessary and how are they placed in the AHU, in the duct or the room.

The parameters with known values used in the UVGI design refer to:

• AHU configuration and dimensions, or duct dimensions
• information about how much fresh air will be provided by the ventilation system
• air flow characteristics (temperature, RH, how much air flow, air speed ...)
• lamp(s) electric power (W) and lamp(s) technical characteristics
• distance between the lamp(s) and the surface treated
• virus type and concentration and possible infection sources.

In the case of overhead or stand-alone devices, it is also important to know the movement pattern of the virus particles in the room.

The output power of a UVC lamp can be calculated using the Keitz formula:

$$P = \frac{I \times 2\pi^2 \times x \times L}{2\alpha + \sin 2\alpha} \tag{4}$$

where
- P = UVC power [W]
- I = irradiance [W/m^2]
- x = distance [m]
- L = lamp arc length [m]
- a = the angle [rad]

The lamp electric power will be:
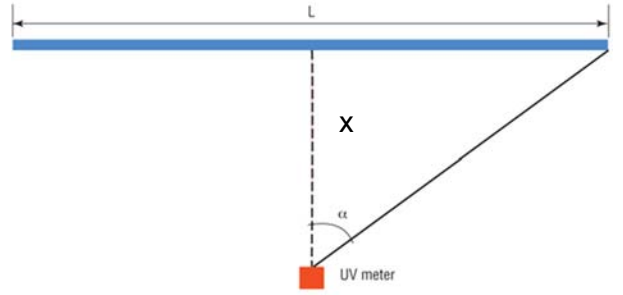
Figure 12 simplified calculation of the UV lamp power in a spot

$$W = \frac{P}{UVC\ lamp\ efficiency(\%)} \tag{5}$$

The radiation view factor from a differential planar element to a cylinder (the lamp), perpendicular to the cylinder axis [6]:

$$F_{d1-2} = \frac{1}{\pi H} ATAN\left(\frac{L}{\sqrt{H^2-1}}\right)$$
$$+ \frac{X-2H}{\sqrt{XY}} ATAN\left(\sqrt{\frac{X(H-1)}{Y(H+1)}}\right)\frac{L}{\pi H}$$
$$- ATAN\left(\sqrt{\frac{H-1}{H+1}}\right)\frac{L}{\pi H}$$

$$\Rightarrow \begin{cases} H = x/r \\ L = l/r \\ X = (1+H)^2 + L^2 \\ Y = (1-H)^2 + L^2 \\ \text{where:} \\ \quad l = \text{length of the lamp segment, cm} \\ \quad x = \text{distance from the lamp, cm} \\ \quad r = \text{radius of the lamp, cm} \end{cases} \tag{6}$$

6. General rules

There is a set of rules that every UV-C user or engineer shall consider:

i. use only officially approved equipment and follow all safety rules indicated in the technical documentation.

ii. UV-C air treatment devices require safety measures and shall be installed only by trained personnel with appropriate risk assessment and controls in place; UV-C

installers and maintenance personnel must respect safety procedures to avoid exceeding occupants' exposure limit with non-enclosed lamps.

iii. UV irradiation level can sometimes be too high for the occupant's eyes, so the irradiation shall be measured immediately after the UV-C device installation and afterwards, periodically. The values shall stay under 0.1 μW/cm^2. Irradiance measurements are generally required for two reasons: (1) validation that the system provides a sufficient UVGI level to ensure microbial inactivation and (2) determination of compliance with occupational safety and health guidelines.

iv. Because ozone generation during UV-C lamps use could harm human health, only ozone-free UV-C lamps shall be considered for spaces occupied during the UV-C air treatment. The maximum allowed human exposure to ozone is 0.05 ppm, according to US Environmental Protection Agency [21], 0.01 ppm according to ASHRAE Environmental Health Committee [22,23], and 0.2 ppm for short exposures of less than 15 min, according to the UK Health and Safety Executive [24]. Therefore, UVGI disinfection equipment shall be tested to verify that the concentration of ozone generated during operation respects the maximum limits. Low-quality UV-C lamps and incorrect system design could generate a level of ozone that is higher than allowed.

v. UVGI lamps are typically mounted downstream from the mixing box and before the filtration section of an AHU; another usual mounting location is downstream from the cooling coil in the AHU or the air duct.

vi. if UVGI systems are installed, RH should be controlled to 40–60% for optimal efficiency [15]; if high humidity conditions are present, increased UV irradiation levels may be necessary to achieve equivalent effectiveness.

Note: Several studies have indicated that UVGI effectiveness decreases as RH increases. Other studies have shown that as RH increases, the ability of some bacteria or viruses to repair UVGI damage to their DNA increases.

vii. UV systems must be fitted with alarms to make the building operator aware of failure (if in duct UV fails, then the air is untreated, and the occupants are at immediate risk);
viii. Finally, UV-C lamps require periodic maintenance such as the irradiation level shall not go under 80% and, consequently, the dirty and dust on the lamps shall be eliminated periodically.

7. Conclusions

1. Germicidal UV-C radiation is a viable decontamination approach against SARS-COV-2 for the air inside buildings during occupying hours; all viruses and almost all bacteria (excluding spores) are inactivated by moderate levels of UV irradiation. Spores are filtered by high-efficiency filters and are not treated with UV.

2. UV-C air treatment is a disinfection, rather than sterilisation, measure; however, there are limited practical examples of the effective application of UV-C to remove respiratory viruses in real buildings.

3. The ozone concentration should be kept below 50 ppb (ideally, below 10 ppb) in indoor environments to protect human health.

4. UV-C is a complementary solution to filtration in mechanically ventilated buildings and a solution to poorly ventilated rooms, like offices and classrooms. Complementary means that UV-C technology is additional. It does not replace ventilation as the first option against air contamination, and proper ventilation to current local regulations must be provided.

5. UVGI is widely available as commercial technology because UV-C devices provide three levels of benefits when applied to HVAC systems:
- at the HVAC-system efficiency level, UV-C eliminates or prevents the build-up of organic material on filters and on cooling coils surfaces, in drain pans, and inside air ducts, keeping the air flow and the heat-transfer levels of cooling coils to 'as-built' conditions, reducing maintenance as well.
- At the **IAQ level**, by reducing pathogens and organic material on filters and cooling coil surfaces, UV-C improves indoor air quality (IAQ) delivered to rooms, with other benefits on occupants' satisfaction and productivity.
- At the **economic level,** UV-C's impact on mechanical systems and occupants translates into substantial economic benefits in energy consumption reduction, carbon footprint reduction, maintenance reduction, reductions in system downtime, and staff time needed for chemical or mechanical cleaning. On average, UV-C could reduce 10–25% of HVAC energy use.

6-. It is very difficult to assess the disinfection effect of a UV-C device; in fact, UV-C efficiency is affected by the distance from the UV-C device and by the 'shadowing' effect (UV radiation cannot penetrate solid material, and bacteria can easily 'hide' inside slightly larger solids). It depends as well on the lamps' state, usage time, and cleanliness.

7. UV-C radiation can produce fast photodegradation of plastic and other materials. From this point of view, materials can be ranked in *no effect* materials like inorganic materials (example aluminium), *minor effect* (copper, EPDM and silicone sealants), *moderate effect* (LPDE, polycarbonate, cast epoxy, paper, HEPA filters for high irradiance values) and *severe effect* materials (HDPE, polyester, cardboard, glass fibre insulation, foam insulation), depending on the damage that UV-C produces on those materials.

8. Commercial methods used to size and design UV-C air disinfection systems are quite empirical. Designers shall consider the room size, the virus dose, the interaction with the ventilation air flow and safety measures. The effectiveness of UV-C air treatment systems is also strongly affected by the type of microorganisms, the irradiation level/type (lamp power and wavelength), duration of irradiation (exposure time), air movement pattern (mixing degree), and temperature and relative humidity. High air speeds will reduce the lamp temperature and, sometimes, the UV output. High RH will reduce the germicidal effect on SARS-COV-2 (decrease the decay rate); however, there are contradictions. Temperature has a low impact on microbial susceptibility to UGVI, but it affects the power of the UVGI lamp.

References

[1] Department of Health and Human Services, Centres for Disease Control and Prevention National Institute for Occupational Safety and Health, Environmental control for tuberculosis: Basic upper-room ultraviolet germicidal irradiation guidelines for healthcare settings, 2009-015.
[2] Z. D. Bolashikov, A. K. Melikov, Methods for indoor air disinfection and purification from airborne pathogens for application in HVAC systems, The 6th International Conference on Indoor Air Quality, Ventilation & Energy Conservation in Buildings IAQVEC 2007, Oct. 28–31, 2007, Sendai, Japan.
[3] C. B. Beggs, E. J. Avital, Upper-room ultraviolet air disinfection might help to reduce COVID-19transmission in buildings: a feasibility study, https://peerj.com/articles/10196.pdf
[4] M. Biasin, A. Bianco, G. Pareschi, et al., UV-C irradiation is highly effective in inactivating SARS-CoV-2 replication. Sci Rep 11, 6260 (2021), https://doi.org/10.1038/ s41598-021-85425-w
[5] J. B. O'Hagan, M. Khazova, Assessment of personal exposures to non-laser optical radiation in entertainment, Health Protection Agency – Centre for Radiation, Chemical and Environmental Hazards, Chilton, Didcot, Oxfordshire OX11 0RQ ISBN 978-0-85951-689-1
[6] W. Kowalski, Ultraviolet Germicidal Irradiation Handbook, UVGI for Air and Surface Disinfection, Springer, Berlin, Heidelberg, Online ISBN978-3-642-01999-9, 2009
[7] http://www.heliosquartz.com/wp-content/uploads/2016/01/Helios-Quartz_UV-LAMPS_ eng.pdf
[8] http://ibse.hk/SBS5312/SBS5312_1718_03-light_sources.pdf
[9] http://www.uvresources.com/blog/the-science-behind-uv-c-energy-uv-in-hvac-systems/
[10] J. Lau, W. Bahnfleth, R. Mistrick, D. Kompare (2012), Ultraviolet irradiance measurement and modelling for evaluating the effectiveness of in-duct ultraviolet germicidal irradiation devices, HVAC&R Research, 18:4, 626–642

[11] https://www.signify.com/global/lighting-academy/browser/webinar/UV-C-disinfection-for-air-surfaces-water

[12] https://lightprogress.com/collections/hvac

[13] https://insights.regencylighting.com/how-much-does-upper-room-germicidal-uv-cost

[14] https://www.smartclima.ro/proiectare-si-fabricare-de-dispozitive-pentru-sterilizare-aer/#comments

[15] ASHRAE Handbook, Applications 2019, Chapter 62 – Ultraviolet air and surface treatment

[16] https://www.ashrae.org/file%20library/technical%20resources/covid-19/final-4-21-2020-ashrae-one-hour-uvgi-course_bh-copy.pdf

[17] A. H. Malayeri, M. Mohseni, B. Cairns, J. R. Bolton, with earlier contributions by G. Chevrefils (2006) and E. Caron (2006), Fluence (UV Dose) required to achieve incremental log inactivation of bacteria, protozoa, viruses and algae (https://uvsolutionsmag.com/stories/pdf/archives/180301_UVSensitivityReview_full.pdf)

[18] https://uvtglobal.com/wp-content/uploads/2020/04/dosage-requirements.pdf

Other resources

[1] REHVA guidance (version 4 and future versions)

[2] G. N. Sze To, C. Y. H. Chao, Review and comparison between the Wells–Riley and dose-response approaches to risk assessment of infectious, respiratory diseases, Indoor Air 2010; 20: 2–16

[3] C. J. Kähler, T. Fuchs, R. Hain, Can mobile indoor air cleaners effectively reduce an indirect risk of SARS-CoV-2 infection by aerosols? https://www.researchgate.net/ publication/343514409, preprint August 2020

[4] K. Nissen et al., Long-distance airborne dispersal of SARS-CoV-2 in COVID-19 wards, Scientific Reports volume 10, Article number: 19589 (2020)

[5] E. Bromage, The Risks – Know Them – Avoid Them; https://www.erinbromage.com/post/the-risks-know-them-avoid-them

[6] Signify webinar, UV-C disinfection for air, surfaces and water, June 2020 (www.signify.com/global/lighting-academy/browser/webinat/ucv-dinsfection-for-air-surfaces -water)

[7] C. Noakes, A. Beswick, Summary of disinfection technologies for microbial control, SAGE meeting paper, 18/05/2020

[8] CIBSE COVID-19 Ventilation Guidance, version 4, Oct 2020

[9] G. Seminara, B. Carli et al., Biological fluid dynamics of airborne COVID-19 infection, Rendiconti Lincei, Scienze Fisiche e Naturali (2020) 31:505–537

[10] S. N. Rudnick, D. K. Milton, Risk of indoor airborne infection transmission estimated from carbon dioxide concentration, Indoor Air 2003; 13: 237–245

[11] R. K. Matharu, L. Ciric et al., Comparative study of the antimicrobial effects of tungsten nanoparticles and tungsten nanocomposite fibres on hospital acquired bacterial and viral pathogens, Nanomaterials 2020, 10, 1017

[12] https://www.timesofisrael.com/for-1-per-person-uv-light-can-help-protect-world-from-virus-scientists-find/

[13] https://www.hpac.com/air-conditioning/article/20927323/rightsizing-UV-C-lamps-for-hvac-applications

[14] https://www.sanuvox.com

[15] O. Lawal, B. Dussert et al., Method for the measurement of the output of monochromatic (254 nm) low-pressure UV lamps, IUVA News/Vol. 19 No. 1

[16] https://www.uvtglobal.com/what-is-uv-c/the-history-of-uv-c/

[17] https://www.intl-lighttech.com/products/ilt2400-uvgi

[18] ISO 15714:2019, Method of evaluating the UV dose to airborne microorganisms transiting in-duct ultraviolet germicidal irradiation devices

[19] ISO 15727:2020, UV-C devices – Measurement of the output of a UV-C lamp

[20] ISO 15858:2016, UV-C devices – Safety information – Permissible human exposure

[21] EPA, https://www.epa.gov/indoor-air-quality-iaq/what-are-ionizers-and-other-ozone-generating-air-cleaners & https://www.epa.gov/indoor-air-quality-iaq/ozone-generators-are-sold-air-cleaners, 2020

[22] ASHRAE, 2011. Emerging Issue Reports: The Ozone and Indoor Chemistry Emerging Issue Report. ASHRAE Environmental Health Committee (EHC), January 2011

[23] M. L. Bell, R. D. Peng, F. Cominici, (2006). The exposure-response curve for ozone and risk of mortality and the adequacy of current ozone regulations. Environmental Health Perspectives, 114(4): 532–536. https://doi.org/10.1289/ehp.8816

[24] HSE, Health and Safety Executive. EH40/2005 Workplace exposure limits containing the list of workplace exposure limits for use with the Control of Substances Hazardous to Health Regulations 2002. (Fourth Edition 2020), London

Study of the durability against carbonation of the concrete formulated with the partial replacement of cement with marble powder

Merah AHMED [1]

1 University AmmarTelidji of Laghouat , Faculty of Civil Engineering and Architecture, Research Laboratory of Civil Engineering (LRGC), Laghouat, Algeria.
a.merrah@lagh-univ.dz, ahmedmerrah@gmail.com

Abstract

The first aim of this study is the use of marble waste powder as a partial replacement with cement (CEMI 42.5) in concrete in order to reduce greenhouse gas emissions results in the cement production and consequently on the manufacturing concrete with less environmental impact.

Moreover, the carbonation phenomenon influences significantly the durability of reinforced concrete structures, in this context, the second aim of this work is the study of the effect of the accelerated carbonation on the durability of concretes formulated with the cement containing the marble waste (MDP) with different percentages. For this purpose, four concrete mixtures containing 0%, 10%, 15%, and 30% MDP as cement replacement by weight basis have been prepared. These mixtures of concretes were submitted to accelerated carbonation to study their durability against this phenomenon.

The series of tests are conducted to study the effect of 10%, 20% and 30% replacement of cement with marble powder on carbonation depth and compressive strength and compare it with the conventional concrete.

The result of this present investigation indicates that the carbonation depth increases with the increase of the rate of the replacement of cement with waste marble powder (10 % to 30%) and the compressive strength decreases slightly with the increase of replacement. the compressive strength remains within the acceptable range of M25 concrete.

Key-words: carbonation, concrete, marble powder

1. Introduction

The consumption of fossil fuels releases trace gases in the atmosphere that affect the climate, such as methane, Sulphur dioxide, nitrogen and carbon dioxide. The latter being responsible for half of the greenhouse effect (Retallack and Conde 2020). (Betts et al 2016) shown that the global carbon dioxide (CO_2) content of the atmosphere reaches the symbolic and significant threshold of 400 parts per million (ppm) for the first time in 2015 and set new records in 2016.

Concrete is the most widely used composite material in the world, given its high strength and stability. this material is mainly composed of cement, aggregates, water and possibly additives, all the components of this material are available in nature with the exception of the cement which requires fossil energy for production which is the main source of pollution air.

(Diet and Schmitt 1996) show that the cement industry generates enormous quantities of carbon dioxide and thus participates in increasing the concentration of CO_2 in the air. this concentration can reach 1% and to produce a ton of cement, the cement industry releases a ton of CO_2.

Furthermore, marble quarries generate marble powder waste that is harmful to the environment. In this context, two objectives are to be expected, the first consists in limiting the CO_2 on emissions due to the manufacture of cement, the second consists in minimizing the effects on the environment by the use of marble powder as a partial replacement for the cement, in this axe of research several researchers have carried out several studies on the effect of this partial replacement of cement with marble powder, among these researchers, (Sadek et al 2016) conducted a study on the possibility of using marble powder in self-placing concrete as a partial replacement for cement, the results of this study showed that the optimal percentage of replacement is around 50% which leads to an increase in compressive strength . (Soliman 2013; Aliabdo et al 2014) studies the effect of the use of marble powder as a partial replacement of cement on the concrete properties, the results obtained shown that the use of marble powder improves workability, compressive and tensile strength. (Kumar and Kumar 2015, Vaidevi 2013; Rodrigues et al 2015; Ergün 2011) studied the effect of different percentage of substitution of cement by marble powder on compressive strength, the results of this research shown that the optimal rate of replacement of cement by powder marble is up to 10%. In the same way, (Singh et al 2017;2019) concluded that an optimum of 15% replacement leads to an improvement in strength and durability of concrete.

In the same way other researchers continued to explore this field ,(Singh et al 2019), concluded that the marble powder incorporated in concrete shows increase in mechanical properties at 15% replacement by weight of cement for lower w/b ratios 0.35 and 0.40, and for w/b ratio 0.45 the strength increases only up to 10% replacement. In their study, (Ulubeyli et al 2016) found out that the use of waste marble in the conventional or self-compacting concrete can improve durability properties of the concrete.

In their study (Vardhan et al 2019) show that waste marble can be used into concrete to improve its strength and permeation properties, with the maximum improvement obtained at 40% replacement level. (Ashish 2018) concluded in their study that the maximum percentage of partial replacement of marble powder in cement don't exceed 20%. The studies cited in this work in the field of partial replacement of cement with marble dust conclude that the replacement of the cement must not exceed 20% of marble dust in order to have acceptable compressive strength of the concrete. High levels of marble dust increase the capillarity of concrete.

On the other hand, many environmental phenomena influence the durability of reinforced concrete structures. Among these phenomena, we can cite the concrete carbonation which is one of the main factors of degradation of unprotected reinforced concrete structures, and those exposed to high concentrations of carbon dioxide (such as road tunnels). This causes corrosion of the reinforcements, causing the concrete to lose its alkalinity and consequently causes the reduction of the service life of reinforced concrete structures. carbon dioxide gas penetrates through the open porosity of concrete to react with interstitial water to give carbonic acid, this in turn reacts with portlandite

$Ca(OH)_2$ (product responsible for the durability of the steels against corrosion while keeping an environment with a basic pH of the order of 13), this reaction produces calcium carbonate $CaCO_3$ which consumes the reserve of portlandite and putting steels without protection. Then, lead to disorders in the construction by swelling and cracking.

Several researchers have studied the effect of carbonation, on the durability of concretes formulated with substitution of cements with marble powder, in their study (Ashish 2019; Gameiro 2014) shows that the depth of carbonation increases with the increase of the replacement.

(Singh et al 2017) shows that with 15% of partial replacement of the marble powder, the resistance for carbonation was improved. According to the experimental study, (Ashish 2018; Rana et al 2015)   also show that the depth of carbonations increased in case of use of powder marble.

In their review study, (Kumar and Thakur 2018) show that the concrete carbonation depth depends on its porosity. Carbonation values also decrease with inclusion of marble powder and reported a similar trend to carbonation depth and water absorption by immersion for the chloride mitigation coefficient.

This paper presents a contribution in this area. this contribution consists on studying the durability of concrete formulated with a partial replacement of cement with marble powder who is the first objective, the second consist to study the effect of using marble powder as partially replace of cement on the durability of concrete against the phenomenon of concrete carbonation.

The result of this investigation indicates that the carbonation depth decreases with the increase of the replacement of cement with waste marble powder (10 % to 30%) and the compressive strength decreases slightly with the increase of replacement. the compressive strength remains within the acceptable range of M25 concrete.

2.   Materials

2.1. Cement

The used cement is a Portland cement CEM I/42.5 produced in the locality of BISKRA in South East of Algeria, the cement density is 3.07 g/cm^3, with the characteristics shows in table 1, 2 and 3

Elements	Content %	Norms
SO_3	2.30	(NA 237) < 3.5%
CL	0.028	(NA 5080) $\leq$ 0.1%
P.A.F	2.04	(NA 237) $\leq$ 5%
C_3S clinker	62	In accordance with Bogue
C_2S clinker	13	In accordance with Bogue
C_3A clinker	1.5	In accordance with Bogue
C_4AF clinker	17	In accordance with Bogue

Table 1: Mineralogic characteristics of used Cement **CEM I 42.5**

Designation	Measures	Norms
Specific surface Blaine (cm^2/g)	3420	(NA231)
Start of taking (min)	180	(NA233) ≥60 min
Hot expansion (min)	0.5	≤10mm(NA232)
Consistence (%)	25.7	T(NA290)

Table 2: Physics proprieties of used cement CEM I 42.5

Mechanic proprieties			
Compressive strength (MPa)	2 days	≥10	21
	28 days	62.5≥R≥42.5	49.5

Table 3: Mechanic proprieties of used cement CEM I 42.5

2.2. Powder Marble

The used marble powder was a waste resulting from the cutting, shaping and lustration of marble stones. This powder was supplied by the company MCA (Marble Tile and Agglo-marble installed in locality of Bordj Bou Arrérdj in Algeria). The physic and the chemical properties of the marble powder are given in Table 4.

Content (%)	Marble powder
CaO	55.6
SiO_2	0.6
AL_2O_3	0.4
Fe_2O_3	0.2
MgO	0.1
$NaCO_3$	90
CL	0.1
LOI	43
Density	2.7
Blaine Specific Surface (cm^2/g)	2126

Table 4: Chemical properties of the marble powder [**23**]
Table 4: Chemical properties of the marble powder (**Bouziani and Benmounah 2013**)

2.3. Aggregates

The used sand is alluvial (0-5 mm) which produced by Oued M'zi quarry of Laghouat, Algeria, two classes of limestone aggregates (3-8 mm and 8-15 mm) were used in the concrete formulation which produced by the quarry (Laghouat).
The table 5 gives the physical proprieties of the used aggregates

Physical proprieties of the used aggregates	Standard	Aggregates		
		Sand	Gravel	
		0/5	3/8	8/15
Apparent Density (g/cm^3)		1.564	1.319	1.255
Absolute density (g/cm^3)		2.6	2.65	2.65
Absorption Coefficient (%)	NF P 18-554	1	1.5	1.5

Table 5: Physical proprieties of the used aggregates.

The used sand has a particle size of 0–5 mm, apparent density of 1.56 g/cm^3 and absolute density of 2.61 g/cm^3. Two sizes of aggregates (3–8 mm), (8–15 mm) are used to formulate the concretes, these aggregates are characterized by a calcareous rock with a high calcium carbonate content (_98% $CaCO_3$), their apparent densities are 1.32 g/cm^3 and 1.26 g/ cm^3 respectively. Their absolute density is 2.6 g/cm^3. The used water is tap water. It meets all the requirements of NFP 18-303 [27] and EN 1008, taking into account the concentrations of suspended solids and dissolved salts.

3.   Methods

3.1. Concrete Formulation

The used concrete formulation method in the present study is DREUX GORISSE method.
The results of the concrete formulation were gives in Table 6:

S/G	W/C	Sand (kg/m^3)	Gravel 3/8 (kg)	Gravel 8/15 (kg)	Cement (CEM I) (kg)	Water (L)	Slump test (cm)
0.60	0.57	683.7	146.7	990.25	374.4	216.42	8

Table 6: Results of control concrete Formulation

Legend:
 S: Sand
 G: Gravels
W: Water
 C: Cement

Table 6: shows the results of the control concrete formulation. According to the synthesis of this results, the concrete formulation has the density, who is a normal concrete according the standard NF EN 12350-6 [28] (Normal concrete with a density between 2000 and 2600 kg/m^3).

From this control concrete formulation, three other concrete mixes were formulated by substituting different percentages (10%, 20% and 30%) of cement replace by weight with marble powder according to Table 7

Concretes formulations	Cement (Kg)	Marble powder (Kg)
B1 (0% replacement)	374.4	0
B2 (10% replacement)	336.96	37.44
B3 (20% replacement)	299.52	74.88
B4 (30% replacement)	262.08	112.32

Table 7: Weights of Marble powder for different concrete formulations.

3.2. Confection and preservation of samples.

Before mixing the concretes, the aggregates, previously washed and dried in an oven at 10 ± 5 ° C for one day (24 h), then cooled in ambient air, then they are introduced, according to mass proportions already known. in parallel with the preparation of the concrete, the moulds (7x7x7 cm3) are prepared for the determination of the compressive strength and for the accelerated carbonation tests. All the samples are kept in the moulds for 24 hours in plastic film, after demoulding, they are immersed in water at $T = 20 \pm 0.5$ ° C according to standard NA 426 for 28 days and according to the recommendation of the AFPC AFREM(P.Rougeau,1997), until the deadlines for the start of tests (Figure 1)

Fig. 1. Samples conservation.

After 28 days of cure, the cubic samples (7x7x7 cm^3) of prepared concrete will be subjected to two test campaigns, compression test and accelerated carbonation test.

3.3. Compressive strength test.

In order to determinate the compressive strength of the four concrete formulations (B1, B2, B3 and B4) cubic samples (7x7x7 cm^3) were used. The compressive strength for cubic samples of carbonated and control concrete samples were determinate at age 7,14 and 28 days.

The compression resistance test was carried out on $7 \times 7 \times 7$ cm^3 cubic samples according to NF P18-406. The hydraulic press used has a loading speed of 0.5 MPa / Sec with a capacity of 3000KN. the rupture stress is given directly by the testing machine with an accuracy of 0.5 MPa (Figure 2.).

Fig.2. Machine for compressive strength test.

3.4. Accelerated carbonation test

The concrete carbonation is a very slow phenomenon in the atmosphere, the concentration of carbon dioxide is not very important (of the order of 0.3%) in the air , the effect of this phenomenon is manifested only after several years of exposure of reinforced concrete structures to this phenomenon, therefore, it is necessary to find a way to accelerate the carbonation of the cementitious material ensuring results representative of this natural phenomenon. This test is called "accelerated carbonation test".

3.4.1. Accelerated carbonation test procedure according to the AFPC-AFREM test protocol.

The test consists in following the evolution of the thickness of the carbonated concrete preserved in an atmosphere rich in carbon dioxide (CO_2).

A.1. Equipment.

✓ **Ventilated oven:** controlled at $40 \pm 2°C$, located in a room with a temperature of $20 \pm 2°C$

✓ **Accelerated carbonation chamber:** the accelerated carbonation test consists in obtaining a gas mixture (50% CO_2 + 50% air) in the carbonation chamber (Figure. 3) with controlling the relative humidity which must be between 40 and 80%. To monitor the relative humidity, a hygrometer was used. The carbonation test is executed using a carbon dioxide (CO_2) incubator according to the AFPC-AFREM test protocol (1997) (P. Rougeau, 1997).
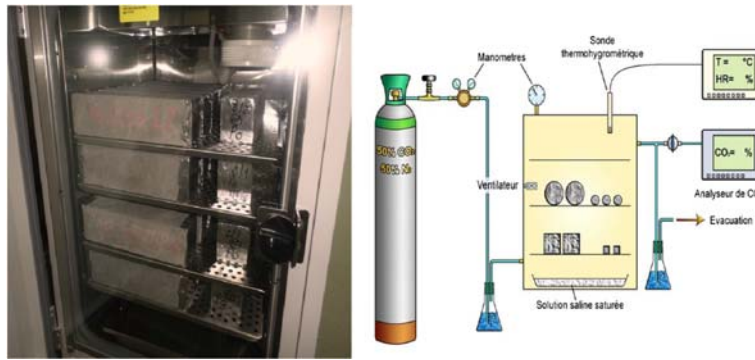
Fig.3. Accelerated carbonation chamber

To start the accelerated carbonation test, the samples must be preconditioned in two phases:

- In the first phase, the specimens undergo a cure in a humid environment (relative humidity greater than 95% or emerged into water) for 28 days (P. Rougeau,1997) then weighed, according to the recommended procedure for determining the bulk density and the water content.

In the second phase, they are placed in an oven at $40 \pm 2°$ C, for two days, then weighed for second time (P. Rougeau,1997). The two faces of each sample must be covered with adhesive aluminium wrapper to guide the diffusion of CO_2, then the samples are subjected to accelerated carbonation in the carbonation chamber for 28 days and placed distant of 2 cm one from the other (figure 4 and figure 5) (P.Rougeau,1997), while other control samples are stored in the laboratory to measure the compressive strength.

Fig. 4.: Preparation of Samples for accelerated carbonation test.

Fig.5. Samples into the chamber of carbonation

At the age 7, 14 and 28 days, concrete samples are weighed and removed from the carbonation chamber to measure the evolution of accelerated carbonation according to the experimental procedures of the AFPC AFREM 1997 recommendations (P. Rougeau,1997). To measure the concrete carbonated depth, the samples are sliced in two parts and the reading is made immediately using the colour indicator recommended by the procedure of standard NF P18-458. It colours the uncarbonated concrete in pink while the carbonated concrete does not change. The colour indicator used to reveal the carbonated concrete is a phenolphthalein solution (Figure. 6). The number of samples required for carbonation test is four: three for measuring the concrete carbonation depth, the fourth is used to follow the evolution of the sample mass during the test. Two additional test specimens may be used to monitor the evolution of concrete subjected to natural carbonation. These samples can be stored in an ambient atmosphere at a temperature of 20 ± 2 _C and a relative humidity of $65 \pm 5\%$. Other cubic samples were prepared for the different concrete formulations according to the recommendations of the French Association of Competitiveness Clusters (AFPC AFREM 1997) (P. Rougeau,1997).

Fig.6. Determination of Carbonation depth with phenolphthalein pulverisation

4.   Results and Discussions

4.1. Densities and water content of samples

In order to conduct the accelerated carbonation test and according to AFPC AFREM 97 (P. Rougeau,1997) recommendations, in the first pre-conditioning phase, the bulk density and water content of the samples must be determined for the accelerated carbonation test.
The table 8 show the results of densities and water content for the four concrete formulation

Concrete formulations	Densities in Kg/m^3	Water content (%)
B1(0% replacement)	**2537.63**	**2.37**
B2(10% replacement)	**2566.14**	**2.32**
B3(10% replacement)	**2602.85**	**2.32**
B4(10% replacement)	**2592.64**	**2.34**

Table 8: Densities and water content for the four concrete formulations

The table 8 show that the densities increases with the increase of substitution (cement with the powder marble) for the four concrete formulations. The water content of the all concrete formulations have the same value, from these results, then, the accelerated carbonation test can be started according to AFPC AFREM 97 (P. Rougeau,1997).

4.1. Effect of the replacement (cement by the powder marble) on the compressive strength for the four concretes formulations

At the age of 28 days, samples were tested with the compressive machine, the table 9 show the effect of the carbonation on the compressive strength of the control concrete and the other concretes with different percentages of replacements of cement with powder marble (10%, 20% et 30%)

Age (days)	Compressive strength (MPa)			
	Formulation B1(control)	Formulation B2 (10%replacement)	Formulation B3 (20% replacement)	Formulation B4 (30% replacement)
28	59.2	55.4	52.9	46.4

Table 9: Compressive strength for different concrete formulations

from Table 9 and the figure 7, it is clearly shown that the compressive strength decreases with increasing percentage of substitution of cement with marble powder. this decrease is slightly (of the order of 11%) up to a percentage of 20% of substitution and it is important of the order of 22% for a substitution of 30%.

Study of the durability against carbonation of the concrete formulated with the partial replacement of cement with marble powder
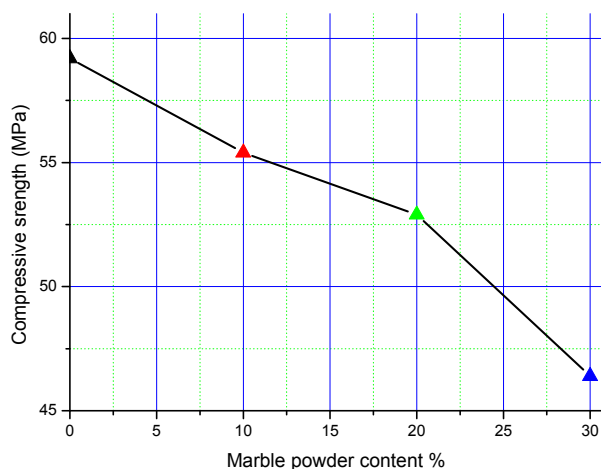
Fig.7.: Compressive strength with marble powder content

The obtained results for the compressive strength of concrete are in agreement with those obtained by (Tayeh 2018). The value of the compressive strength of 46 MPa corresponding to a substitution of cement with 30% of marble powder is acceptable for the realization of structural elements of reinforced concrete. this result will lower cost of making reinforced concrete structures, with condition to protecting the exposed concrete against carbonation.

4.2 Effect of the carbonation on the gain mass for the four concrete formulations

The table 10 show the effect of the carbonation on the gain mass for the four concrete formulations at the different ages 7,14 and 28 days,

Age (days)	Mass gain (g)			
	Concrete B1 (control)	Concrete B2 (10% replacement)	Concrete B3 (20% replacement)	Concrete B4 (30% replacement)
7	853.24	865.92	881.7	913.3
14	856.8	869.2	886.8	923.1
28	858.2	870.6	889.1	925.6

Table 10: Mass gain (g) for different concrete formulations.

From this table, we draw the following curve (Figure 8)

238
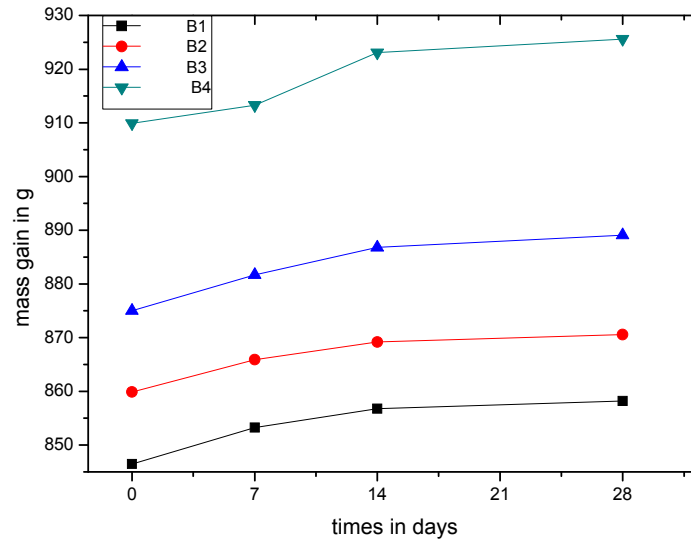
Fig.8.: Mass gain for the four concretes formulations

Figure. 8 show that the carbonation increases the mass of samples with the increase of the substitution (cement by marble powder (10%, 20%, 30%). This increase is due mainly to the concrete carbonation who makes changes in the microstructure of carbonated concrete (replacement of portlandite by calcite).

4.3. Effect of the accelerated carbonation on the four concretes formulations.

The carbonate depth was determined, according to the AFPC-AFREM 97 procedure (P.Rougeau,1997), by a phenolphthalein method described above, applied to the face of the cubic samples ($7 \times 7 \times 7$ cm^3) after cutting into two parts with the 'ages 7, 14 and 28 days. Table 11: shows the evolution of the depth of carbonation at different ages for the four concrete formulations.

Age (Days)	Carbonation depth (mm)			
	Concrete B1 (Control)	B2 (10% replacement)	B3(20% replacement)	B4(30% replacement)
7	1	3	4	6
14	2	5	7	8
28	3	6	7.5	9.5

Table 11: Evolution of carbonation depth at different ages for the four concrete formulations

From the table 11, we draw the following curve (figure 9).
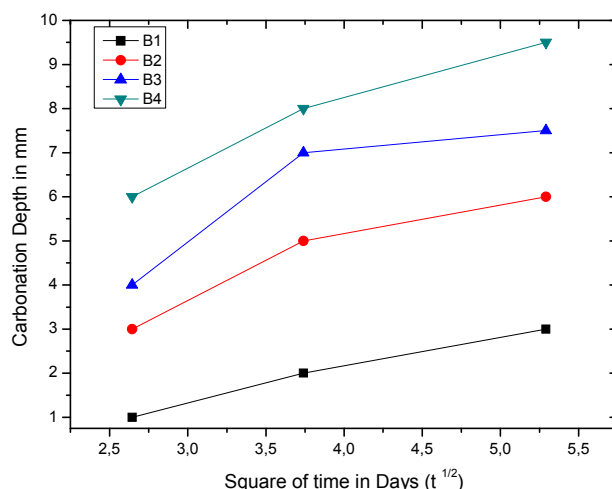
Fig.9.: Carbonation depth for the four concrete formulations

According to the curve of the evolution of the carbonation depth with the square of time for the different concretes, we note that the depth of the carbonation increases with the substitution of cement by the marble powder (10%, 20%, 30%).

In addition, it can be seen from the previous curve (Figure 9) that the evolution of the carbonation depth is relatively fast from 7 days to 14 days and stabilizes at almost constant values until the 28th days. This for all concretes (B1, B2, B3, B4). This result can be explained as follows:

-        During the 7 to 14-day period, the available amount of portlandite is larger, resulting in faster carbonation with calcite formation.

-        For the period between 14 and 28 days, the available amount of portlandite becomes low as it is consumed during the first period. this will reduce the carbonation rate.

This reduction is caused by clogging of pores caused by the formation of calcite which has a molar volume greater than the molar volume of portlandite.

On the other hand, it can be concluded that the depth of carbonation increases with the increase of the percentage of replacement of powder marble.

4.4. Correlation between the mass gain and the carbonation depth

The figure 10 show the mass gain with carbonation depth
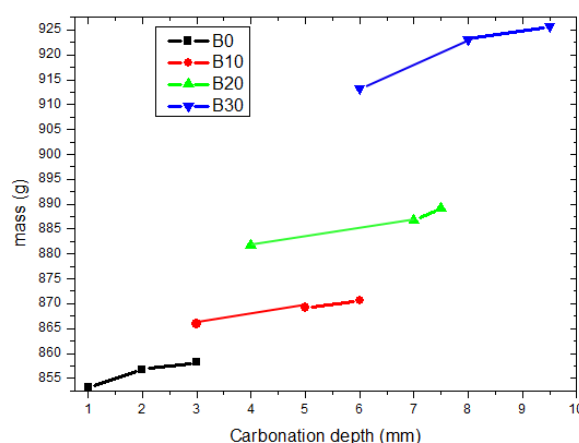
Fig 10. Mass gain with the carbonation depth

From the figure 10, it can be seen that the mass of the carbonated samples increases with the increase of the carbonation depth, which shows an important relation between the gain of the mass and the carbonation depth, which leaves to think that there is a relation which links the gain of mass to the depth of carbonation, that is to say that one can estimate the depth of carbonation from a simple weighing, thus avoiding the use of solution of phenol.

5.   Conclusions

From this study, the following conclusions can be written
-       The depth of carbonation increases with the time of exposure in the enclosure of accelerated carbonation.
-       The increase in the substitution of cement by powdered marble increases the depth of carbonation. this is due to the replacement of cement by the marble powder which makes decreased, the rate of portlandite and consequently, it accelerates the consumption of this one by the reaction of carbonation.
-       The increase in the mass of carbonate samples increases with the increase in the depth of carbonation, this is mainly due to the carbonation of portlandite giving rise to calcite denser than portlandite
-       The compressive strength decreases with substitution of the cement by the marble powder. this decrease is slight and remains within values acceptable by Algerian standards.
-       Partial replacement of cement with marble powder up to 30% can give a quality concrete (Acceptable compressive strength according to Algerian standards). moreover, this replacement contributes to reducing the harmful effects of marble waste on the environment.
-       To protect this concrete and make it durable against carbonation, it must be protected by an anti-carbonation coating.

References

Retallack, G.J., Conde, G.D., 2020. Deep time perspective on rising atmospheric CO2. Global and Planetary Change 103177.

Betts, R.A., Jones, C.D., Knight, J.R., Keeling, R.F., Kennedy, J.J., 2016. El Niño and a record CO 2 rise. Nature Climate Change 6, 806.

Diet, A., Schmitt, A., 1996. Electricity of France and renewable energies: this is part Solar systems (Review) 17–23.

Sadek, D.M., El-Attar, M.M., Ali, H.A., 2016. Reusing of marble and granite powders in self-compacting concrete for sustainable development. Journal of Cleaner Production 121, 19–32.

Soliman, N.M., 2013. Effect of using marble powder in concrete mixes on the behavior and strength of RC slabs. International Journal of Current Engineering and Technology 3, 1863–1870.

Kumar, R., Kumar, S.K., 2015. Partial replacement of cement with marble dust powder. International Journal of Engineering Research and Applications 5, 106–114. Vaidevi, C., 2013. Study on marble dust as partial replacement of cement in concrete. Indian journal of engineering 4, 14–16.

Singh, M., Srivastava, A., Bhunia, D., 2019. Long term strength and durability parameters of hardened concrete on partially replacing cement by dried waste marble powder slurry. Construction and Building Materials 198, 553–569.

Singh, M., Srivastava, A., Bhunia, D., 2017. An investigation on effect of partial replacement of cement by waste marble slurry. Construction and Building Materials 134, 471–488.

Aliabdo, A.A., Elmoaty, A.E.M.A., Auda, E.M., 2014. Re-use of waste marble dust in the production of cement and concrete. Construction and building materials 50, 28–41.

Rodrigues, R., De Brito, J., Sardinha, M., 2015. Mechanical properties of structural concrete containing very fine aggregates from marble cutting sludge. Construction and Building Materials 77, 349–356.

Singh, M., Srivastava, A., Bhunia, D., 2019. Analytical and experimental investigations on using waste marble powder in concrete. Journal of Materials in Civil Engineering 31, 04019011.

Ergün, A., 2011. Effects of the usage of diatomite and waste marble powder as partial replacement of cement on the mechanical properties of concrete. Construction and building materials 25, 806–812.

Ulubeyli, G.C., Bilir, T., Artir, R., 2016. Durability properties of concrete produced by marble waste as aggregate or mineral additives. Procedia engineering 161, 543–548. Vardhan, K., Siddique, R., Goyal, S., 2019. Strength, permeation and micro-structural characteristics of concrete incorporating waste marble. Construction and Building Materials 203, 45–55.

Ashish, D.K., 2018. Feasibility of waste marble powder in concrete as partial substitution of cement and sand amalgam for sustainable growth. Journal of Building Engineering 15, 236–242.

Ashish, D.K., 2019. Concrete made with waste marble powder and supplementary cementitious material for sustainable development. Journal of cleaner production 211, 716–729.

Singh, M., Choudhary, K., Srivastava, A., Sangwan, K.S., Bhunia, D., 2017. A study on environmental and economic impacts of using waste marble powder in concrete. Journal of Building Engineering 13, 87–95.

Gameiro, F., De Brito, J., da Silva, D.C., 2014. Durability performance of structural concrete containing fine aggregates from waste generated by marble quarrying industry. Engineering Structures 59, 654–662.

Rana, A., Kalla, P., Csetenyi, L.J., 2015. Sustainable use of marble slurry in concrete. Journal of Cleaner Production 94, 304–311.

Kumar, A., Thakur, A., 2018. A State of Art Review: On Usage of Waste Marble Powder In Concrete Production.

P. ROUGEAU, " AFREM crossover test results, Accelerated carbonation test," CERIB, 1997.

Bouziani, T., Benmounah, A., 2013. Correlation between v-funnel and mini-slump test results with viscosity. KSCE Journal of Civil Engineering 17, 173–178.

Tayeh, B.A., 2018. Effects of marble, timber, and glass powder as partial replacements for cement. Journal of Civil Engineering and Construction 7, 63–71.

Calculul densităţii sarcinii termice pentru birouri clasa A și B

Calculation of fire load for class A and B offices

Ovidiu MIHALACHE[1], Ion ANGHEL[2], Iulian-Cristian ENE[3]

[1]Academia de Politie "Alexandru Ioan Cuza" – Facultatea de Pompieri
București, sector 2, Șoseaua Morarilor, nr.3, România
ovidiu@3mexpert.ro

[2]Academia de Politie "Alexandru Ioan Cuza" – Facultatea de Pompieri
București, sector 2, Șoseaua Morarilor, nr.3, România
ion_anghel2003@yahoo.com

[3]Academia de Politie "Alexandru Ioan Cuza" – Facultatea de Pompieri
București, sector 2, Șoseaua Morarilor, nr.3, România
iuliancristianene@gmail.com

Rezumat. Densitatea de sarcină termică din interiorul unui compartiment de incendiu, alături de fluxul căldurii degajate de incendiu, reprezintă doi parametri esențiali în domeniul ingineriei securității la incendiu, fiind utilizați în special ca parametri de intrare în modelarea incendiilor. Acest studiu începe cu o prezentare a evoluției modului în care a fost calculată, de-a lungul timpului, densitatea sarcinii termice. În continuare, sunt redate două metode de calcul a densității sarcinii termice, prima metodă fiind utilizată în conformitate cu standardul SR EN 10903-2: 2016, iar cea de-a doua, în conformitate cu standardul SR EN 1991-1-2-2016. În cadrul celor două metode sunt analizate două scenarii: un spațiu cu destinația de birou clasa A, utilizată de 120 lucrători, caracterizată de o suprafața de 10 m^2 aferentă unui lucrător; un spațiu cu destinația de birou clasa B, utilizată de 216 lucrători, caracterizată de o suprafața de 5 m^2 aferentă unui lucrător. În ambele scenarii, suprafața celor două birouri este identică, având valoarea de 1232,50 m^2.
În urma analizei rezultatelor obținute prin utilizarea celor două metode se constată că spațiile cu destinația de birou utilizate de un număr mai mare de lucrători au o sarcină termică mai mare decât în cazul spațiilor utilizate de mai puțini lucrători. Folosind metoda SR EN 10903-2: 2016 se obțin valori mai mari ale densității sarcinii termice decât prin folosirea metodei SR EN 1991-1-2-2016. De asemenea, se constată că riscul de incendiu este mic, valorile densității sarcinii termice fiind sub valoarea de 420 MJ/m^2.

Cuvinte cheie: densitate de sarcină termică, metode de calcul, birou clasa A și B

Abstract. In the field of fire safety engineering there are two key parameters being used mainly as input parameters in fire modeling, namely the fire load inside a the fire compartment, along side the heat flow released by the fire. This study begins with a presentation of the evolution of the calculation mode of the heat load density, over time. There are presented two methods of calculating the heat load density, the first method used

Ovidiu MIHALACHE, Ion ANGHEL, Iulian ENE

is according to standard SR EN 10903-2:2016, and the second, in accordance with the standard SR EN 1991-1-2-2016. Two scenarios are analyzed under the two methods: A „class A office room" used by 120 workers, each worker having atributed an area of 10 m²; A „class B office room" used by 216 workers, each worker having atributed an area of 5 m². In both scenarios, the area of the two offices is identical, at 1,232.50 m².
The results obtained through the use of the two methods show that office rooms used by a higher number of workers have a higher thermal load than the ones used by a smaller number of workers. By using the SR EN 10903-2:2016 method, there were obtained higher values of the fire load as opposed to using the SR EN 1991-1-2-2016 method. The analysis also shown that the fire risk is low, the values of the fire load being under 420 MJ/m^2.

Key words: fire load, calculation methods, class A and B office

1. Introducere

Sarcina termică reprezintă cantitatea totală a căldurii degajate de incendiu obținută prin arderea tuturor materialelor combustibile aflate într-un compartiment de incendiu. Sarcina termică reprezintă un parametru important în cadrul modelării incendiilor și se măsoară în MJ. Sarcina termică se poate determina, folosindu-se diferite metodologii, prin analizarea unui model reprezentativ de clădiri, a dimensiunilor încăperilor, a materialelor combustibile fixe sau movibile și a caracteristicilor acestora.

În domeniul ingineriei securității la incendiu este utilizat conceptul curbei modelului de incendiu, reprezentat de principalul parametru, și anume, fluxul căldurii degajate de incendiu, denumit și HRR (eng: heat release rate). Acest parametru reprezintă cantitatea de căldură generată de un incendiu în unitatea de timp, fiind măsurat în J/s sau W.

Modelele de incendiu sunt caracterizate, în principal, prin raportarea fluxului căldurii degajate de incendiu la timp, densitatea sarcinii termice, utilizată independent de alți parametri, nefiind suficientă pentru determinarea cu exactitate a curbei unui model de incendiu.

2. Evoluția modului de calcul al densității sarcinii termice

Proiectarea construcțiilor și instalațiilor aferente se realizează pe baza standardelor prescriptive și/sau de performață. Un criteriu foarte important în stabilirea măsurilor de securitate la incendiu pasive și active pentru o clădire îl reprezintă riscul de incendiu.

Riscurile de incendiu se determină pentru fiecare încăpere și pentru compartimentul de incendiu în ansamblul lui. Nivelul riscului de incendiu poate fi stabilit în funcție de destinația spațiului său, respectiv în funcție de densitatea sarcinii termice, exprimată în MJ/m².

Densitatea sarcinii termice constă în raportul dintre sarcina termică totală dintr-o încăpere și suprafața acestei.

În 1976, în România a fost aprobată o primă metodă de calcul [1], aceasta fiind ulterior revizuită în anul 1979 [2]. Astfel, formula de calcul pentru sarcina termică este:

$$S_Q = \sum_{i=1}^{n} Q_i M_i \qquad\qquad (1)$$

unde

S_Q reprezintă sarcina termică [MJ];

Q_i - puterea calorifică inferioară materialului [MJ/kg] sau [MJ/m³N];

M_i - masa materialelor combustibile de același fel, aflate în spațiul supus analizei [kg] ([m³N], pentru gaze);

n - numărul materialelor de același fel aflate în spațiul supus analizei.

Pentru determinarea puterii calorifice inferioare, Q_i [3], este necesară luarea în considerare a tuturor materialelor combustibile, fixe sau mobile, care sunt în spațiul respectiv sau care intră în componența elementelor de construcții, a instalațiilor, a utilajelor tehnologice, a mijloacelor de transport, inclusiv a celor din componența pardoselilor, a tâmplăriei, a finisajelor (exceptând zugrăvelile și zonele vopsite), a izolațiilor, a rafturilor, a containerelor, a paleților sau a ambalajelor.

Nu se iau în considerare materialele combustibile aflate într-o stare în care aprinderea lor nu este posibilă (de exemplu, cele aflate într-o stare de umiditate ridicată).

Densitatea sarcinii termice se determină cu formula

$$Q_S = \frac{S_Q}{A_S} \qquad\qquad (2)$$

unde

Q_S reprezintă densitatea sarcinii termice [MJ/m²];

A_S – suma ariilor pardoselilor încăperilor ce alcătuiesc spațiul luat în considerare (o încăpere sau un grup de încăperi neseparate cu elemente rezistente la foc între ele) [m²].

Cantitatea de căldură degajată în urma unui incendiu care va acționa asupra elementelor de construcție, se poate scrie conform relației [3]:

$$S_A = cp \sum_{i=1}^{n} m Q_i M_i \qquad\qquad (3)$$

unde

S_A reprezintă cantitatea de căldură degajată în urma unui incendiu [MJ];

c – coeficient prin care se ține seama de mărimea dimensiunilor geometrice ale spațiului supus analizei, valorile acestui coeficient fiind standardizate [3] (conform tabelului 1 din STAS 8790-71);

p – coeficient prin care se ține seama de numărul de niveluri ale construcției, respectiv de condițiile de ventilare și disipare a căldurii, valorile acestui coeficient fiind standardizate [3] (conform tabelului 2 din STAS 8790-71);

m – coeficient prin care se ține seama de capacitatea de ardere a materialelor, în condiții de incendiu, valorile acestui coeficient fiind standardizate [3] (conform tabelului 3 din STAS 8790-71);

În ceea ce privește masa materialelor combustibile de același fel, M_i, aflate în spațiul supus analizei, nu se iau în considerare:
- Pardoselile lipite direct pe un suport incombustibil masiv;
- Gazele și lichidele pentru lubrefiere sau răcire din interiorul utilajelor tehnologice fixe sau al conductelor, care nu pot fi avariate înainte sau în caz de incendiu;
- Lichidele din conducte și recipienți ficși, de maxim 1 m³.
- Cărbunele sau coxul depozitate temporar în buncăre din beton sau zidărie.

Densitatea cantității de căldură care se apreciază că va acționa asupra elementelor de construcție în caz de incendiu se poate determina conform relației

$$q_a = \frac{S_A}{A_a} \qquad (4)$$

unde

q_a reprezintă densitatea cantității de căldură care se apreciază că va acționa asupra elementelor de construcție [MJ];

A_a – aria corespunzătoare suprafeței A_S, planșeele având rezistența la foc de minim 1 ora (REI 60), fără goluri sau cu goluri protejate, ori goluri neprotejate mai mici de 0,5 m^2 fiecare, aria însumată fiind de maxim 5% din A_S [m^2].

Conform standardului SR EN 10903-2 [4] aprobat în anul 2016, sarcina termică se determină astfel

$$S_Q = \sum_{i=1}^{n} Q_i M_i \qquad (5)$$

Puterea calorifică Q_i se determină conform SR EN ISO 1716:2010 [5], revizuit în anul 2018, acest standard înlocuind standardul STAS 8790-81 [3].

Trebuie precizat că standardul [5] permite utilizarea puterii calorifice indicate atât în literatura de specialitate, cât și în specificațiile tehnice ale produselor datorită gamei foarte largi de produse si materiale existente.

Densitatea sarcinii termice se determină cu aceeași formulă

$$q_s = \frac{S_Q}{A_S} \qquad (6)$$

Anterior acestui standard european [5] s-au aprobat o serie de documente, denumite generic Eurocoduri, pentru armonizarea tehnică a legislației necesară inginerilor în scopul proiectării structurilor de rezistență.

Astfel, conform SR EN 1991-1-2:2004: Eurocod 1 [6], densitatea sarcinii termice se determină cu formula

$$Q_{fi,k} = \sum M_{k,j} \cdot H_{ui} \cdot \Psi = Q_{fi,k,j} \qquad (7)$$

unde

$Q_{fi,k}$ reprezintă densitatea sarcinii termice [MJ];

$M_{k,j}$ – cantitatea de material combustibil despre care se presupune că nu variază pe timpul duratei de viață a unei structuri și reprezentată prin valori care nu să fie depășite în 80% din timp [kg];

H_{ui} – puterea calorifică inferioară determinată conform SR EN ISO 1716 [5] [MJ/kg];

Ψ – coeficient facultativ care permite evaluarea sarcinii termice protejate.

Trebuie precizat că standardul [6] indică puterea calorifica inferioară a anumitor solide, lichide și gaze.

Densitatea sarcinii termice se determină pe baza unor clasificări naționale a sarcinilor termice după destinație și/sau de maniera specifică pentru un proiect individual, prin efectuarea de studii privind sarcina termică. Formula utilizată este

$$d_{f,d} = q_{f,k} \cdot m \cdot d_{q1} \cdot d_{q2} \cdot d_{nj} \qquad (8)$$

unde

$d_{f,d}$ reprezintă densitatea sarcinii termice [MJ/m^2];

$q_{f,k}$ – densitatea sarcinii termice caracteristice [MJ/m^2];

m - coeficient de ardere;

d_{q1} – coeficient care ține seama de riscul de inițiere a incendiului datorat mărimii compartimentului;

d_{q2} – coeficient care ține seama de riscul de inițiere a incendiului datorat destinației;

d_{nj} – coeficient care ia în considerare diversele măsuri active de luptă împotriva incendiului;

Densitatea sarcinii termice caracteristice, $q_{f,k}$, este definită prin relația

$$q_{f,k} = Q_{fi,k}/A \tag{9}$$

unde

A – aria planșeului (A_f) sau aria suprafeței interioare (A_i) a compartimentului analizat ori a spațiului de referință [m^2];

3. Clasificarea riscului de incendiu

În Romania, clasificarea riscului de incendiu se face potrivit normativului P 118-1999 „Normativ de siguranță la foc". Astfel, pentru clădirile civile, riscul de incendiu este determinat, în principal, de densitatea sarcinii termice (qi) stabilită prin calcul și de destinația respectivă.

In funcție de densitatea sarcinii termice, riscul de incendiu în clădiri civile, poate fi:

mare: qi = peste 840 MJ/m^2;
mijlociu: qi = 420 - 840 MJ/m^2;
mic: qi = sub 420 MJ/m^2.

În alte țări membre ale Uniunii Europene, clasificarea riscului de incendiu se face, de regulă, în funcție de funcțiunea locală, respectiv generală, a compartimentului, coroborat uneori cu caracteristicile de arie și volum. Există și limitări ale densității sarcinii termice pentru anumite funcțiuni.

4. Calculul densității sarcinii termice utilizând SR EN 10903-2: 2016

Exemplu de calcul pentru un nivel de birouri cu spații open space/peisagere, 2 săli de curs IT a 16 persoane, sală de sedinţe cu 10 persoane, sală de mese, sală de recreere, vestiar, circulaţii:

4.1. Calculul densității sarcinii termice pentru un birou clasa A (10 mp/1 pers) S = 1.232,50 m^2 – 120 lucrători.

Tabel 1

Calculul densității sarcinii termice utilizând SR EN 10903-2-2016 pentru un birou clasa A

Materiale combustibile	Arie [m²] sau bucăți	Masă [kg]	q [MJ/Kg]	Q
dulap lemn pentru documente-rollbox	8	18	19.25	2,772.00
birou din lemn și metal pentru documente	120	25	19.25	57,750.00
scaun metalic cu poliuretan	120	1	37.70	4,524.00
calculatoare	120	5	33.00	19,800.00
hârtie	120	10	16.30	19,560.00
fotoliu	16	30	27.00	12,960.00
masă din lemn și metal	12	10	16.30	1,956.00
dulap lemn pentru haine $1{,}0 \cdot 0{,}5 \cdot 2{,}0$ [m]	13	50	16.30	10,595.00
dulap mic vestiar $0{,}3 \cdot 0{,}4 \cdot 1{,}0$ [m]	120	10	16.30	19,560.00
parchet laminat	1232.5	1.5	21.80	40,302.75
ușă interioară lemn	1	10	21.80	218.00
textile	120	5	20.95	12,570.00
∑Q=				202,567.75
qs =	202567.8	/	1232.5	**164.36**

→ densitatea sarcinii termice are valoarea sub 420 MJ/m² → risc mic de incendiu. Trebuie menționat că toate cantitățile de materiale combustibile pentru obiectele de mobilier sunt estimate, iar materialele luate in considerare au fost PAL simplu si PAL melaminat.

Nota: pentru diferentierea spațiilor de birouri între ele din punct de vedere al amplasării, echipării, accesibilității se utilizează încadrarea acestora în trei clase: A, B si C potrivit ANSI/BOMA Z65.1-2017 Standardul de Clasificare și Evaluare a birourilor propus de **B**uilding **O**wners and **M**anagers **A**ssociation (BOMA).

4.2. Calculul densității sarcinii termice pentru un birou clasa B (5 mp/1 pers) S = 1232,50 mp – 216 lucrători.

Tabel 2

Calculul densității sarcinii termice utilizând SR EN 10903-2-2016 pentru un birou clasa B

Materiale combustibile	Arie [m²] sau bucăți	Masă [kg]	q [MJ/Kg]	Q
dulap lemn pentru documente-rollbox	8	18	19.25	2,772.00
birou din lemn și metal pentru documente	216	25	19.25	103,950.00
scaun metalic cu poliuretan	264	1	37.70	9,952.80
calculatoare	216	5	33.00	35,640.00
hârtie	216	10	16.30	35,208.00
fotoliu	16	30	27.00	12,960.00

Calculul densităţii sarcinii termice pentru birouri clasa A şi B

masă din lemn şi metal	12	10	16.30	1,956.00
dulap lemn pentru haine 1,0 · 0,5 · 2,0 [m]	13	50	16.30	10,595.00
dulap mic vestiar 0,3 · 0,4 · 1,0 [m]	179	10	16.30	29,177.00
parchet laminat	1232.5	1.5	21.80	40,302.75
uşă interioară lemn	1	10	21.80	218.00
textile	184	5	20.95	19,274.00
∑Q=				302,005.55
qs =	302005.6	/	1232.5	245.03

→ densitatea sarcinii termice are valoarea sub 420 MJ/m^2 → risc mic de incendiu. Se pastrează menţiunea de la calculul anterior.

Tabelul 3

Tabel comparativ rezultatele obţinute în cazul utilizării SR EN 10903-2/2016

Tipul spaţiului şi elementele considerate	Densitatea sarcinii termice [MJ/mp]
Birou clasa A cu 120 persoane fără pardoseală flotantă şi fără pereţi combustibili	164,36
Birou clasa B cu 216 persoane fără pardoseală flotantă şi fără pereţi combustibili	245,03

Se constată că dublarea numărului de utilizatori, respectiv de mobilier nu schimbă încadrarea în risc mic de incendiu a nivelului de clădire recompartimentat.

Posibilitatea utilizării pereţilor amovibili şi a pereţilor modulari din materiale combustibile adaugă un spor de putere calorifică la totalul din acel spaţiu. În acest sens s-a facut calculul pentru acelaşi nivel de birouri cu spaţii peisagere, 2 săli de curs IT a 16 persoane, sală de sedinţe cu 10 persoane, sală de mese, sală de recreere, vestiar, zonă de circulaţie.

5.   Calculul densităţii sarcinii termice utilizând SR EN 1991-1-2-2016

Exemplul de calcul conform SR EN 1991-1-2-2007, anexa E s-a determinat într-o manieră specifică pentru un proiect individual cu un nivel de birouri cu spaţii peisagere, 2 săli de curs IT a 16 persoane, sală de sedinţe cu 10 persoane, sală de mese, sală de recreere, vestiar, zonă de circulaţie. Astfel, calculul densităţii sarcinii termice pentru un birou clasa A (10 mp/1 pers) S = 1.232,50 mp – 120 lucrători şi Ai = Ac cu pardoseala x 2 + Arie laterala fatade + Arie laterala Nod 1 + Arie laterala Nod 2 + Arie laterala nod lifturi = 1.232,5 x 2 + 634,0 +65,9 + 65,9 + 85,6 = 3.306,40 m^2.

5.1.   Calculul densităţii sarcinii termice pentru un birou clasa A (10 mp/1 pers) S = 1.232,50 m^2 – 120 lucrători.

Tabel 4

Calculul densității sarcinii termice utilizând SR EN 1991-1-2-2016 pentru un birou clasa A

Materiale combustibile	Arie [m²] sau bucăți	Mk‚j [kg]	Hui [MJ/Kg]	Q fi,k [MJ]	Ψi [%]	Q fi,k‚j [MJ]
dulap lemn pentru documente-rollbox	8	18	19.25	2,772.00	10	3,049.20
birou din lemn şi metal pentru documente	120	25	19.25	57,750.00	10	63,525.00
scaun metalic cu poliuretan	120	1	37.70	4,524.00	10	4,976.40
calculatoare	120	5	33.00	19,800.00	10	21,780.00
hârtie	120	10	16.30	19,560.00	10	21,516.00
fotoliu	16	30	27.00	12,960.00	10	14,256.00
masă din lemn şi metal	12	10	16.30	1,956.00	10	2,151.60
dulap lemn pentru haine 1,0 · 0,5 · 2,0 [m]	13	50	16.30	10,595.00	10	11,654.50
dulap mic vestiar 0,3 · 0,4 · 1,0 [m]	120	10	16.30	19,560.00	10	21,516.00
parchet laminat	1232.5	1.5	21.80	40,302.75	10	44,333.03
uşă interioară lemn	1	10	21.80	218.00	0	218.00
textile	120	5	20.95	12,570.00	10	13,827.00
∑Q fi,k‚j = sarcina termică caracteristică						222,802.73
Ai = aria suprafetei interioare a spatiului analizat						3,306.39
q f,k = ∑Q fi,k‚j / Ai = Densitatea sarcinii termice caracteristice	222,802.73	/	3,306.39			67.39

→ densitatea sarcinii termice are valoarea sub 420 MJ/m².

5.2. Calculul densității sarcinii termice pentru un birou clasa B (5 mp/1 pers) S = 1232,50 mp – 216 lucrători:

Tabel 5

Calculul densității sarcinii termice utilizând SR EN 1991-1-2-2016 pentru un birou clasa B

Materiale combustibile	Arie [m²] sau bucăți	Mk‚j [kg]	Hui [MJ/Kg]	Q fi,k [MJ]	Ψi [%]	Q fi,k‚j [MJ]
dulap lemn pentru documente-rollbox	8	18	19.25	2,772.00	10	3,049.20
birou din lemn şi metal pentru documente	216	25	19.25	103,950.00	10	114,345.00
scaun metalic cu poliuretan	264	1	37.70	9,952.80	10	10,948.08
calculatoare	216	5	33.00	35,640.00	10	39,204.00
hârtie	216	10	16.30	35,208.00	10	38,728.80
fotoliu	16	30	27.00	12,960.00	10	14,256.00
masă din lemn şi metal	12	10	16.30	1,956.00	10	2,151.60
dulap lemn pentru haine 1,0 · 0,5 · 2,0 [m]	13	50	16.30	10,595.00	10	11,654.50

Calculul densității sarcinii termice pentru birouri clasa A și B

dulap mic vestiar 0,3 · 0,4 · 1,0 [m]	179	10	16.30	29,177.00	10	32,094.70
parchet laminat	1232.5	1.5	21.80	40,302.75	10	44,333.03
ușă interioară lemn	1	10	21.80	218.00	0	218.00
textile	184	5	20.95	19,274.00	10	21,201.40
∑Q fi,k,j = sarcina termică caracteristică						332,184.31
Ai = aria suprafeței interioare a spațiului analizat						3,306.39
q f,k = ∑Q fi,k,j / Ai = Densitatea sarcinii termice caracteristice	332,184.31	/	3,306.39			100.47

→ densitatea sarcinii termice are valoarea sub 420 MJ/m^2.

Tabel 6

Tabel comparativ rezultatele obținute în cazul utilizării SR EN 1991-1-2-2016

Tipul spațiului și elementele considerate	Densitatea sarcinii termice [MJ/mp]
Birou clasa A cu 120 persoane fără pardoseală flotantă și fără pereți combustibili	67,39
Birou clasa B cu 216 persoane fără pardoseală flotantă și fără pereți combustibili	100,47

Notă:
- îmbunătățirea performanței la acțiunea focului a diverselor materiale de constructii nu modifica densitatea sarcinii termice.

6. Concluzii

Conceptul de proiectare al unei clădiri are în vedere, printre numeroasele cerințe, și un număr de utilizatori pe o suprafață dată. Darea în exploatare a acestei construcții executate, poate să aducă modificări solicitate de beneficiar / administrator / chiriaș din punctul de vedere al numărului de persoane, în sensul creșterii gradului de ocupare și utilizare.

Mărirea numărului de utilizatori are implicații directe asupra multor parametri și instalații, cum ar fi instalațiile de ventilare și climatizare, instalațiile electrice, compartimentările sau tipul de mobilier.

Din perspectiva securității la incendiu, creșterea numărului de persoane dintr-un spațiu cu destinația de birou tip open-space/peisager se traduce în primul rând prin creșterea numărului de piese de mobiler. Această modificare presupune posibile îngustări ale circulațiilor deschise, posibile creșteri ale lungimilor de evacuare și, desigur, creșterea densității sarcinii termice.

Prin calculele efectuate se observă că, la o dublare a utilizatorilor, rezultă o creștere de 60 % a densității sarcinii termice indiferent de metoda de calcul utilizată.

Ovidiu MIHALACHE, Ion ANGHEL, Iulian ENE

Tabel 7

Tabel comparativ cu toate variantele obținute

Tipul spațiului și elementele considerate	Densitatea sarcinii termice pe baza SR EN 10.903-2 [MJ/mp]	Densitatea sarcinii termice pe baza SR EN 1991-1-2 [MJ/mp]
Birou clasa A cu 120 persoane fără pardoseală flotantă și fără pereți combustibili	164,36	67,39
Birou clasa B cu 216 persoane fără pardoseală flotantă și fără pereți combustibili	245,03	100,47

În același timp, dupa cum reiese din tabelul nr. 7, nu se observă o modificare a încadrării în riscul de incendiu, potrivit normativului Romanesc P118-1999, respectiv risc mic de incendiu.

Trebuie menționat faptul că diferențele rezultate din cele două metode de calcul a densității sarcinii termice pot avea semnificații importante asupra măsurilor pasive de securitate la incendiu.

Articolul a analizat variația densității sarcinii termice în funcție de clasificarea tipului de spații de birouri, clasa A si B, conform BOMA, lăsând deschisă posibilitatea continuării studiului și asupra implicațiilor îmbunătățirii performanțelor la foc ale diferitelor materiale de construcții cu grafen, în sensul dezvoltării unui incendiu într-un spațiu dat cu materiale convenționale identificate în calculul densității de sarcină termică pentru destinația birou versus materiale modificate cu grafen.

Referințe

[1] STAS 10903/2-76, Masuri de protectie impotriva incendiilor. Determinarea sarcinii termice in constructii, 1976.
[2] STAS 10903/2-79, Masuri de protectie impotriva incendiilor. Determinarea sarcinii termice in constructii, 1979.
[3] STAS 8790-71, Măsuri de siguranță contra incendiilor. Determinarea puterii calorifice, 1981.
[4] SR 10903-2, Masuri de protectie contra incendiilor. Determinarea sarcinii termice in constructii, 2016.
[5] SR EN ISO 1716:2010, Încercări de reacție la foc ale produselor pentru construcții. Determinarea căldurii de ardere, 2010.
[6] SR EN 1991-1-2:2004: Eurocod 1: Actiuni asupra structurilor. Partea 1-2: Actiuni generale – Actiuni asupra structurilor expuse la foc, 2004.
[7] P 118 – 1999 Normativ de siguranta la foc a construcțiilor.
[8] MP 008 - 2000 Manual privind exemplificari, detalieri si solutii de aplicare a prevederilor normativului P 118-99.

The effect of granulate porosity on the evolution of the thermal conductivity of an resin concrete exposed to high temperatures

Benoudjafer imane[1], Benoudjafer ibtissam[2], Tomoaia-Cotisel Maria[3,4]

[1]Laboratory of Mechanical and Structures,University Tahri Mohammed of Bechar , Algeria.
E-mail: imenousse@yahoo.fr

[2]Laboratory ENERGARID, Department of Architecture, University Tahri Mohammed of Bechar , Algeria.

[3]Laboratory of Mechanical and Structures,University Tahri Mohammed of Bechar , Algeria.

[4] Babes-Bolyai University of Cluj-Napoca, Romania.

Abstract. *As the aggregates occupy about three-quarters of the volume of concrete, it's not surprising that their properties can, not only, to limit its resistance, but also to affect the durability and structural performance of concrete. In this context, the study's main objective to study the influence of the aggregate porosity on the evolution of the thermal conductivity of a resin concrete exposed to high temperatures. the experimental results show that the porosity of the aggregates has a significant influence on the evolution of the thermal conductivity of the concretes tested.*

Key words: *aggregates, porosity, durability, thermal conductivity, concrete, temperature*

1. Introduction

The presence of internal pores in the aggregates is directly related to the density of the aggregates and indeed the characteristics of these pores are very important in the study of aggregate properties [6]. The porosity of aggregates and their absorption influence some of their properties: their bond with the hydrated cement paste, their chemical stability and resistance to abrasion [8]. The size of the aggregate pores is very variable: the larger ones can be seen under a microscope or even with the naked eye; the smallest are barely larger than the pores of the cement paste. Some pores are completely inside the aggregates; others emerge on the surface [1].

The cement paste, due to its viscosity, cannot penetrate to a great depth as it does in the largest pores; it is then the overall volume of the grains which is considered as solid for the determination of the quantities or proportions of aggregates in the concrete [4]. Whatever it is, water can penetrate the pores; the amount and the rate of penetration depending on their size, their communication with each other and their total volume [5]. When all the aggregate pores are full of water, that is when the latter

are saturated and superficially dry, if left in dry air, some of the water in the pores will evaporate and the aggregates will no longer be superficially dry [4]. Prolonged drying in an oven will reduce the humidity in the aggregates until no more water evaporates, the aggregates will be called dry [3].

In the porous space of aggregates we can distinguish two groups of voids: open pores and closed pores. The open pores form a continuous or blind porous system in the material [14]. The closed pores are isolated and are not interconnected. Only the open pore system can contribute to the transport of the material in the material [2]. the pores are interconnected, the higher the water absorption [6] [7]. The open porosity of the aggregates is an important characteristic which directly influences their hygrometric property and consequently the workability of the concrete and the water behavior of the cement paste with which they are in contact [2]. Porosity is, by definition, the ratio of the volume of voids to the total volume [1] [8].

The elevation of temperature causes strong cangements at the microstructure of concrete changes that will drive a shift in mechanical properties especially [17]. Indeed, heating leads to a mechanical deterioration of the concrete through the formation of microcracks[10]. These increase the conductivity of the material and therefore make the transport phenomena even more important [6]. A knowledge of the thermal properties is necessary for descption the behavior of concrete at high temperatures [14].

The study of thermal conductivity is of great technological interest, especially for applications that require the use of materials based or with high thermal conductivity[1,6]. This physical magnitude characterizing the materials during the heat transfer caused by a temperature difference between two region of a same medium or between two media in cntact (conduction) [18]. it is not, strictly, a property of the material since it sometimes depends on a large number of parameters including the method of manufacture [15] [20] [21], the history and the nature of the material, the temperature, the pressure, the humidity , the presence of cracks and even the surface state [6]. From a numerical point of view, it is the amount of heat-energy transferred per unit of isothermal area in a unit of time under a unit temperature gradient [2]. The thermal conductivity of various materials is generally determined experimentally by measuring methods based mostly on measuring surface flux and temperature gradient [6] [14] . In this text, the main objective of this work is to study the influence of the porosity of aggregates on the evolution of the thermal conductivity of a resinous concrete exposed to high temperatures.

2. Procédure éxpérimentale
2.1. Matériaux
Five types of aggregates tested are of three different types: limestone, silico-limestone and silica. The characteristics of the aggregates are presented in table 1. For

each density and intergranular porosity, the values retained are the average of three tests. They are named by their nature and their form: the first letter refers to the mineralogical nature of the aggregate used (C for limestone, SC for silico-limestone and S silicon), and the following letter distinguishes the shape of the aggregates: Rolled (R) or Crushed (C). Fine aggregates have a maximum diameter between 3 to 5 mm and large aggregates have a maximum diameter between 8 and 15 mm.

Tabel 1

Caracteristics of aggragates

Aggregates		Densities (Kg/m3)					intergranular porosity (%)
		ρ_{vra}	ρ_{rs}	ρ_{re}	ρ_{app}	ρ_{abs}	Pint
Sands	SC1-R	1621	2453	2443	2516	2615	34
	SC2-R	1662	2614	2654	2582	2503	37
	SSC-C	1500	2565	2667	2650	2734	44
Gravels	GC-C1	1350	2213	2631	2721	2700	49
	GC-C2	1420	2295	2675	2723	2700	47

A global analysis shows that, whatever the type of density, the classification according to their values remains identical. The actual densities of the aggregates vary between 2213 and 2614 kg / m³, which corresponds to common aggregates of limestone and silico-limestone origin as indicated by their geological formation. Their apparent densities are between 1350 and 1662 kg / m³. We also note that the limestone sands (SC2-R and SC1-R) are characterized by the lowest absolute densities and the sand-lime sand (SSC-C) which is characterized by the highest value. However, the aggregates (GC-C1 and GC-C2) have an identical density characteristic intrinsic to the material for which the voids volumes are not taken into account.

The values of the intergranular porosity are relatively close for the two classes of gravel GC-C1 and GC-C2 of limestone nature, slightly higher than that of sand-lime sand (SSC-C). the latter which has fine elements and a greater granular extent, has the highest intergranular porosity than limestone sands (SC1-R and SC1-R) carrying similar values. The open porosity of the aggregates is an important characteristic which directly influences their hygrometric property and consequently the workability of the concrete and the water behavior of the cement paste with which they are in contact [2]. Porosity is, by definition, the ratio of the volume of voids to the total volume. The results of the porosity calculations are presented in the form of a histogram in Figure 1.

Analysis of the total porosities shows that the highest values are obtained for limestone aggregates. We find in descending order the limestone sands (6.57% for SC1-R and 6.03% for SC2-R) then the limestone gravel (5.31% for GC-C2 and 5.24% for GC-C1), and the sand-lime sand (2.45% for SSC-C). The highest open porosity is also observed for GC-C1 gravel (3.3%). Those of limestone sands are close (between

2.90% and 2.78%). The minimum value is measured for sand-lime sand SSC-C (0.64%) unlike water absorption. The minimum value corresponds to that of sand-lime sand, as for the total porosity. The aggregate porosities are comparable. It can also be noted that the porosity accessible to water represents 44 to 46% of the total porosity for limestone sands, 33% for gravel GC-C2, and 26% for sand-lime sand. However, this ratio reaches a value greater than 60% for the gravel GC-C2. Finally, there is a certain variability in the closed porosity values and a classification which does not follow those of the open or total porosities. Limestone aggregates are characterized by the highest values of closed porosity.
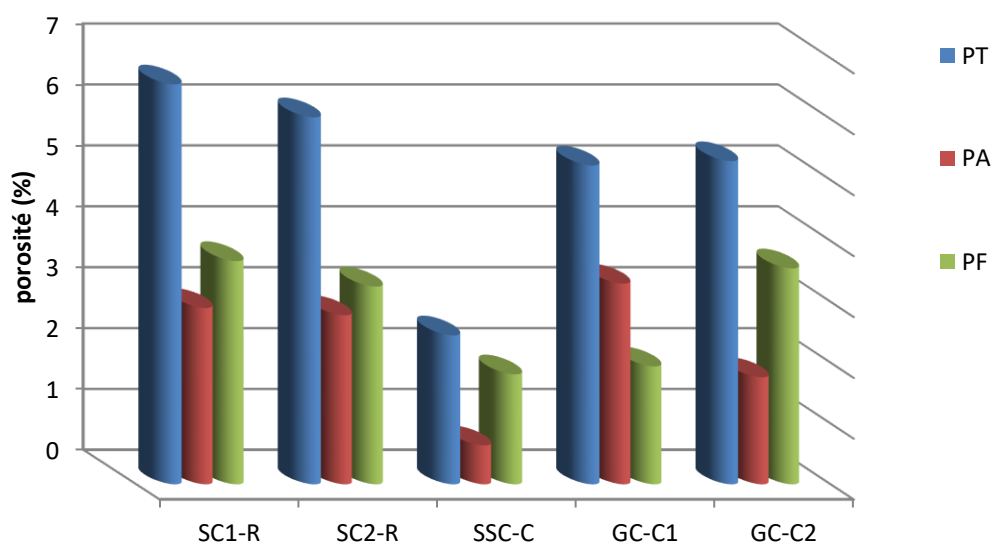

Fig. 1. Closed, total and accessible porosities with water of the various aggregates

2.1. Making of concrete

The epoxy resin used in this study is issue a mixture of Eponal 371V1 resin and hardener of the same denomination. A super-plasticizer type Cimfluid 3020, based on modified plycaboxylates, was used to ensure satisfactory plasticity of the different formulations without varying the amount of binder paste relative to that of the granular skeleton. This adjuvant, in accordance with the standard [EN 206-1], has a density of 1078 kg / m3, a dry extract of 30.81% [NF EN 480-8] and a viscosity of 59 cps at 25 °C. The recommended dosage varies from 0.2 to 2.5 kg per 100 kg of cement a mineral flame retardant was used the pure polymer concrete fireproofing.

Before proceeding with the actual manufacture proper of the resin concrete, preliminaries steps are necessary to obtain a product identical to itself and to minimize the effect of the elements related to the state and the quality of the incoming materials. in the composition of the resin concrete to be manufactured and as well also to the method of manufacture. The constituents must therefore be stored under favorable conditions according to the instructions of the manufacturer or the rules of the state of the art .Indeed, granulats should be dried at 105 °C, for more; 24 hours and the resin

must be stored in the room at temperature-controlled. The measurements were performed on samples. The prismatic moulds were filled on three layers, and each layer received 40 shots with a metal bar. This phase is moving by the levelling of the upper surface of the specimens, with a rule according to saw movement Demolding of the samples are conserved in the room controlled at temperature and humidity (25 ° C and 50% RH), until a maturity of the experimental tests. The surfaces of the samples have been rectified with a diamond disc, to get two surfaces enough that were sufficiently level so that there was as little air as possible between the probe and the samples.

2.3. Thermal conductivity measurement

As part of this experimental study, the Hot Disk method was used to experimentally measure the thermal conductivity of the varieties of concrete tested using prismatic test pieces (4x7x14 cm) after 90 days. It represents the most robust technique for direct and absolute measurement of this thermal property which therefore does not require any prior calibration or any corrective factor [2]. In order to ensure a constant water content, the test pieces were kept in an oven until their mass did not change more than 0.2%. The Hot Disk probe is placed between two samples of the same concrete tested. This probe is used both as a heat source and as a temperature sensor. The system is based on the technology of the transient plane source ("Transient Plane Source" in English), in which the variation of electrical resistance linked to a variation of temperature [ISO 22007-2].

The principle of the TPS method consists in providing constant power for a limited time to the Hot Disk probe in order to raise the temperature of the type of concrete studied by a few degrees. It is also the probe which is used to measure the rise in temperature, thanks to the recording of the variation of its electrical resistance via a very precise Wheastone bridge [6]. The characteristics of the temperature increase, directly linked to the evolution of the electrical resistance of the probe, are precisely recorded and the analysis of this variation (transient regime) [9]. It is interesting to mention, that no contact agent (water, thermal paste, ...) was required because the effects of contact resistance are systematically detected by the device and removed by the operator [13].

2.4. Thermal cycle

In this study, we applied a hot heating cycle the ambient temperature to 25°C until exposure temperatures (bearing) equal to 105 ° C, 150 ° C, 200 ° C and 250 ° by means of an oven. The specimens were placed in an oven in a way allowing the heat to be distributed homogeneously in the enclosure with a ventilation system. A K type thermocouple is placed in contact with the surface of a control sample and another is embedded in the center in order to determine changes in temperature. Measurements
 of thermal conductivity of concrete studies were performed according to the following steps:

✓ Measurement of the thermal conductivity at room temperature. The measurement was performed three times with a regular time interval of 45 min.
✓ Heating the specimen at a rate of 1 °C/min, until the next measurement temperature.
✓ Maintenance of the temperature measurement for 15 h to ensure the heat and water homogeneity of the sample.
✓ Each measurement of thermal conductivity was carried out 3 times with a time interval of 45 min.
✓ Heating the specimen to the next temperature and repeating the cycle until the last temperature measurement (250 °C).

3. Experimental results

The variations in residual compressive strength and its deviation, for the three of the concrete mixes B (CR), B (C'-R) and B (SC-C), as a function of temperature, are plotted on Figures 2 and 3 respectively.
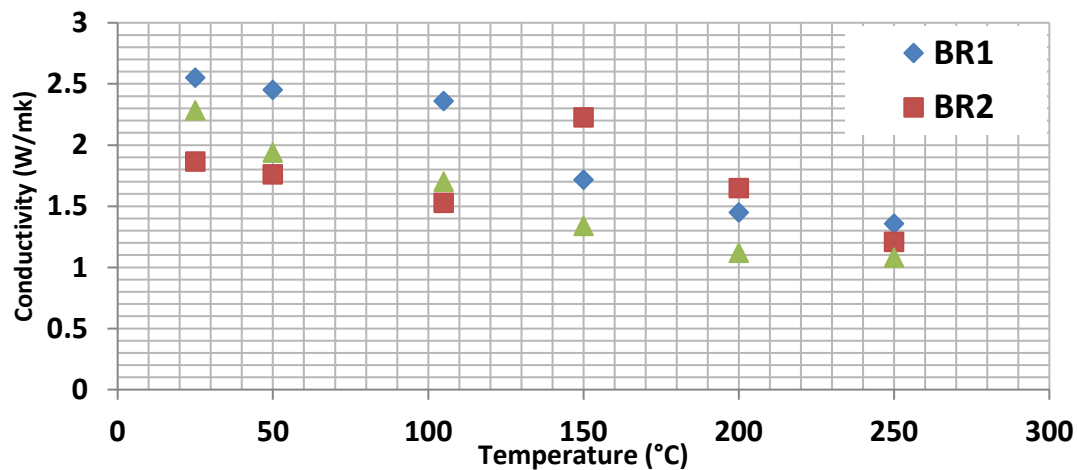

Fig. 2. Evolution of the thermal conductivity of concretes tested as a function of temperature
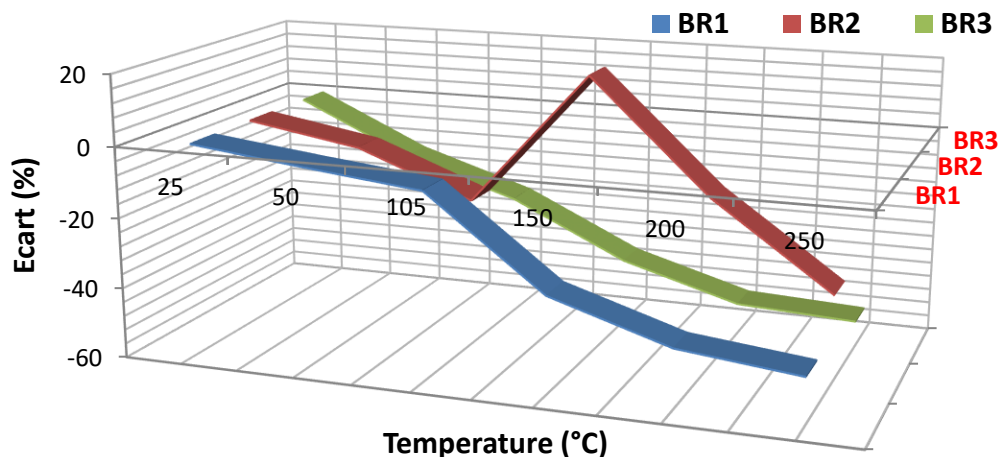

Fig. 3. Evolution of the ecart of thermal conductivity of concretes tested as a function of temperature

258

From these figures, we mainly notice that the thermal conductivity, for the three types of concrete tested, varies as a function of temperature. We can distinguish three consecutive phases in the evolution of compressive strength with temperature:

Phase (I) (ranging from 25 ° C to 105 ° C): in this first phase, the thermal conductivity of the different concretes is significantly lower than that recorded at room temperature. Between 25 ° C and 50 ° C, the composition BR1 has good thermal conductivity than that of the concretes BR3 and BR2 respectively. It reaches values higher than 2.4 W / mk when it is heated to 50 ° C.

Phase II (from 105 ° C to 200 ° C): In this temperature range, there have been various changes in thermal conductivity as a function of temperature. BR2 concrete has an equivalent increase from 105 ° C to 150 ° C and then a slight decrease from 150 ° C to 200 ° C. On the other hand, the two mixtures of concretes BR1 and BR3 show a strong decrease in thermal conductivity, reaching values less than 1.10 W / mk, when it is heated to 200 ° C.

Phase (III) (ranging from 200 ° C to 250 ° C): For temperatures between 200 ° C and 250 ° C, we observe that the positioning of the evolution values of the thermal conductivities begins to show gaps lines, that is to say the three categories of concrete, formulated based on different types of aggregate and porosity, do not keep the same classification of the evolution of thermal conductivity with respect to temperature.

The analysis of these experimental results allows us to make the following interpretations:
the decrease in the thermal conductivity of the concretes tested for temperatures between 25 ° C and 250 ° C, is mainly linked to the evaporation of free water. According to several authors [1], [9] and [10], this evaporation has been observed when the concrete is exposed to temperatures between 30 and 90 ° C. According to different studies [5], [9], and [14], the thermal conductivity of concrete depends on the thermal conductivity of each of its components according to more complex mixing laws than that used for the specific heat [5]. In particular, these mixing laws take into account the spatial distribution of the components in addition to the volume proportions of each. However, it is generally accepted that the thermal conductivity of concrete depends essentially on that of aggregates (Bazant and Kaplan 1996 [9]).

According to various studies [1], [2], [8], [9] [10] and [12], the presence of water in the form of steam at high temperature can also modify the physical and chemical structure of the cement paste. According to Basheer and al., the combination of hygrothermal conditions, can cause changes in the nature of hydrates [7]. These changes depend mainly on the C / S ratio (CaO / SiO2), the temperature and the pressure prevailing in the material [2]. The value of this ratio influences the formation of various forms of hydrates resulting in the creation of various forms of hydrates with different mechanical properties [9]. It is necessary to mention that the properties of the

material will also depend on the interaction between the paste and the aggregates and on the behavior of the transition halo [5].

In addition, the remarkable variation in the difference noted in the evolution of the thermal conductivity from one concrete to another, during the temperature variation, can be explained by the effect of the mineralogical nature of the constituent aggregates of these concretes on the evolution of thermal conductivity with temperature. According to several authors [1], [4] and [13], the behavior of aggregates at high temperatures is completely different. Similarly differents authors have shown that limestone aggregates exhibit good thermal behavior at high temperatures [1] [4] [9] [12] [13] [16] [18] and [19], and Benoudjafer also confirmed that the type of aggregate influences the behavior of concrete at high temperatures [16]. The loss of thermal conductivity is considerably less when the aggregate does not contain silica (some forms of silica undergo a dimensional change); this is the case with limestones [9].

4. Conclusion

The evolution of thermal conductivity varies with temperature. The causes of this variation are the same as that of the variation in mechanical resistance to compression (leaving water and increasing porosity REF. Leaving water by drying makes it possible to cause a non-negligible reduction in the conductivity of the material, because it is characterized by a high thermal conductivity, on the other hand, the creation of voids is due to the increase in porosity and the appearance of cracks.

The objective of this study was to study the influence of the porosity of aggregates on the thermal conductivity of the varieties of concrete tested. The materials which are the subject of this study are concretes of composition set up especially for the needs of the study. The characteristics studied were established in the reference state and compared with those determined at the various thermal gradients.

The synthesis of the observations and the experiments carried out noted that the evolution of thermal conductivity is strongly linked to the departure of free water, and to the evolution of the microstructure of concretes. This results in the variation of the porosity during the experimental procedure. Among the parameters significantly influencing the behavior of concrete material at high temperature is the presence of water in the material.

Références bibliographiques

[1] ACKER, P., J. TORRENTI, ET F. ULM , „Concrete behavior at a young age", Mechanics and materials engineering , Hermès, 2004.

[2] ACKER, P., TORRENTI, J., ULM, F , „Mechanical behavior of concrete", LAVOISIER, ISBN 2-7462-0980-2, 2005.

[3] AKÇAOGLU, T., M. TOKYAY, ET T. ÇELIK , „Effect of coarse aggregate size and matrix quality on ITZ and failure behavior of concrete under uniaxial compression", Cementand Concrete Composites,2004, 26(6), 633-638.

[4] ALARCON-RUIZ, L., GALLE, C., MASSIEU, E, „Analysis of the evolution of the porosity of cement pastes at high temperature ", Materials 2002, towers.

[5] BARON, J., ET R. SAUTEREY , „ Hydraulic concrete ", Press of the National School of Bridges and Roads", Paris, 1982.

[6] BARON, J., OLLIVIER, J.P, „ Concretes, databases and data for their manufacture ", Paris: Edition Eyrolles, 1996.-522 p.

[7] BASHEER, L., P. BASHEER, ET A. LONG , „Influence of coarse aggregate on the permeation, durability and the microstructure characteristics of ordinary Portland cement concrete", Construction and Building Materials, 2005, 19, no. 9(9), 682-690.

[8] BAZANT Z.P,THONGUTHAI W, „ Pore pressure in heated concrete walls ",Magazine of Concrete Research, 1979, Vol 107, n° 31, p 67-79.

[9] BAZANT Z.P. and KAPLAN M, „Concrete at high temperature : Material behaviour and Mathematical Modelling ", London: Longman Concrete Design and Construction Series, 1996. 412p.

[10] Benoudjafer I.m., LABBACI B. and Benoudjafer I.b., „An Experimental Investigation on the Thermal Effect on the Mechanical Behavior of Concrete", International Review of Civil Engineering (I.R.E.C.E.), Vol. 8, N. 2, ISSN 2036 – 9913, 2017.

[11] Benoudjafer I.m., LABBACI B. and Benoudjafer I.b., „Study of the improvement of the energy performance of residential buildings in dry and hot climates ", Knowledge Courier., N°26, 2018.

[12] Benoudjafer I.m., LABBACI B. and Benoudjafer I.b., „Experimental characterization of a concrete subjected to high temperatures by vibration analysis", Energineering and Technologie, vol 39 pp 19-24, ISSN 2556-5608, 2018.

[13] Benoudjafer I.m., LABBACI B. and Benoudjafer I.b., „Mechanical Characterization of Resin Concrete Subjected to High Temperatures by Vibration Analysis", Materials Science Forum , Advanced Materials and Processing Technologies volume 962, p-p236-241,2019.

[14] Benoudjafer I.m., Benoudjafer I.b and LABBACI B.,, „The effect of nature the granulate on the evolution of the thermal conductivity of an resin concrete exposed to high temperatures" , Revista Română de Inginerie Civilă , Volume 10 N 2 p-p 171-179, 2019.

[15] Benoudjafer I.b. and Benoudjafer I.,, „improvement of the energy performance of a residual building (case of the city of Béchar)" , International Journal of Scientific Research & Engineering Technologie (IJSET), Vol.11 pp.25-31, ISSN 1737-9296, 2019.

[16] Benoudjafer I.m and Benoudjafer I.b.,, „Comparison between the elasticity modules of a self-compacting concrete exposed to high temperatures by two resonance frequency methods" , International Journal of Scientific Research & Engineering Technologie (IJSET), Vol.11 pp.20-24, ISSN 1737-9296, 2019.

[17] Benoudjafer I.m., LABBACI B. and Benoudjafer I.b., „ influence of the nature of aggregates on the behavior of concrete in its climatic environment ", 2nd International Conference on Composite Materials and Structures, University of Science and Technology Mohamed Boudiaf. 28-30 November 2011, Algeria.

[18] Benoudjafer I.m., and LABBACI B., „ Experimental study of the mechanical properties of concrete subjected under hot temperature'', 1st international seminar on risks and civil engineering. University of Batna, 26 and 27 Nov. 2012, Algeria.

[19] Benoudjafer I.m., and LABBACI B., „ Experimental study on mass transfer of self-compacting concrete subjected to high temperatures '', 2nd International Seminar of Civil Engineering GCB 2015 U, Béchar, 2015, Algeria

[20] Benoudjafer I.m., and LABBACI B., „ Effect of local temperature during service on the mechanical properties of concrete » », the 3rd International Conference on Fluid Flow, Heat and Mass Transfer (FFHMT'16), Ottawa, May 2 –3, 2016 ,Canada.

[21] Benoudjafer I.m., LABBACI B. and Benoudjafer I.b., „Non-destructive identification of the elasticity module of concrete by experimental modal analysis "International Seminar of Civil Engineering (SIGC 2018), ENPO-MA, November 27-28, 2018, Oran, 2018, Algeria.

Studiu comparativ privind coroziunea în timp a electrozilor în sol, Partea 2 – Analize microbiologice

Comparative study regarding corrosion in time of the ground electrodes, Part 2 – Microbiological analyses

Ştefan PAVEL[1], Ioan Bogdan PASCU[2], Nicoleta NEMEŞ[2], Romeo NEGREA[3], Emilia DOBRIN[4], BURIAC Oana[2]

[1]Universitatea Politehnica Timişoara-ICER,
Timişoara, str. G.Musicescu, nr. 138, Romania
e-mail:pavelstefanel@gmail.com
[2]Universitatea Politehnica Timişoara-ICER*;*
e-mail: i.bogdan.pascu93@gmail.com; nicoleta.nemes@upt.ro; oana.grad@upt.ro
[3]Universitatea Politehnica Timişoara-Departamentul de Matematică
Timişoara, P-ţa Victoriei, nr. 2, Romania
e-mail: romeo.negrea@upt.ro
[4]Institutul Naţional de Cercetare-Dezvoltare în Sudură şi Încercări de Materiale Timişoara
Timişoara, B-dul Mihai Viteazul, nr. 30, Romania
e-mail: emi_dobrin@yahoo.com

Rezumat:Obiectivul lucrării este de a prezenta, aspecte referitoare la: coroziunea metalelor acoperite şi neacoperite cu zinc în solul oraşului Timişoara (electrozi de împământare a Instalaţiei de Legare la Pamânt aferentă Instalaţiilor Electrice din Construcţii), analiza parametrilor de sol, prototipuri de electrozi, măsurători electrice, microbiologice şi analiza de prognoză-predicţie matematică, materiale şi dicţionare de termeni aferenţi. Un alt aspect prezentat în acest material este efectuarea de măsurători ale spectrului câmpului elecromagnetic oscilografiat al elementelor de metal acoperite şi neacoperite cu zinc din sol.

Cuvinte cheie: coroziune, electrod de împământare, sol, legare la pământ, microbiologia solului

Abstract: The objective of this paper is to present aspects related to: corrosion of metals covered, and not covered with zinc in the soil of Timişoara (grounding electrodes of a grounding installation related to Electrical Installations of Constructions), analysis of soil parameters, prototype electrodes, electrical, microbiological analysis and mathematical prognosis analysis-prediction, materials, and dictionaries of related terms. Another aspect presented in this material are the measurements related to the spectrum of the oscillograph electromagnetic field of the grounding electrodes, which are covered, and not covered with zinc.

Key words: corrosion, ground electrode, soil, grounding, soil microbiology

Ştefan PAVEL, Ioan Bogdan PASCU, Nicoleta NEMEŞ, Romeo NEGREA, Emilia DOBRIN, Oana BURIAC

1. Microbial analysis of the soil

Due to the fact that the soil quality legislation, respectively the national soil quality monitoring strategies are based only on determinations of the physical and chemical parameters, therefore they do not include elements of soil microbiology, there is little research on microbial activity in the soils of our country. This is also due to the fact that a microbiological research is very laborious, difficult to quantify and especially very expensive. Numerical determinations of different categories of microorganisms performed by many researchers have highlighted their dependence on the soil horizon, the depth from which they were harvested, the peculiarities of humidity, pH, content of organic substances and the degree of oxygenation. No technique for the estimation of the number of bacteria in the soil can reflect their exact and real situation, as the specific nutritional requirements of each type of bacteria are extremely diverse and complex, no culture medium can simultaneously meet this great complexity. In order to characterize the soil in which the monitoring poles were implanted, samples were collected at a depth of 1.5 m and 2.3 m. The soil samples were characterized by physical, chemical and microbial activity. To characterize microbiologically, the soil samples were crushed and sieved, then the soil sample was extracted. 3 successive dilutions (10-3-10-8) of the soil samples were made, the dilutions being made with distilled water. The total number of germs was determined by the plate culture method, using a solid nutrient medium with meat and yeast extract. Successive dilutions of the soil samples were seeded (1 ml of inoculum) on the solid culture medium, by incorporation, after previously adjusting the pH of the medium to 7.2. After incubation for 48 hours at 36°C, the obtained values from the count were multiplied by the dilution factor, giving the number of colonies forming per 1 g of soil. Bacterial colony counting was done with the Yul Flash & Go automatic colony counter. The results are shown in the following table. Bacteria (col/ml) determined by automatic counting with the Yul Flash & Go colony counter.

Table 1

Microbiological analysis results

Dilution	No. of colonies at 1.5 m depth	Bacteria (col/ml) at 1.5 m depth	No. of colonies at 2.3 m depth	Bacteria (col/ml) at 2.3 m depth
10^{-3}	83	$1,09*10^5$	43	$5,65*10^4$
10^{-6}	29	$3,81*10^9$	13	$1,7*10^7$
10^{-8}	27	$3,55*10^7$	3	$3,94*10^8$

Relative to the total soil mass, Alexander (1971) proposes as a calculation basis, a volume of 1 μm^3/cell and a wet weight of 1.5 x 10^{-12} g / cell. At a density of 10^8 cells/g dry soil, bacteria occupy 0.01% of the total volume of the soil, and at a density of 10^9 bacteria, 0.1%. In terms of weight, at the density of 10^8 cells, the bacteria represent 0.015%, and in the case of 10^9 cells, 0.15% of the total soil mass.
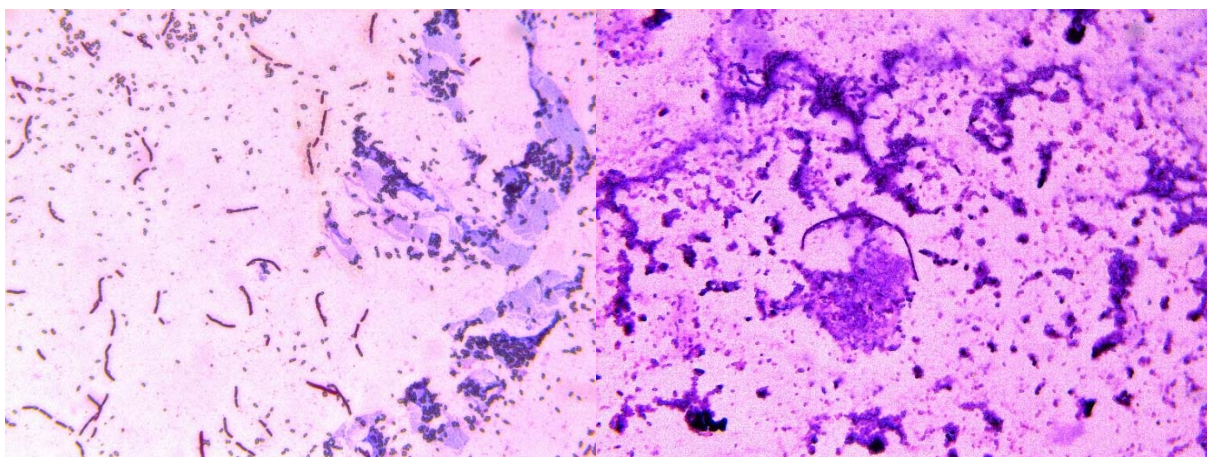
Fig. 1. Gram stain smear made from the bacterial culture at the depth of 1.5m

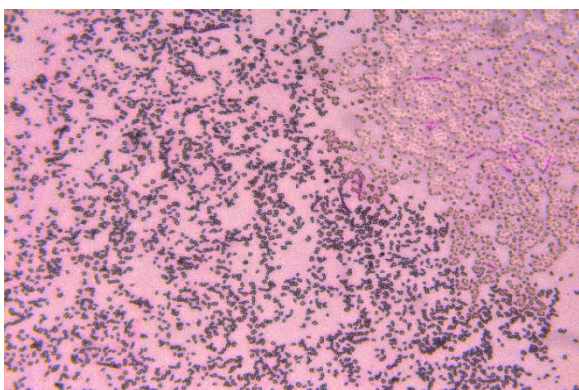Fig. 2. Gram stain smear made from the bacterial culture at the depth of 2.3m

Fig. 3. Gram stain smear made from the bacterial culture at the depth of 1.5m
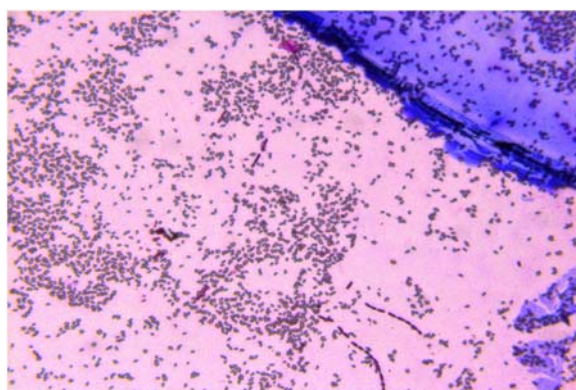

Fig. 4. Gram stain smear made from the bacterial culture at the depth of 2.3m
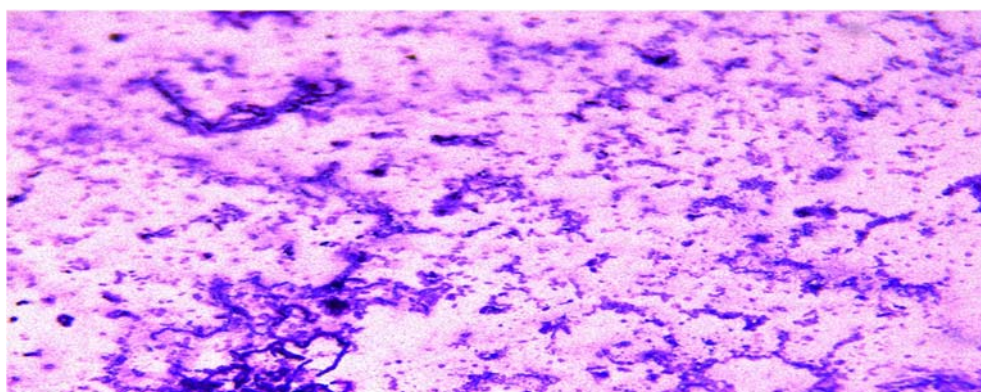

Fig. 5. Gram stain smear made from the bacterial culture at the depth of 1.5m

From the analysis of the smears made after the gram staining, as shown in Fig. 1 and Fig. 2 gram-negative bacteria are predominant. The predominant microbiota at 1.5 m depth consists of filaments of gram-negative bacilli, and a few gram-negative short bacilli, and gram-positive cocci, irregularly arranged. At a depth of 2.3 m, gram-negative are predominant, agglomerated, and irregularly arranged. There are present long filaments of gram-positive bacilli, and cocci chains of gram-positive bacteria.

In the literature [1], the authors mention: *"According to the literature, zinc is easily affected mainly by bacilliform bacterium and can be coated with biofilm. In addition, the binding of bacteria (biofilm) to zinc has led to a more frequent rate of corrosion. Research has shown that Bacillus mycoides accelerates the corrosion of a galvanized metal.* **Coccus bacteria also have an corrosive effect onto metals.** *As example; cocci bacteria were found on a corroded rail. According to the summary resulted from the literature it is clear that some biofilms (especially bacillus type) have a corrosion effect onto zinc. In this study, the corrosion of the zinc anode electrode occured. These informations are accepted by the literature. In this study, during this process, a biofilm developed, and the corrosion of zinc occured. The corrosion rate (CR) is calculated according to the formula* $CR = \frac{W}{At}\%$ *where CR is the corrosion rate, w is the weight at the beggining of the experiment, reported to the final weight. A is the metal surface and the exposure time.*

[3] Fig. 6. Bacillus mycoides accelerates the corrosion rate on a galvanized metal
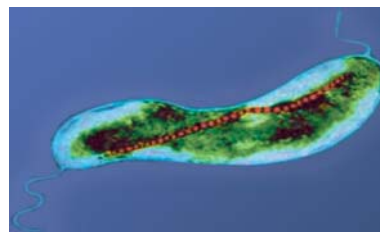
[4] Fig. 7. Magnetotactic bacterium

In the literature [2] it is confirmed that the bacterium *Thiobacillus* (gram negative bacterium) uses sulfur as energy and is abundant present in clay soil, the bacterium oxidises sulfur and produces sulfuric acid, and sulfate, FeS_2 – iron disulfide, $Fe2(SO4)3$ – iron (III) sulfate, and $CaCO_3$ – calcium carbonate – compounds that are in the soil.
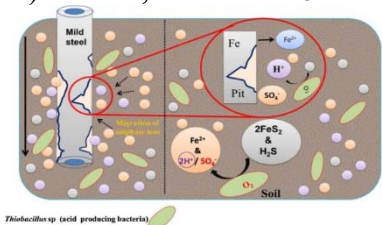

Fig. 8. [2]Corrosion of the galvanized steel in a clay soil, and the acid produced by *Thiobacillus*

[5] Fig. 9. Thiobacillus ferrooxidans are responsible for the oxidation of iron and inorganic sulfur compounds

References

[1]
https://www.researchgate.net/publication/321836416_Examination_of_Zinc_Electrode_Performance_in_Micro bial_Fuel_Cells

[2] https://www.sciencedirect.com/science/article/pii/S1878535218302272
[3] https://www.pinterest.cl/pin/179932947595684910/
[4] https://www.pinterest.cl/pin/251638697900538581/
[5] https://www.sciencephoto.com/media/798832/view

Effect of metakaolin as partially cement replacement on the compressive strength of standard mortars

Amrane Belaid[1], Souici Khaled[1], Hami Brahim[1], Kennouche Salim[1], Safi Brahim[2], Nadir Mesrati[3]

[1]Department of Civil Engineering, Faculty of Science, Bouira University, 10000, Algeria
am_belaid@yahoo.fr   khaledsouici@gmail.com,   brahim22011980@hotmail.fr,
kennouchesalim@gmail.com),
[2]Processes Engineering department, Faculty of Technology, M'hamed Bougara University, Boumerdes, 35000, Algeria
safi_b73@univ-boumerdes.dz
[3]Laboratary of materials science and engineering, National Polytechnic School, Algeriers, Algeria
n_mesrati@yahoo.fr

Abstract
This study presents the effect of incorporating synthesized metakaolin on the compressive strength of standard mortars for a constant water/binder ratio of 0.5. Synthesized metakaolin mixtures with cement replacement of 5, 10, 15 and 20% were tested.
From the results, it was observed that 15 % replacement level was the optimum level in terms of compressive strength. Beyond 15 % replacement levels, the strength was decreased but remained higher than the control mixture. Compressive strength of 52 MPa was achieved at 15 % replacement. This investigation has shown that it is possible to produce high strength mortars using local kaolin.

Key-words: metakaolin, mortar

1. Introduction

Metakaolin is a highly reactive pozzolan obtained by calcination of kaolin at high temperature (700-1200°C). It enhances the strength, durability, and workability of Portland cement concrete and other cement-based products.

The use of metakaolin as partial substitute of cement in concrete/mortar pastes has been widely investigated in the previous years. However, the researchers have not been able to reach agreement on a unique conclusion regarding the optimum metakaolin replacement percentage for obtaining maximum strengths of concretes and mortars. Different replacement levels have been reported in the literature:

Rabehi et al. [1] partially replaced cement in mortars with calcined kaolin at levels of 0%, 5%, 10%, 15%, and 20%, by weight. Fixed w/b ratio of 0.5 was used. The results indicated that 5% metakaolin exhibited the highest compressive strength.

Said-Mansour et al. [2] partially replaced cement in mortars with metakaolin at levels of 0%, 10%, 20%, and 30%, by weight. Fixed w/b ratio of 0.5 was used. 0.9% of SP was used for mixture containing 30% metakaloin. The results indicated that 10% metakaolin exhibited the highest 28 days compressive strength while the inclusion of 30% metakaolin reduced it by 5.42%.

Goel [3] partially replaced cement in mortars with metakaolin at levels of 0%, 5%, and 10%, by weight. W/b ratios of 0.46 and 0.5 were used. The results indicated that 5% metakaolin exhibited the highest compressive strength at w/b ratio of 0.46, whilst the inclusion of 10% metakaolin exhibited the highest compressive strength at w/b ratio of 0.5.

Potgieter, Vermaak and Potgieter [4] investigated the optimum compressive strength, at age of 28 days, of mortars containing 0%, 10%, 20%, and 30% South African metakaolin as partially cement replacement. They used fixed w/b ratio of 0.375. The results showed that 10% metakaolin exhibited the highest 28 days compressive strength.

Courard et al. [5] partially replaced cement in mortars with metakaolin at levels of 0%, 5%, 10%, 15%, and 20%, by weight. Fixed w/b ratio of 0.5 was used. The results indicated that 15% Metakaolin exhibited the highest 28 days compressive strength.

Khaleel and Abdul Razak [6] partially replaced cement in mortars with metakaolin at levels of 0%, 5%, 10%, and 15%, by weight. Fixed w/b ratio of 0.32 and various dosages of Superplasticizer were employed. The inclusion of 10% metakaolin exhibited the highest 28 days compressive strength.

Vu et al. [7] partially replaced cement in mortars with metakaolin at levels of 0%, 5%, 10%, 15%, 20%, 25%, and 30%, by weight. W/b ratios ranging from 0.4 to 0.53 were used. 1.3% and 0.5% of SP were employed for mixtures containing w/b ratios of 0.4 and 0.44, respectively. The results indicated that 15% metakaolin exhibited the highest 28 days compressive strength at w/b ratios of 0.44 and 0.47, whilst the inclusion of 20% metakaolin exhibited the highest 28 days compressive strength at w/b ratios of 0.4, 0.5, and 0.53. The inclusion of 30% metakaolin reduced it by 1.38%.

Parande et al. [8] partially replaced cement in mortars with metakaolin at levels of 0%, 5%, 10%, 15%, and 20%, by weight. Fixed w/b ratio of 0.4 was used. The results

indicated that 15% metakaolin exhibited the highest compressive strength. The enhancement in the 28 days compressive strength was 50%, and 45% with the inclusion of 15%, and 20% metakaolin, respectively.

Khatib et al. [9] partially replaced cement in mortars with Metakaolin at levels of 10% 20%, 30%, 40% and 50%. Fixed w/b ratio of 0.5 was used. Compared to the control, the results showed an increase in the compressive strength with the inclusion of 10%, 20%, and 30% metakaolin, whilst the inclusion of 40% metakaolin showed slightly lower compressive strength. The inclusion of 50% metakaolin showed approximately 20% reduction in the compressive strength. The inclusion of 20% metakaolin exhibited the highest 28 days compressive strength.

Roy et al. [10] partially replaced cement with metakaolin at levels of 0%, 7.5%, 15%, and 22.5%, by weight. Fixed w/b ratio of 0.36 was used. The results indicated that 7.5% metakaolin exhibited the highest 28 days compressive strength.

Venu Malagavelli, Srinivas Angadi, J S R Prasad and Subodh Joshi [11] partially replaced cement in mortars with metakaolin at levels of 5%, 10%, 15%, 20% weight. They used fixed w/b ratio of 0.3. The results showed that 10 % metakaolin exhibited the highest 7 and 28 days compressive and flexural strengths.

Antoni et al. [12] partially replaced cement in mortars with 30% metakaolin, by weight. Fixed w/b ratio of 0.5 was used. The results showed that the inclusion of metakaolin improved the compressive strength at ages of 7, 28, and 90 days by 7%, 19% and 4%, respectively.

Accordingly, results differ regarding the optimum metakaolin replacement percentage for obtaining maximum strengths of concrete/mortar/pastes.

2. Materials and methods

2.1 Materials used

Materials used in this investigation were:

-        Processed kaolin clay, hereafter indicated KT.

-         Portland Cement CPJ CEM II/A 42.5 N

-         Standardized alluvial sand from El Oued in the southeast of Algeria.

-         Alkaline liquid (Activation solution), hereafter indicated SA was prepared in the laboratory.

The processed kaolin KT used for metakaolin synthesis was provided by the SOAKLA Complex of kaolin in El Milia (in eastern Algeria).

The sand used for cement and geopolymer mortar mixtures is normalized siliceous sand conforming to norm ASTM c778-06.

Alkaline activator was prepared in the laboratory by mixing aqueous solutions of sodium hydroxide (NaOH (12M)) and sodium silicate.

2.2 Sample testing

- The chemical compositions of KT kaolin and Cement were determined using a Philips PW 1404 X spectrophotometer.

- X-Ray Diffraction Analysis (XRD) with a Siemens D5000 diffractometer was employed to characterize the processed KT kaolin and the synthesized metakaolin.

-The particle size distribution of the sand was determined by laser granulometry.

- Specific surface areas of cement and MK metakaolin were measured using Blaine testing instrument according to EN 196-6 Standard [13].

- The Fourier Transformed Infra-Red (FTIR) analysis was used to follow the KT kaolin calcination process. It was carried out with a spectrometer equipped with ATR diamond of total attenuated reflectance.

- The compression tests carried out, according to EN 196-3:2005 standard [14] on 40mm x 40mm x40mm cubic specimens was meant to determine the geopolymer optimal formulation and the optimal replacement rate of cement by metakaolin in mortars.

2.3 Thermal treatment of started kaolin clay (KT)

Metakaolin was obtained by calcination of processed kaolin clay in the laboratory. Indeed, the main process important for production high reactivity pozzolana from kaolin clay is calcination.

At this stage of the study, the optimum temperature for heating kaolin in order to obtain Metakaolin with a high pozzolanic index and the heating period are still exactly

undetermined. They are still different from one researcher to another which explains the benefits of this study.

The goal of this part of study is to determine optimal calcination parameters for obtaining metakaolin from treated Algerian kaolin clay (KT), for the use as cimentitous material.

In order to obtain optimal calcination parameters, processed kaolin (KT) samples of about 30 g were heat treated in the laboratory furnace at different temperatures (650, 750 and 850 °C) and at different heating times (30, 60, 90, 120 min.).

X-ray diffraction and Fourier transform infrared spectroscopy FT-IR were adopted to investigate the influence of temperature on the metakaolin synthesis process.

After heating, the samples were subjected to room temperature at ambient conditions to avoid crystallization of amorphous metakaolin. The weight of the samples before and after the thermal treatment was measured in order to determine weight loss during calcinations process.

2.5 Effect of synthesized MK-metakaolin as partially cement replacement on the compressive strength of standard mortars

Hereafter we will explore how the synthesized MK-metakaolin affects the compressive strength of standard mortars based on CPJ CEM II/A 42.5 N cement in which MK-metakaolin was used as cement replacement. In addition, the optimum content of MK-metakaolin which exhibited the highest 28 days compressive strength was investigated.

We partially replaced cement in mortar mixtures with MK-metakaolin at levels of 0%, 5%, 10%, 15%, and 20%, by weight. Fixed w/b ratio of 0.5 was used. Beyond 20%, we observed that MK reduced the workability. Formulations studied are listed on table 1.

Table1

Various Mix proportion of MK-Metakaolin Blend mortar

Material	Mix				
	MK0	MK5	MK10	MK15	MK20
CPJ CEM II/A 42.5 N cement (g)	450	425	400	375	350
MK (g)	0	25	50	75	100
Water (g)	225	225	225	225	225

The mortars were mixed in a 5L mixer according to EN 196-1 and ISO 679:2009 standards with the mixing water. Standard sand (EN 196-1 and ISO 679:2009 standards) of a particle size between 0 and 2 mm was used. The mortar specimens were cast in 4x4x4 cm cubic metal moulds. All specimens were cured at 20°C and 95% R.H. for 24 hours and then demoulded and stored under the same conditions until testing.

The compression tests were performed on cubic specimens of dimensions 4x4x4 cm (fig.1) according to EN 196-1 standard.

Fig.1 MK-metakaolin/Portland cement mortar specimens

3. Results and discussion

3.1 Raw materials characterization

3.1.1 Sand sieve analysis

Figure 2 plots the particle size distribution of the sand. As it can be seen, sand is mainly constituted of fine aggregates.
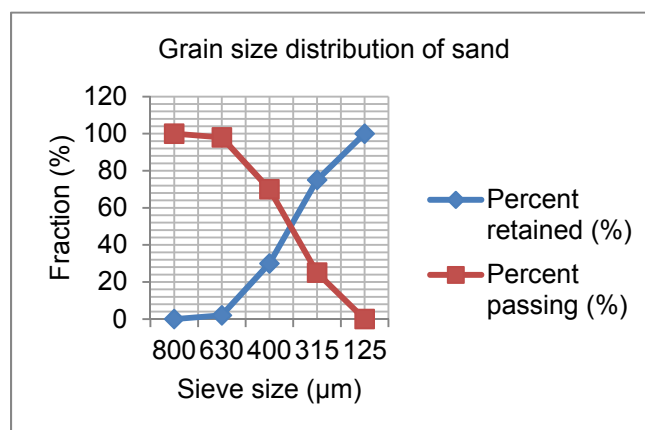

Fig.2. Grain size distribution of sand

3.1.2 Chemical analysis of raw materials

The chemical analysis of KT kaolin, Portland cement was determined by X-Ray Fluorescence (XRF). Results are given in Table 2.

Table 2

Chemical composition of raw materials

Chemicals	SiO$_2$	Al$_2$O$_3$	Fe$_2$O$_3$	CaO	MgO	SO$_3$	K$_2$O	Na$_2$O	LOI[1]	I.R[2]	TiO$_2$
Cement	20.34	5.37	3.00	61.69	1.80	2.20	0.76	0.14	0.97	1.12	-
Kaolin (KT)	49.30	33.00	2.38	0.08	0.40	-	2.93	0.09	-	-	0.24

(1) LOI: Loss in ignition; (2) I.R: Insoluble Residue;

3.1.3 FTIR characterization

FTIR technique was used to show the functional groups contained in Kaolin and Metakaolin. In order to confirm the characteristic bands of kaolinite in raw sample and the absence of these bands in thermally treated samples, a FTIR spectrophotometer Nicolet 6700 Thermo Scientific was used. IR spectra obtained for KT Kaolin starting clay and thermally treated samples are presented in Figures 3a, 3b, 3c and 3d. The results of IR spectroscopy of KT starting clay (Figure 3a) show the characteristic bands of kaolinite [15]: OH− at 3700, 3600 cm^{-1}; Al–OH at 913 cm^{-1}; Si–O at 1032, 1008, 469 cm^{-1} and Si–O–Al^{VI} at 538 cm^{-1}.
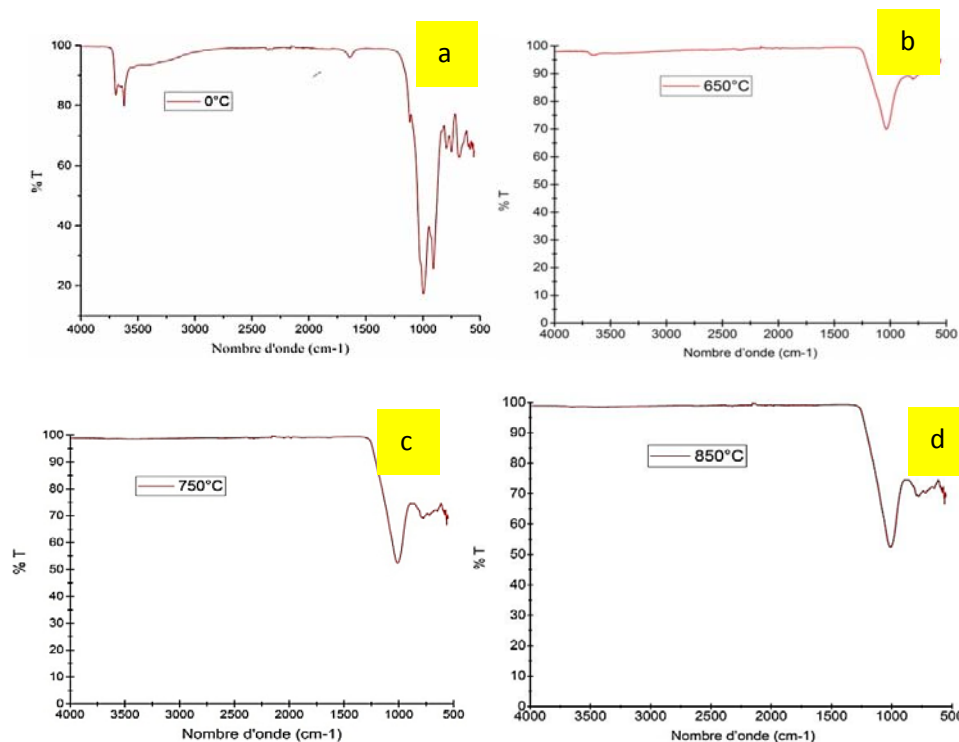

Fig. 3. IR spectra of starting kaolin (a) and calcined Kaolin for 90 min at: 650°C (b), 750°C **(c)** and 850°C (d)

Absence of the detectable Al–O–H bands at 3700 and 3620 cm^{-1}, due to KT deshydroxylation is evident from figure 3c and figure 3d. Absence of the band at 539 and 913 cm^{-1} and the appearance of a new band at 800 cm^{-1} can be related to the change from octahedral coordination of Al^{3+} in kaolinite to tetrahedral coordination in metakaolinite. The bands at 1100 and 1200 cm^{-1} are assigned to amorphous SiO_2.

After KT calcination, absence of bands at 1113, 1024, 998 and 908 cm^{-1} and apparition of the band about 1044 cm^{-1} on the MK spectral, confirm the process of Kaolinite-Metakaolinite conversion, as well as the presence of amorphous silica in metakaolin. Absence of the band at 908 cm-1 after kaolinite amorphisation at 750 °C and the appearance of the band at 546 cm^{-1} (Al - O, Al^{IV}) can be related to the change from octahedral coordination of Al^{3+} in kaolinite to tetrahedral coordination in metakaolinite. [16]

3.2.1 XRD Analysis

In order to confirm disappearance of kaolinite peaks, after thermal treatment, the XRD patterns of starting and calcined kaolin were compared (Figures 4a and 4b). It is evident that the major mineral constituents of the starting clay are kaolinite, quartz, Muscovite and albite minerals (Fig. 4a). After calcination at 750 °C, Kaolin was transformed into an amorphous phase, which is Metakaolin ($2\theta/20–35$), in addition to the formation of Anorthite after its reaction with CaO decomposed from Calcite, and other minerals like Quartz and Leucite resulting from the transformation of Muscovite (Fig. 4b).
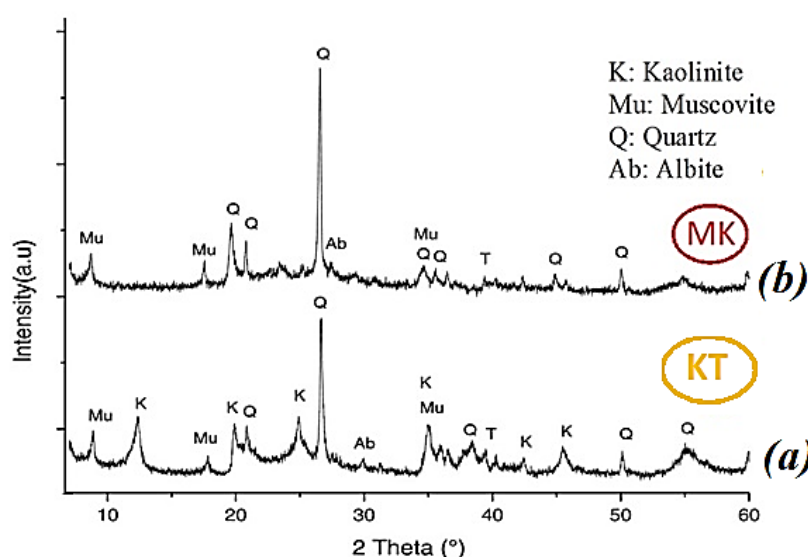

Fig. 4 XRD patterns of KT starting kaolin clay (a) and thermally treated KT kaolin at 750°C for 90 minutes (b)

After determining optimal calcination parameters, a sufficient quantity of the KT was calcined in a 3m³ gas furnace. The calcined kaolin is then ground into fine powder in a ball mill and then sieved through a sieve with apertures of 80 μm. Figure 5 shows the synthesized MK-metakaolin powder.

Fig.5. Crushed MK-metakaolin

The main physical and chemical characteristics of the synthesized MK metakaolin were investigated.

3.2 MK metakaolin characterization

3.2.1 Main physical properties: Absolute density and Specific surface area

The main physical properties values of Portland cement and metakaolin are reported on table 3. It should be noted in particular that the MK metakaolin specific surface value is over 15 times higher than Portland cement. By contrast, the absolute dry density of cement exceeds that of MK metakaolin.

Table 3

Main physical characteristics of Portland cement and the synthetized Metakaolin

Property	MK Métakaolin	CPA-CEM II/A 42.5N cement
absolute dry density (g/cm3)	2.70	3.10
specific surface area (m²/g)	15.00	0.34

3.2.1 XRF analysis

The chemical composition results of metakaolin MK determined by X-ray fluorescence (XRF) is listed in Table 4.

Table 4

Chemical composition of Synthetized Metakaolin

Type	SiO$_2$	Al$_2$O$_3$	Fe$_2$O$_3$	CaO	MgO	K$_2$O	Na$_2$O	TiO$_2$
Percent by mass	55.08	36.87	2.66	0.09	0.45	3.27	0.10	0.27

3.3 Effect of MK metakaolin as partially cement replacement on the compressive strength of standard mortars

Effect of MK-metakaolin as partially cement replacement on the compressive strength of standard mortars was investigated. Formulations studied are listed on table 6 above.

Figure 6 shows evolution of the compressive strength of mortar at 7 and 28 days for different formulations, as a function of the metakaolin replacement levels.
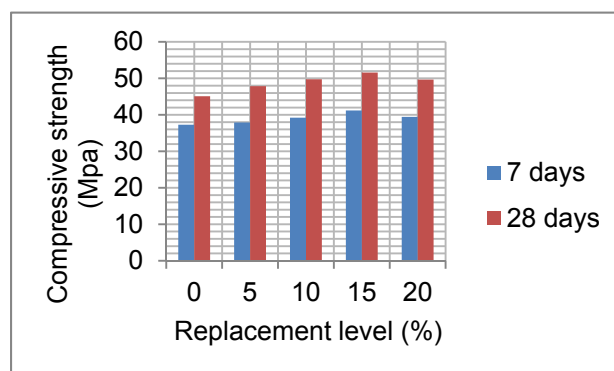

Fig.6. Effect of metakaolin (MK) on the compressive strength of mortars

The results indicated that 15% Metakaolin exhibited the highest 28 days as well as the 7 days compressive strength followed by 10% metakaolin, 20 % metakaolin and 5% metakaolin respectively.

Realistically, the optimum percentage of metakaolin that exhibited the maximum compressive strength is dependent on the cement type and content, type and dosage of admixtures, and also on the age of testing. In addition, some authors believed that the w/b ratio is the main factor that governs the optimum content of metakaolin [7] while others believed that the calcination temperature and its period is the main factor that governs the optimum metakaolin content. As well, other authors believed that the chemical composition constitutes the major factor that affecting the optimum metakaolin content.

In general the optimum percentage of metakaolin that exhibited the maximum compressive strength is dependent on the cement type and content, type and dosage of admixtures, and also on the age of testing [12].

Accordingly, results differ regarding the optimum metakaolin replacement percentage for obtaining maximum strengths of concrete/mortar/pastes. However, the vast majority of authors agree that the pozzolanic reaction between metakaolin and Calcium Hydrates (CH) improves the mechanical characteristics (compressive strength) [5, 10, 17] mainly at early ages [18].

4. Conclusion

The conclusions of this study can be summarized as following:

1) Metakaolin, pozzolanic additive, may be obtained by calcination of processed Algerian kaolin clay from El Milia at a temperature of 750 °C with a heating time of 90 min.

2) The optimum replacement level of CEM II/A 42.5 N cement by MK-metakaolin is 15 %, which gave the highest compressive strength in comparison to that of other replacement levels.

References

[1] Bahia Rabehi, Khaled Boumchedda1 and Youcef Ghernouti " Study of calcined halloysite clay as pozzolanic material and its potential use in mortars" International Journal of the Physical Sciences ISSN1992-1950 ©2012 Academic Journals Vol. 7(31), pp. 5179-5192, 16 August, 2012,.

[2] Mohamed Said-Mansour, El-Hadj Kadri, Said Kenai, Mohamed Ghrici and Rachid Bennaceur, Influence of calcined kaolin on mortar properties Construction and Building Materials 25 (2011) 2275.

https:// doi:10.1016/j.conbuildmat.2010.11.017

[3] Amita Goel, Effect of aggressive environment on durability of metakaolin based cement mortar (Master Thesis, Deemed University, Department of Civil Engineering, June 2006).

https://docplayer.net/29459862-Effect-of-aggressive-environment-on-durability-of-metakaolin-based-cement-mortar.html

[4] S. S. Potgieter-Vermaak and J. H. Potgieter, Metakaolin as an Extender in South African Cement, Journal of Materials in Civil Engineering 18 (2006) 619.

https://doi.org/10.1061/(asce)0899-1561(2006)18:4(619)

[5] Luc Courard,Anne Darimont,Marleen Schouterden and Fabrice Ferauche Durability of mortars modified with metakaolin, Cement and Concrete Research 33 (2003) 1473.

https://doi.org/10.1016/S0008-8846(03)00090-5

[6] O. R. Khaleel and H. Abdul Razak, The effect of powder type on the setting time and self compactability of mortar, Construction and Building Materials 36 (2012) 20.

https://doi.org/10.1016/j.conbuildmat.2012.04.079

[7] D.D. Vu, P. Stroeven and V.B. Bui, Strength and durability aspects of calcined kaolin-blended Portland cement mortar and concrete Cement & Concrete composites 23 (2001) 471.

https://doi.org/10.1016/S0958-9465(00)00091-3

[8] Anand Kuber Parande, Babu B. Ramesh and Karthik M. Aswin, Study on strength and corrosion performance for steel embedded in metakaolin blended concrete/mortar, Construction and Building Materials 22 (2008) 127

https://doi.org/10.1016/j.conbuildmat.2006.10.003

[9] J. M. Khatib, E. M. Negim and E. Gjonbalaj, High Volume Metakaolin as Cement Replacement in Mortar World Journal of Chemistry 7 (2012) 7.

https://doi/10.5829/idosi.wjc.2012.7.1.251

[10] D. M. Roy, P. Arjunan and M. R. Silsbee, Effect of silica fume , metakaolin and low-calcium fly ash on chemical resistance of concrete, Cement Concrete Res 31 (2001) 1809.

https://doi.org/10.1016/S0008-8846(01)00548-8

[11] Venu Malagavelli, Srinivas Angadi, J S R Prasad and Subodh Joshi, Influence of Metakaolin in Concrete as Partial Replacement of Cement, International Journal of Civil Engineering and Technology, 9(7), 2018, pp. 105–111.

http://www.iaeme.com/IJCIET/issues.asp?JType=IJCIET&VType=9&IType=7

[12] M. Antoni, J. Rossen, F. Martirena and K. Scrivener, Cement substitution by a combination of metakaolin and limestone, Cement and Concrete Research 42 (2012) 1579.

https://doi.org/10.1016/j.cemconres.2012.09.006

[13] EN 196-6, Methods of testing cement, Part 6: *Determination of fineness*.

[14] EN 196-1, Methods of testing cement-Part 1: *Determination of strength*

[15] Russel J.D., Infrared Spectroscopy Of Inorganic Compounds, Laboratory Methods in Infrared Spectroscopy, Wiley, New York, 1987.

[16] Farmer V.C. The infrared spectra of minerals. London Mineralogical Society Monogram (1988) p539.

Effect of metakaolin as partially cement replacement on the compressive strength of standard mortars

[17] Badogiannis, E., Kakali , G., Dimopoulou , G., Chaniotakis ,E., Tsivilis, S.,(2005). Metakaolin as a main cement constituent. Exploitation of poor Greek kaolins. Journal of Cement & Concrete composites, 27, pp. 197–203

https://doi.org/10.1016/j.cemconcomp.2004.02.007

[30] X. Jin and Z. Li, Effects of Mineral Admixture on Properties of Young Concrete, J Mater Civil Eng. 15 (2003) 435. https://doi.org/10.1061/(asce)0899-1561(2003)15:5(435)

Comparative study between the materials used to design the blades of a wind farm

Emilia Dobrin[1]

[1]Timişoara Polytechnic University
Victoriei Square 2, Timişoara 300006, România
E-mail: emi_dobrin@yahoo.com

Abstract. *This study considered four alternatives, namely reinforced fiberglass plastics, fiberglass reinforced materials, carbon fiber reinforced materials, Kevlar, Al5754, Al6082, Al7075 alloys to determine the most good material for the blades of a wind turbine.*

Key words: composite materials, glass fiber reinforced plastics, reinforced materials based on fiberglass, carbon fiber reinforced materials.

1. Introduction

Our goal is: to select a suitable material for creating the blades of a horizontal wind farm, which can operate in a region with low wind speed [1].

The ideal blade should be durable, corrosion resistant, high wear resistance, lightweight and most importantly, cost effective.

The main components of horizontal axis wind turbines include the rotor blades, the rotor hub, the main shaft, the gearbox, the generator and the power converter, all housed in a nacelle supported by a bed plate which is mounted on the resistance tower and rotates due to a guide bearing system [2].

The blades represent the main element of conversion of wind energy into electricity, their geometry, material, number and length contributing decisively to the efficiency of the wind farm. The stresses to which a wind turbine blade is subjected are generated by centrifugal force, gravitational force, aerodynamic loading, vibrations all this leading to complex stresses. Aggressive environmental factors (UV radiation, variations in temperature and humidity, impact with birds, etc.) potentiate the risks to which the blades are subjected [3], [4].
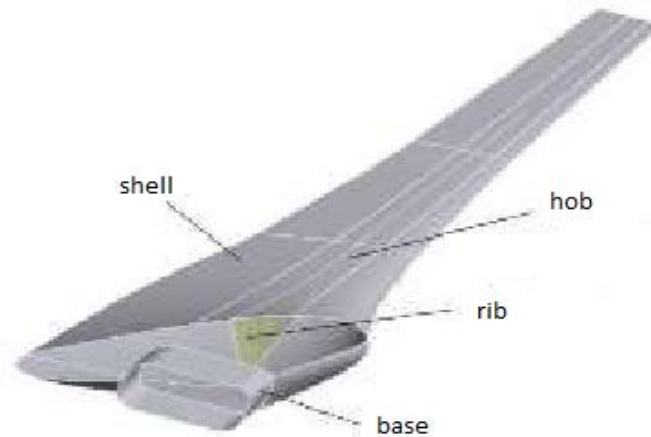
Fig. 1.1 Blade structure [5]

Generally, a wind turbine is designed to operate for about 30 years without the need for maintenance. For this we must have minimal deformation of the blades, effects of fatigue as little as possible (due to gravitational forces on rotation and wind loading) [3]. Given these requirements, we will use only materials with very good mechanical and chemical resistance, the lowest possible mass, low maintenance costs, with a diversity of shapes and design dynamics [6].

The choice of blade material is a serious problem facing the manufacturing industry. The main selection indices for blade materials should be based on the following material properties:

- the quality of the material (both the quality of the surfaces, the elastic, chemical and thermal characteristics of the fibers and matrix in the composite structure, the quality of the joints between the reinforcing elements and the other components) [4];

- a high rigidity of the materials to ensure that the blades maintain the optimal aerodynamic shape while being subjected to strong wind loading conditions;

- low mass density to minimize gravitational loading;

- high fatigue resistance to high cycles to ensure the required 20-year life cycle with high reliability [7].
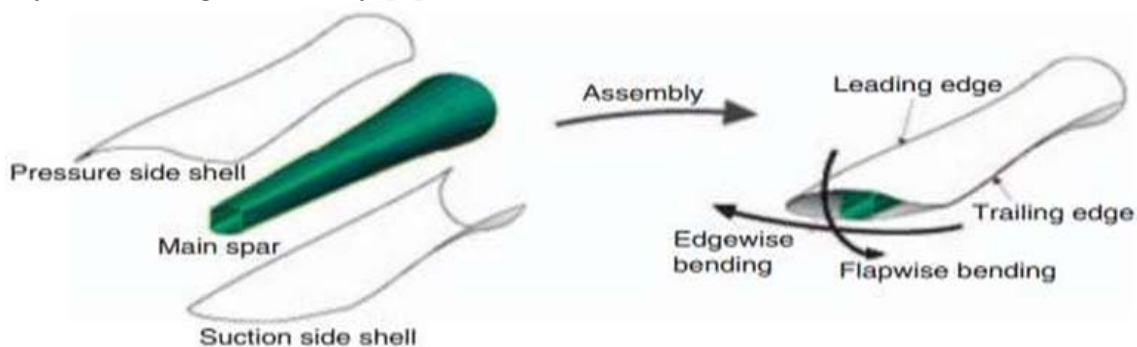

Fig.1.2 The composition of the blade of a wind farm [8]

2. Composite Materials

They are materials that contain strong fibers surrounded by a matrix. The matrix and the fibers joined efficiently in the composite manufacturing process in order to increase their properties, being distinguished by tensile strength, shock resistance and high abrasion, having a much lower weight than the traditional materials they replace [9, 10]. Presentation of the usual composite materials used for blades:

- glass fiber reinforced plastics;
- reinforced materials based on fiberglass;
- carbon fiber reinforced materials;
- kevlar;
- alloys de Al5754, Al6082, Al7075.

As a composite material, fiberglass-reinforced plastic is used to design the rotor blade. Fiberglass is in the form of fine fibers, which are made of molten glass. The strength / weight ratios of fiberglass composites are higher than those of most other materials, and their impact resistance is phenomenal. Moreover, they possess good electrical properties, resistance to humidity and weather in the open air and resistance to heat and chemicals. These properties are combined with ease of manufacture [11]. Following the tests, this type of blade withstands loads ten times higher than the normal work force and the field performance test showed that the rotor blade has an average measured power factor of 41.2% [2]

Fiberglass reinforced plastic
Most glass-reinforced products are made of E glass, which has a good electrical and mechanical properties and high heat resistance. Type E glass fibers are usually mixed with heat-resistant (epoxy) resins are used to build the turbine blade, which are more expensive, but have higher strength characteristics and higher fatigue strength. The stiffness of the composite depends on the stiffness of the fibers and the percentage of their volume. The percentage of fiber volume if 65% and can lead to reduced stiffness to composite fatigue. This is due to the existence of dry regions between the fiber and the resin [12, 13].

Carbon fibers are composed of almost pure carbon, which forms a crystallographic lattice with a hexagonal shape called graphite. In recent years, carbon fibers have become increasingly popular due to the increasing demands of rotor blades and the declining price of carbon fibers. Carbon fibers have an excellent combination of very high rigidity, high strength, low weight and low density. Carbon fibers have more rigidity than glass fibers. They have a lower density than fiberglass, but are more rigid. This led to the development of a lighter and more rigid turbine. The compressive strength of carbon fibers is lower than glass fibers [12, 14, 15].

Kevlarul
Kevlarul is an organic polymer with aramid fiber with exceptional properties (shock

and abrasion resistance, high tensile strength, strength and stability up to 500 ° C, vibration damping capacity, low density - 1.7 g / cm3, insensitive to action of chemical agents and microorganisms). Applications of Kevlar fibers as such, or in carbon-Kevlar composites and hybrids, refer to sheathing components, fairings and interior design and have the effect of reducing the weight of those components by about 30%, costs by 50% and increasing their durability. 2 to 5 times. Aramid fibers (aromatic polyamides) are characterized by excellent thermal and thermal stability, static and dynamic fatigue strength and impact resistance. These fibers have the highest tensile strength (strength / density ratio) of any commercially available continuous filament yarn. Aramid - reinforced thermoplastic composites have excellent wear resistance. Aramid fibers have low or very low densities [15], [17].

Alloys aluminum

Aluminum is a silvery white metal with a density of about one-third that of steel. Aluminum was only implemented in test situations because it was found to have a lower level of fatigue than steel. Aluminum is ductile and a good conductor of heat. Aluminum is a low-priced metal, but it has good reliability and a low level of tensile strength. Aluminum is light, but weaker and less rigid than steel [15].

Aluminum is extremely malleable and can be formed into almost any shape. An extruded product is the result of heating an aluminum ingot to 500 ° C and pressing it through a mold in the form of a finished part or extrusion. With the right alloy and the right heat treatment, extrusions offer endless application opportunities. Extruded aluminum is suitable in climate screens for offshore transformer stations. Due to their low weight and anti-corrosion properties, extrusions ensure a long service life, easy installation, low maintenance and low use of other materials [18].

3. Analyze materials

The behavior of composite materials is influenced by a variety of mechanical and physical parameters. Homogeneity and quality of manufactured materials are essential [19].

Tabel 1

Mechanical characteristics:

Composite materials	Modulus of elasticity E[a]	Tensile strength Rm [MPa]	Flow limit resistance Rp0.2 [N/mm^2]	Elongation to break A50[%]	Ratio Poissons	Hardness a Brinell HB [daN/mm^2]
Fiberglass reinforced plastic	2.76-6.65	26200	3500	2.00-8.00	0.25	175-239
Reinforced materials based on fiberglass E	72.4	3445	1200	4.8	0.20	83
Carbon fiber reinforced materials	2.14-27.6	110	1300	0.29-1.79	0.10	100-125

Studiu comparativ între materialele utilizate pentru proiectarea palelor unei centrale eoliene

Kevlar	130	480	500	3.6	0.36	262-321
Al5754	70.3	205	105	24	0.33	60
Al6082	70	350	310	11	0.33	105
Al7075	71.7	540	465	9	0.33	175

Tabel 2

Physical characteristics:

Composite materials	Density g/cm^3	Water absorption %	Filler content %	Melt flow g/10 min
Fiberglass reinforced plastic	1.05-1.25	0.0100	10.0-20.0	-
Reinforced materials based on fiberglass E	2.54-2.60	0.0500-0.300	5.00-40.0	1.10-60.0
Carbon fiber reinforced materials	1.21-1.42		10.0-40.0	
Kevlar	1.44			
Al5754 ENAW-AlMg3 Peraluman - 300	2.67			
Al6082 AlSi1MgMn Anticorodal	2.70			
Al7075 ENAW-AlZn5.5 MgCu Planoxal 70/Perunal 215	2.8			

4. Conclusion

Composite materials compared to traditional materials have important advantages and bring many functional advantages: good mechanical and physical strength, low mass, low maintenance costs, a diversity of shapes and the dynamics of blade design.
The most efficient composite materials in terms of breaking strength / weight ratio are fiberglass (GFRP), carbon fiber (CFRP) and kevlar. More than three times stronger and stiffer than glass, carbon fiber is an alternative to commonly used glass-reinforced plastic. This helps designers build longer blades while maintaining the necessary rigidity.
As a strength / weight ratio, it is currently the best material that can be produced is Kevlar.

Bibliografie

[1] I.Okokpujie, U.Okonkwo, Implementation of multi-criteria decision method for selection of suitable material for development of horizontal wind turbine blade for sustainable energy generation, Heliyon 6 (2020) e03142, 2020;
[2] S.M. Habali, I.A. Saleh, Energy Conversion & Management 41 (2000) 249±280, 2000;
[3] L. Mishnaevsky Jr., Composite materials in wind energy technology, Thermal to mechanical energy conversation: Engines and Requirements, Denmark;
[4] M. Stanciu, I. Curtu, Analiza riscurilor integriății structurale a palelor turbinelor eoliene, Buletinul Agir nr. 2, 2005;

[5] M. Guțu, Optimizarea structurii de rezistență a palelor aerodinamice pentru turbine eoliene, teza doctorat, Chișinău, 2017;

[6] https://www.tuiasi.ro/uploads/files/Rezumat_Emanuela_Marin.pdf;

[7] LLC. Ancona, J. McVeigh, Wind Turbine - Materials and Manufacturing Fact Sheet Prepared for the Office of Industrial Technologies, Princeton Energy Resources International, 2001;

[8] O. Thomsen, Sandwich Materials for Wind Turbine Blades - Present and Future, Journal of Sandwich Structures and Materials , 2009;

[9] https://sim.tuiasi.ro/wp-content/uploads/2018/01/output-carte-2.pdf;

[10] S. Kumar, A. Krishnan, Vibrational Fatigue Analysis of NACA 63215 Small Horizontal Axis Wind Turbine Blade, Materials Today: Proceedings 5 (2018) 6665–6674;

[11] https://textilelearner.blogspot.com/2012/09/glass-fiber-composites-properties-of.html;

[12] S. Bhadoria, A. Maurya, Materials for Wind Turbine Blades, Loading and Manufacturing Methods, International Journal of Engineering Research & Technology (IJERT) ISSN: 2278-0181, 2020;

[13] K. Senthil, A.S. Krishnan, Vibrational Fatigue Analysis of NACA 63215 Small Horizontal Axis Wind Turbine blade, Materials Today: Proceedings 5 (2018) 6665–6674, 2018;

[14] K. Babu, N.V. Raju, The material selection for typical wind turbine blades using a MADM APPROACH& ANALYSIS of blades, MCDM 2006, Chania, Greece, June 19-23, 2006

[15] D. Popescu, Tehnologia materialelor / metode si procedee tehnologice, https://slideplayer.ro/amp/17577456;

[16] https://sapm.upm.ro/docs/Cursuri/An2/StudiulMaterialelor.pdf;

[17] https://www.hydro.com/en;

[18] S. Kumar, A.S Krishnan, Vibrational Fatigue Analysis of NACA 63215 Small Horizontal Axis Wind Turbine blade, Materials Today: Proceedings 5 (2018) 6665–6674;

[19] M. Jawaid, Effect of Kevlar and carbon fibres on tensile properties of oil palm/epoxy composites, Conference Paper in AIP Conference Proceedings December 2017.

Reacted and Activated Rubber effect on Stiffness Modulus and Cracking Resistance of Bituminous Mixtures

Zeine E. Boudnani[a,*], Bachir Glaoui [b], M'hamed Merbouh [c], Jorge B. Soussa[d]

[a,b,c] Laboratoire de Fiabilité des Matériaux et Structures dans Les Zones Sahariennes, UTMBéchar, Algérie

[d] : CONSULPAV, Consultores e Projectistas de Pavimentos, Lda., Rua da Zona Industrial, No.6 A, Casais da Serra. 2665-305 Milharado, Mafra, Portugal.

Abstract

Traditionally, asphalt rubber (AR) mixtures have been difficult to produce. Their production requires specialized plants and equipment, which has resulted in their high cost to manufacture. In part this difficulty is due to the need to produce AR binder by blending it at high temperatures for a significant period of time (typically at about l90°C for 45 min to 1 h). A new technology that produces a reacted and activated rubber (RAR), which is an elastomeric asphalt extender, has been developed by hot blending and activation of a rubber granulate with a selected asphalt binder and activated mineral binder stabilizer. The objective of this study was to evaluate and characterize the performance of Reacted and Activated Rubber (RAR) modified dense graded asphalt mixtures in order to recommend a suitable RAR content to produce a mix that provides superior pavement performance characteristics. The research effort encompassed investigation of shear stiffness modulus and cracking resistance for performance evaluation of six dense graded asphalt mixtures, including one conventional and five modified mixes covering 48 samples. The stiffness modulus was increased as RAR increases, the cracking resistance results showed an increase of fracture energy as RAR increased. 15% RAR was found as the most appropriate content based on its performance characteristics.

Key words: RAR, bitumen, stiffness, cracking resistance, performance.

1. Introduction

The need for improved material performance has spurred the adoption of modified asphalt systems. Rubber has been used as a modifier on road projects in the United States since the late 1940s [1]. A few years after the first roads were repaved; the process to add crumb rubber from waste tires was developed in Phoenix, Arizona, in 1965. This process is a well-developed system of asphalt modification with nearly 50

years of development. Today, however, asphalt rubber (AR) mixtures are still difficult to produce and require specialized plant and equipment, which results in their high cost to manufacture. This difficulty is due in part to the need to produce AR binder by blending it at high temperatures for a significant period of time (typically at about 190°C for 45 min to 1 h) [1]. The complexities in the process have caused AR mixes to be significantly more expensive to produce than conventional paving mixtures.

According to Sousa et al. (2013), RAR was produced by mixing in heat and activated for a short period of time, then specially designed to form dry rubber granulated active rubber. RAR can be added to any type of Hot Mix Asphalt (HMA) to replace the asphalt part of the binder with different proportions. In Asphalt Mixing Plant RAR mixing was added directly to the pug mill or drum dryer. According to Medina and Underwood (2017), the soft asphalt used in RAR aims to reduce some of the increase in hardening caused by rubber, consequently enabling the production of asphalt with RAR at the same mixing and compaction temperatures. Crumb rubber used comes from the truck and car tires, which are processed and milled with ambient or cryogenic processes. RAR has a particle size distribution ranging from 0.595 mm to 0.075 mm sub [2].

Previous research by the authors investigated the effects of the addition of RAR with two different base binders at various dosages from 5 to 25% by utilizing a series of advanced arheological testing processes [4]. An overall reduction in the viscosity-temperature susceptibility property was found with increasing RAR content irrespective of the base asphalt binder. Additionally, an improvement in the complex shear moduli indicated higher rut resistance with RAR as well as higher recovery of these modified asphalts with lower strains accumulated for higher RAR based asphalts.

As part of this research [5], there was also a need for a detailed study on the performance evaluation of RAR modified asphalt mixtures using advanced materials characterization tests currently being used by the pavement community. Furthermore, the response of the RAR modification to the various environmental and loading conditions was essential to understand the suitability of RAR materials in conventional dense graded mixtures most commonly used worldwide. Thus, the objective of this study was to evaluate and characterize the performance of RAR modified dense graded asphalt mixtures in order to recommend a suitable RAR content to produce a mix that provides superior pavement performance characteristics [3].

However, the cracking resistance of a mixture, as most mechanical properties, is not only influenced by the binder type and content, but also by a wide range of factors

such as the type andcontent of filler that constitutes the mastic or the amount and nature of the fines.

Recently, numerous researchers have investigated the influence of asphalt binders on the cracking resistance of mixtures by establishing a correlation between the rheological propertiesof the binders using conventional tests, e.g. elastic recovery test, bending beam rheometer or dynamic shear rheometer, and the cracking performance of asphalt mixtures at a defined temperature, e.g. overlay tester or indirect tension test [24,25].

Others have tried to establish a correlation between the critical cracking temperature for both asphalt binders and mixtures at low temperatures [26,27]. However, relationships between binder tests and mixtures tests have not been fully established due to significant differences in the test temperature. Based on the encountered discrepancies, this study aims to directly characterize the cracking resistance that different asphalt binders withstand by applying a direct tensile stress under different test temperatures.

Understanding the ability of an asphalt pavement to resist fractures from repeated loading condition is essential for developing superior HMA pavement designs. Previous studies have been conducted to understand the occurrence of fatigue and how to extend pavement life under repetitive traffic loading [28,29]. The use of CRM, expanded to HMA, continues to evolve since the CRM binders enhance the performance of asphalt mixtures by increasing the resistance of the pavements to permanent deformation and thermal and fatigue cracking. Many researchers have found that utilizing crumb rubber in pavement construction is both effective and economical [30].

Therefore, this paper evaluates the stiffness modulus using ITSM, ductility and tenacity that different types of asphalt binders provide to a mixture under one fixed environmental condition by applying the Fénix test [21,22]. This test, developed by the Road Research Laboratory of the Technical University of Catalonia, evaluates the crack resistance of asphalt mixtures by calculating the dissipated energy during mixture cracking [22].

2. Background

The components of RAR are asphalt, crumb rubber, and an activated mineral binder stabilizer. Conceptually, asphalt cements (or bitumen in Europe and elsewhere) can be any straight-run, plain, soft bitumen. The use of soft asphalt grades enables production of HMA at conventional mixing and laying temperatures without the loss of the proper workability, despite the addition of crumb rubber. Usually, the crumb rubber

consists of scrap tires that are processed and finely ground by any proven industrial method. The scrap tires consist of a combination of automobile tires and truck tires, and should be free of steel, fabric, or fibers before they are ground. To produce RAR, the crumb rubber particles should be finer than 1.0 mm. A 30-40 mesh maximum particle size is preferred. AMBS is a new binder stabilizer that was developed to prevent excessive drainage of the bitumen in SMA mixes during mix haulage, storage, and laydown. This stabilizer (industrially known as "iBind") is an activated, micro ground, raw silica mineral (40 μm and finer), which is a waste by product of phosphate industries' mining. Activation, by nano monomolecular particle coating, is intended to obtain thixotropic and shear-thinning properties for the asphalt.

The binder film and mastic in the mix should possess high viscosity at rest (haulage, storage, after lay) to reduce drain down, and low viscosity in motion (mixing and laying) is needed to maintain the proper workability (2). During research and development, RAR was produced and tested at different formulations, dictated by the type and relative proportions of its three components [1]. On average, a typical RAR blend contains about 62% crumb rubber, 22% soft bitumen, and 16% AMBS. After the material has reacted in the blending equipment, another 10% AMBS is added in a coating mixer unit to prevent re-coagulation of the product. RAR has been found to enhance the properties of the plain bitumen to levels higher than polymer modified asphalt, and to levels even higher than conventional AR blends [1]. A hypothesized basic model for the mechanism of RAR as a bitumen enhancer is illustrated in Figure I.
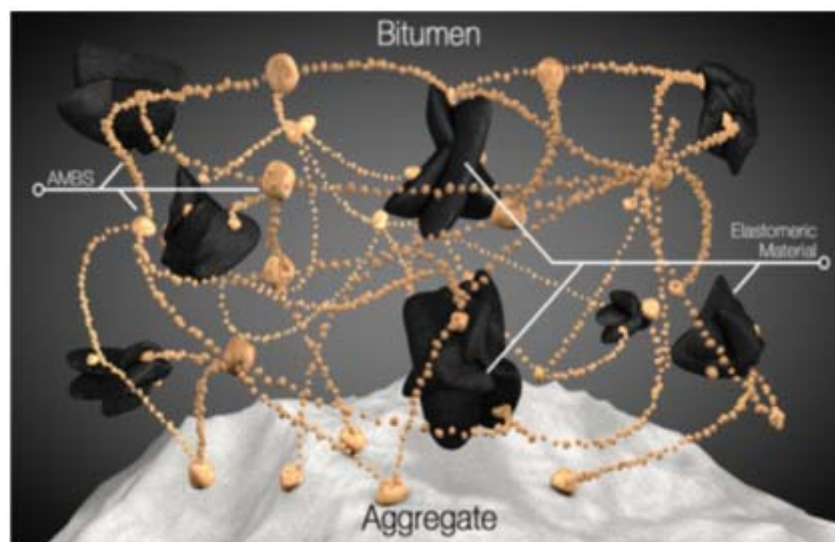

Figure 1: Suggested model for mechanism of RAR as asphalt extender [1].

2. Objective

The main objective of this study is to evaluate and examine the effect of reacted and activated Rubber on the laboratory performance of bituminous mixtures.

3. Materials

3.1 Reacted and activated rubber (RAR)

RAR is composed of soft asphalt (bitumen), finely ground scrap tire rubber and fillers reacted at optimal proportions and temperatures as reported in [6]. **Fig. 2** represents a the gradation of reacted and activated rubber (RAR) [3]. Generally, RAR consists of about 62–65% crumb rubber, 20–25% soft asphalt, and 15–20% filler. During the production of the RAR material, the asphalt used will be a softer kind to enable an improvement in the viscosity, and also ensure the workability of the binders even at higher rubber contents. The rubber particles used in the composition of RAR are of the maximum size of 600 lm. The fillers used in the RAR conglomerate are microscale additives to reduce moisture sensitivity of the asphalt mixes [7]. The activation was achieved by nano monomolecular particle coating. The base binder was modified by different contents of RAR ranging from 5 to 25% by mass of bitumen.
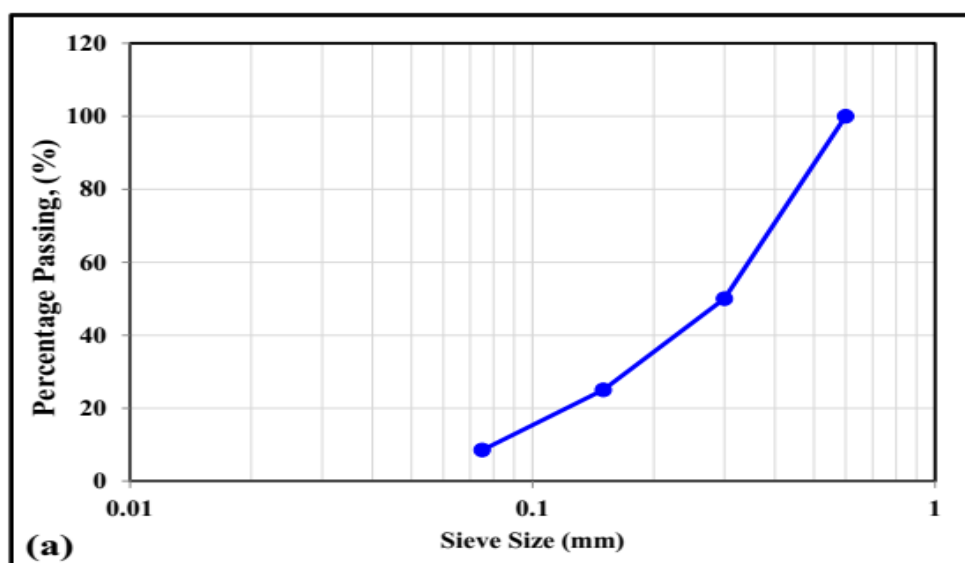
Figure 2: Gradation of reacted and activated rubber

3.2 Binders

The base binder that was used in this study was 35/50 penetration grade typically used for construction of pavements in Algeria; this binder was obtained from national bitumen Contractor. Different modified RAR binders were prepared, the first set of RAR

binders were prepared by heating the base binder 180°C and adding the different percentages of RAR, 5, 10, 15, 20 and 25% by weight of the binder for testing, Since the blending process of the RAR modified binders does not have a standard procedure, the mixing time and temperature range for these binders, which were respectively, 5 min and 170–180°C were chosen to simulate the mixing process in the pugmill, transport, and laydown[4]. Also, the speed of the motor while blending was about 3000 rpm, A high laser thermometer was used to maintain the mixing temperature around 180°C. Physical tests were conducted on the un-modified and RAR modified binders, these tests are Penetration [8], softening Point [9], Ductility [10] and Elastic Recovery [11].

3.3 Mixtures

To select the aggregate gradation of the mixture to be evaluated in this study, the gradations of aggregates of dense graded and RAR modified mixtures used in paving projects in Algeria were examined. Based on that, the selected asphalt mixture had a 14 mm nominal maximum aggregate size (NMAS) and was designed to meet the European Standards specifications for EN 13108-1 for high traffic surface mixtures (class 3). **Fig 3** showed gradation limits and target mixture specifications for the dense graded mixture, this later is named BBSG 0/14 (bétons bitumineux semi-grenus -half granulated bituminous concrete-) in the standard. It is noted that designed mixture included: 31% crushed aggregates 8/14mm, 24 % crushed aggregates 3/8mm and 45% manufactured sand 0/3mm. The mechanical characteristics of aggregates are summarized in the **Table1**, it is noted that the mix design was targeted to construct a new bituminous pavements.
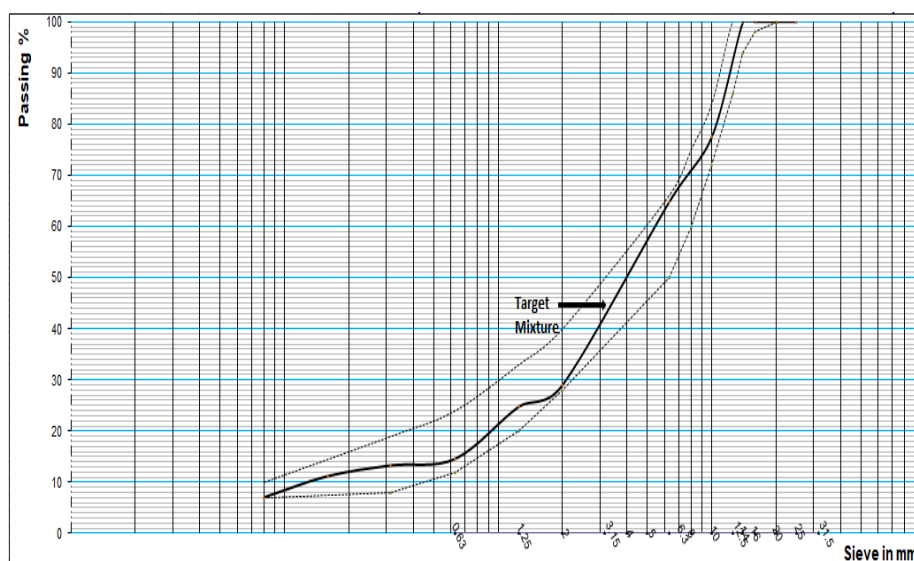

Figure 3: Gradation of target mixture BBSG 0/14 according to EN13108-1

Aggregates were heated for 4 hours at 180°C in the oven. Then the bitumen, aggregates and reacted and activated rubber were mixed at 180°C for 4 minutes to ensure homogenous mixing, the mixture was kept in the oven for 1h 30min to simulate the short term aging. **Table 2** illustrates the binder content for each of the seven mixtures. Same base binder content was kept constant for all mixtures to isolate the effect of RAR content.

Table 1: Mechanical characteristics of aggregates

Aggregates	Standard Test	0/3	3/8	8/15
Specific Density (t/m³)	ASTM C127-15 C128-15	2.71	2.71	2.71
Absorption (%)	ASTM C127-15 C128-15	0.6	0.5	0.5
Finesse Modulus %	EN 933-1:2012	2.56	-	-
Sand Equivalent (%)	EN 933-8	60	-	-
Methylene Blue Test (%)	EN 933-9	0.03	-	-
Los Angeles (%)	EN 1097-2:2010	-	18	17
Micro Deval (%)	EN 1097-1:2010	-	16	14

Table 2: Different bitumen contents for different RAR content

RAR Content (%)	Bitumen Content (%)
0	5.60
5	5.88
10	6.16
15	6.44
20	6.72
25	7.00

4. Mixtures Testing

A laboratory testing program was performed to evaluate the performance of the control and the RAR modified mixtures with respect to Indirect Tensile Stiffness Modulus and Cracking Resistance. The following sections provide details about tests conducted on mixtures considered in this study. The Air voids were kept between 5 and 9% returning to EN13108-1.

To analyze the effect of reacted and activated rubber on the cohesion and bearing capacity of the bituminous mixes, the six mixes were designed with an identical mineral skeleton. The mixes were short term aged in the over for 1h30min at 160C for conventional and 180C for RAR modified mixes. The manufacturing temperature for

the conventional 35⁄50 reference mix was 160–165°C. The RAR mixes were elaborated at a slightly higher temperature because the addition of reacted and activated rubber increased mix viscosity. The higher temperature thus guaranteed the workability of the mix.

The mixtures were designed, based on the results of the SGC test (EN 12697 – 31). In the gyratory compaction test, three sets of specimens were evaluated for each of the mix formulas. Each specimen had a diameter of 100 mm was compacted by the application of a vertical stress (normally 600KPa) via end platens to a known mass of asphaltic mixture within a 100 or 150mm internal Ø mould. The longitudinal axis of the mould is rotated (gyrated) at a fixed angle to the vertical whilst the platens are kept parallel and horizontal. (The size specified in each formula). During compaction the height of the sample is automatically measured and both the mixture density and void content calculated. Once the optimal bitumen content was determined for each mix,

4.1 Indirect Tensile Strength Modulus according to EN 12697-26

Stiffness modulus is an important mechanical characteristic of the road base and surface layers. This test describes a material stiffness that most closely simulates the behavior of material under a moving wheel [21]. Basically, the term stiffness refers to stress divided by corresponding strain [22]. The stiffness can be easily measured by Indirect Tensile Stiffness Modulus Test. by using ITSM Testing Machine. The test conducted was in accordance to EN 12697-26 Method for the determination of the indirect tensile stiffness modulus of bituminous mixtures which is a non-destructive test [23]. The test was conducted by applying five pulse loads with a suitable waveform (**fig 5**). This repeated load generates movement (strain) along the vertical plane of cylindrical specimen. The load was applied for a period of 0.1 seconds and rest period (load is released) of 0.9 seconds. Therefore, the stiffness modulus, S_m can be determined using the equation 1 below:

Figure 5: Indirect Tensile Stiffness Modulus Machine

$$Sm = F \times (m + 0.27) \div (z \times h) \tag{1}$$

S_m: indirect tensile stiffness modulus (MPa),
F: applied load (N),

z: mean amplitude of horizontal deformation obtained from 5 applied of the load pulse (mm),
h mean thickness of the test specimen (mm);
m: Poisson's ratio - 0.35 for temperature 15°C.

4.2 Fénix Test

A new experimental test has been developed by the Road Research Laboratory of the Technical University of Catalonia, Barcelona, Spain, to evaluate cracking resistance of asphalt concrete mixtures by calculation of the dissipated energy during the cracking process [21]. The Fénix test is used to calculate the dissipated energy during the cracking process, which is a combination of all energies released during material deformation and cracking [22]. The testing device can be seen in Figure 6 [21]. The evaluation of this energy is an effective way of measuring cracking resistance of asphalt concrete mixtures. In addition, the Fénix test generates tensile stresses around the cracking area, using the work done to propagate the crack across the induced plane **Figure 6**.
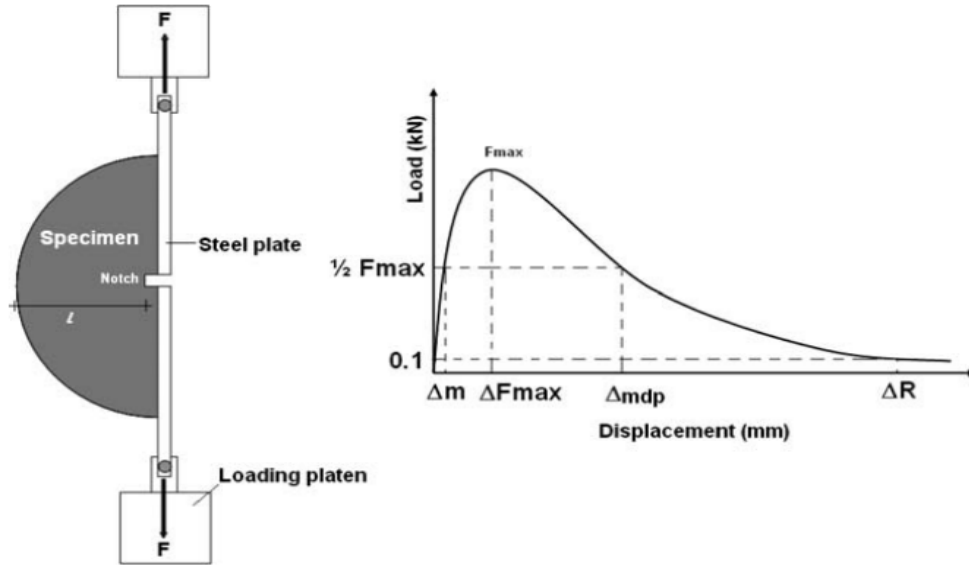
Figure 6: Fénix Test Setup and load-displacement output Curve [21].

The test procedure consists of subjecting one-half of a 63.5-mm thick cylindrical specimen with a diameter of 101.6 mm prepared by Marshall or gyratory compaction to a tensile stress at a constant displacement velocity (1 mm/min) and specific temperature [21]. A 6-mm deep notch is made in the middle of its flat side where two steel plates are fixed. The specimen is glued to the steel plates with a thixotropic adhesive mortar containing epoxy resins. Each plate is attached to a loading platen so that they can rotate about fixing points.

Load and displacement data are recorded throughout the test to calculate the parameters involved in the cracking process. The fracture energy during cracking, G_F, is calculated by Equations 1 [22]:

$$G_F = \frac{\int_0^{df} F(u) \cdot du}{S} \tag{1}$$

where
G_F: fracture energy (J/m^2)
F: load (kN)
u: displacement (mm)
S: specimen fracture surface (m^2)
df: displacement at the end of the test (mm). It is considered that the test ends at $4. 10^{-2}$ m of displacement.

The Tensile Stiffness Index (IRT) represents the slope of the stress-displacement curve between 25% and 50% of the peak load [22], and it is related to the mixture modulus. It is obtained using Equation 2:

$$\text{IRT} = \frac{0.5Fmax - 0.25Fmax}{d0.5Fmax - d0.25Fmax} \tag{2}$$

Where
IRT = tensile stiffness index) (kN/mm),
Fmax = peak load (kN), and
$d_{0.25Fmax}$ and $d_{0.5Fmax}$: displacement before peak load at 25 and 50% of the peak load (mm), respectively

The toughness index (TI) is defined as the fracture energy during the post-peak part of the curve, weighted by the displacement between the maximum load and 50% of maximum post-peak load, Eq. (3) [22]:

$$\text{TI} = \text{GF}.\Delta d = \frac{\int_{dfmax}^{df} F(u) \, . \, du}{S} . \left(d_{0.5PostFmax} - d_{Fmax} \right) \tag{3}$$

where
 TI: toughness index (J.mm/m^2)
 F: load (kN)
 u: displacement (mm)
 S: fracture surface (m^2)
dFmax and d0.5PostFmax: displacement at maximum load and displacement at 50% post-peak load (mm), respectively

Finally, the displacement at 50% post-peak load (d0.5PostFmax) has been considered as a parameter directly related to the ductility of the mixture, since it allows evaluating the type of fracture [22]

The experimental phase was made by preparing two Marshall Specimens for every mixture from control to modified mixtures. A sum of 12 Marshall Specimens were prepared to set the Fénix test on these mixtures. The test temperature was fixed at 25°C for all mixtures and the only factor that has been changed is the RAR content. A high accuracy laser thermometer was used to maintain the temperature at the value of 25°C. The Specimens were kept at the test temperature for 4 hours at least before testing.

5. Results and Discussion

5.1 Binders Testing Results

Table3 showed the results conducted on the un-modified and modified binders by physical testing to characterize the changes in their physical properties.

Table3: Conventional binder testing results for base and RAR binders.

RAR (%)	Penetration (1/10mm) - EN 1426-	Softening point (°C) -EN 1427-	Ductility (cm) -ASTM D113-07-	Elastic recovery (%) -EN 13398-
0	39,8	50,3	120	25,5
5	33	52,5	20,55	37,5
10	30,3	53	17,05	52,5
15	27,5	56	12,5	54,6
20	25,1	57,6	11,05	57,5
25	24,8	66,2	10,5	N/A

5.1.1 Standard penetration test (needle penetrometer) -EN 1426-

Needle penetrometer test is a method for measuring the consistency of bituminous binders, consistency in general is the way in which a substance holds together, the value of penetration is meant as indicator of how stiff the binder is at preselected temperature of 25°C, this penetration is measured in tenth of a millimeter.

Higher penetration values indicate softer binders while lower values indicate stiffer binders. Reacted and activated rubber (RAR) additive was used to modify the original bitumen 35/50 with different percentages 0, 5, 10, 15, 20 and 25% three replicates at 25°C of each sample were prepared and three readings of penetration values were taken for each replicate.

The results showed from **figure 7** that penetration values decreased with increase in RAR content. It indicates that penetration value at given temperature and for 35/50 binder was decreased with RAR content increased.
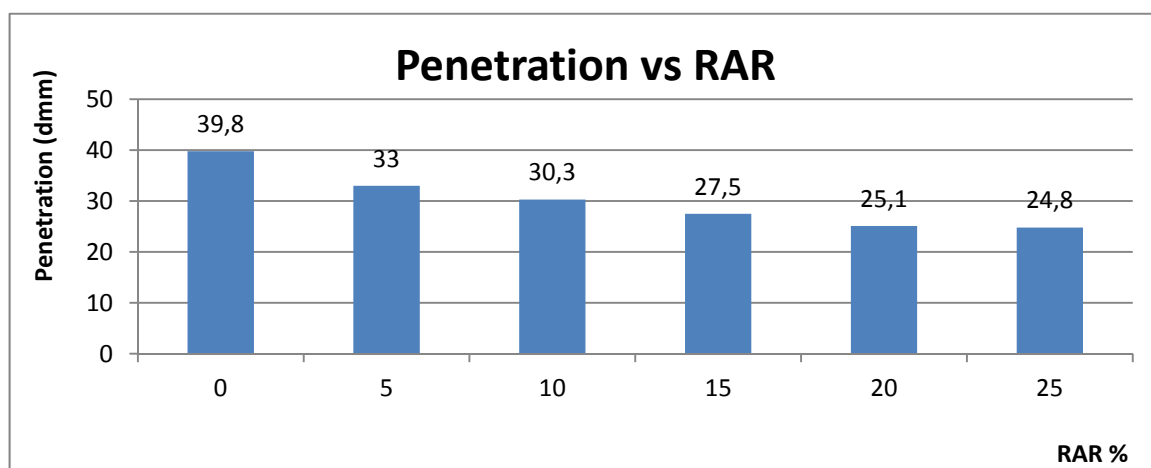
Figure 7: Penetration vs RAR %

Penetration Values obtained indicates that modified binder with RAR content will be performing better compared to neat bitumen to resist fatigue temperatures. The optimum value of RAR based upon the Standardized penetration test conducted would be 25%. Based upon the trend analyzed, even less penetration can be achieved with increasing RAR content.

5.1.2 Softening point (ring and ball) -EN 1427-

The softening point of bitumen is the temperature at which the substance attains certain degree of softening. So it the temperature in Celsius (°C) at which a standard ball passes through a sample of bitumen in mold and falls through a height of 2.5cm, when heated under water at specified conditions of test. The determination of softening point helps to know the temperature up at which a bituminous binder should be heated for various use applications. A binder should have sufficient fluidity before its application.

Two replicates of neat and other different modified bituminous binders were tested for their softening point. Temperature readings are collected when each of the steel ball touch the bottom plate. Two temperature readings were averaged for each replicate. The results of softening points are summarized in the **fig 8.**
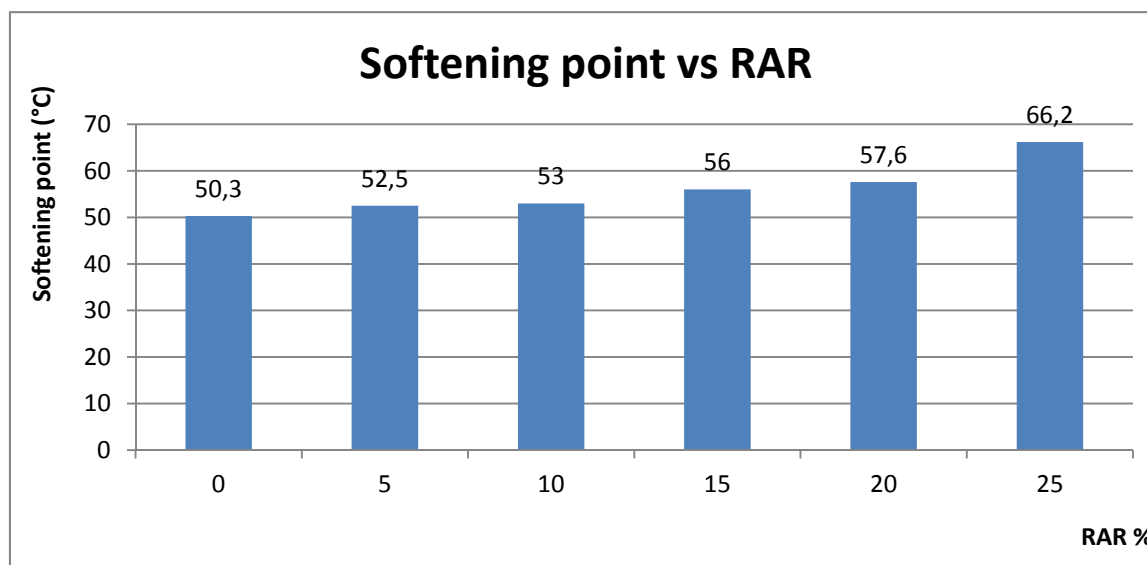
Figure 8: Softening point vs RAR %

The data of the fig supports that the greater the percentage of RAR, the greater the softening point. The more RAR, the stiffer the binder and the higher the temperature is needed to attain the softening point. Higher softening points indicate lower temperature susceptibility, and mitigation of rutting. Therefore, the optimum recommended value of RAR based upon the softening point test conducted would be 25 %, Higher values than 25% could be recommended to be studied further. Based upon the trend analyzed, the softening point can be increased.

5.1.3 Ductility -ASTM D113-07-

Ductility is the property of bitumen that permits it to undergo great deformation or elongation. Ductility is defined as the distance in cm, to which a standard sample or briquette of the material will be elongated without breaking. Dimension of the briquette thus formed is exactly 1 cm square. The bitumen sample is heated and poured in the mould assembly placed on a plate. These samples with molds are cooled in the air and then in water bath at 25°C temperature. Three replicates of neat and other modified binders were tested for their ductility test, elongation in cm were averaged for all the binders. The results are showed in the **figure 9.**
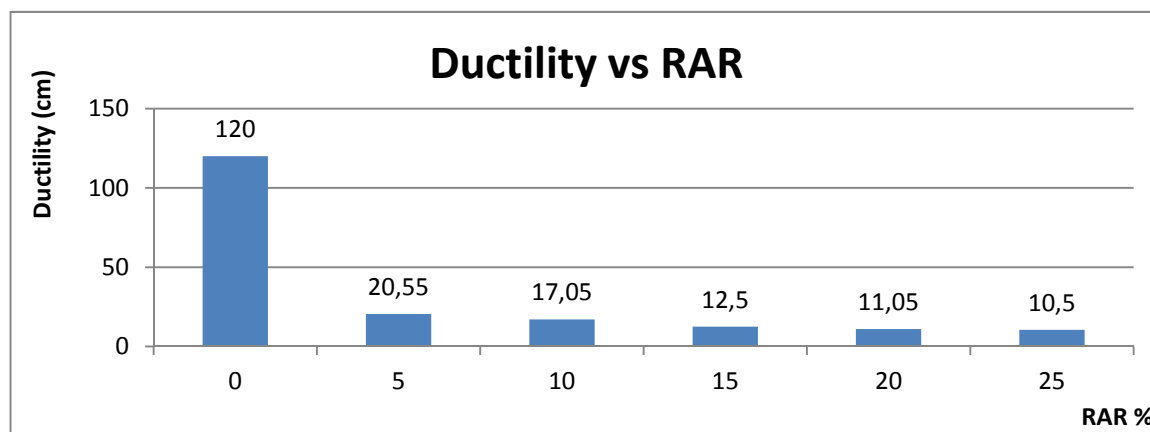
Figure 9: Ductility vs RAR %

The collected data form the fig showed that the modification of neat bitumen is sensitive for ductility test whatever the percentage of RAR. A decrease by 83% of ductility just for 5% of RAR, where the greatest decrease was showed for 25% of RAR by 91%. The analyzed trend is showing that slight changes in ductility of the modified binders have been seen. The optimum RAR content would be 5% of RAR. Better ductility could be seen for less RAR contents than 5%.

5.1.4 Elastic recovery -EN 13398-

The elastic recovery is a measure of the tensile properties of the polymer modified asphalt cement. The elastic recovery is measured by the percentage to which the asphalt cement residue will recover its original length after it has been elongated to a specific distance at a specified rate of speed and then cut in half. The distance to which the specimen contracts during a specified time is measured and the elastic recovery is calculated.

Three replicates for neat and modified bituminous binders were tested for their elastic recovery, the following **fig10** showed the results.
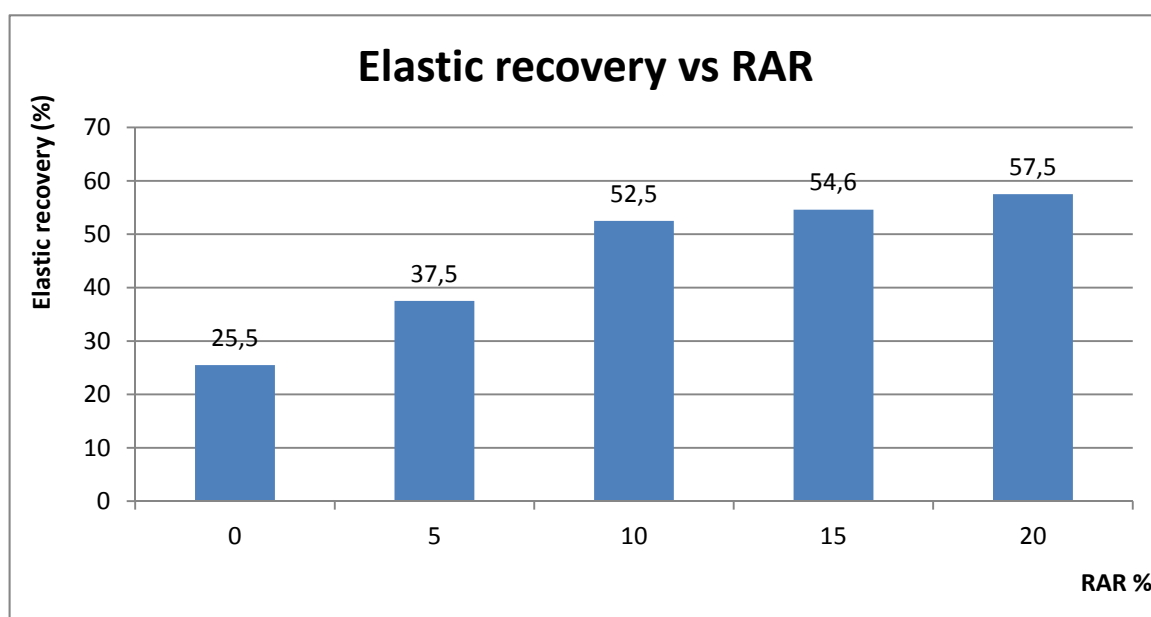
Figure 10: Elastic recovery vs RAR %

The collected data showed that the addition of reacted and activated rubber (RAR) has an effect on the elastic properties of modified bitumen binders, by increasing its elastic recovery. As it can be seen from the fig, the RAR content should not be equal or greater than 25% (elastic recovery not available). The optimum RAR content for 35/50 neat bitumen is 20%, higher elastic recovery may be reached for RAR content between 20 and 25%. The addition of RAR to neat bitumen improves the elastic properties.

5.2 Mixtures Testing Results

5.2.1 Shear Gyratory Compaction

We can find that the compactability of neat mixture when mixing temperature is 160℃ is equivalent to that of hot RAR mixtures when its mixing temperature is 180℃ for 5 and 10% RAR.

From the below fig 11, we can show that the apparent density and air voids of the control, 5 and 10 RAR is approximately the same, this is due to the low un-dispersed swelled RAR contents (low weight) and the difference in viscosity also of the modified bitumens. So it is clearly that the effect of un-dispersed RAR particles and viscosity of modified bitumens play a role very important on the apparent density of the mixtures.
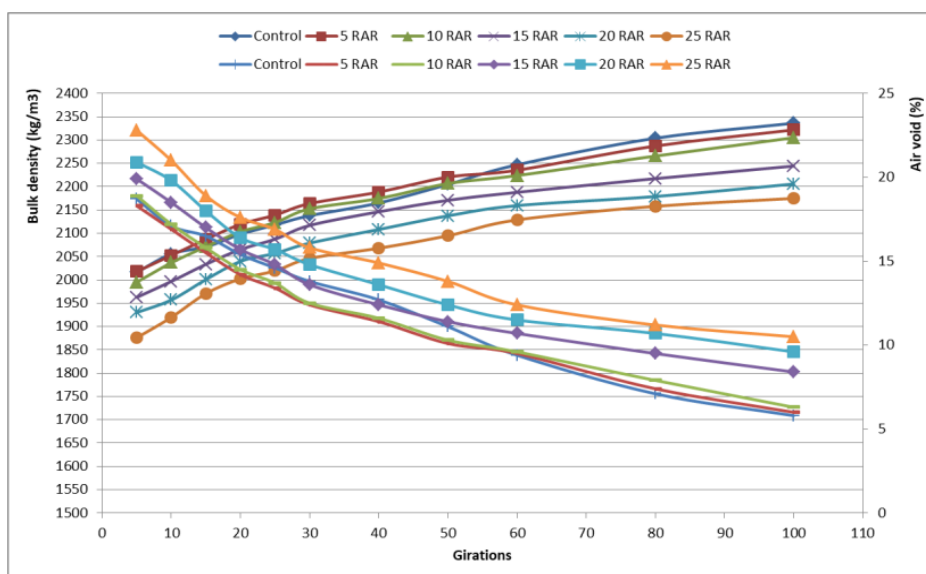
Figure 11: Effect of RAR content on the Apparent Density and air voids of the Mixtures

For 15, 20 and 25% RAR, we see lower densities and higher air voids of the mixtures respectively which is expected because of the high RAR contents that increase considerably the viscosity, for example, at 80 gyrations the lowest density is 2150kg/m³ (25% RAR) and the highest one is 2200kg/m³ (15% RAR)which confirms previous comments. So, starting from 15% RAR, the compactability become an issue due to the increase in viscosity. For 25% RAR the density decreased considerably because of the increase in viscosity.

As it can be seen from the above fig 11, the effect of increasing gyrations number result in reducing the Air voids for all Mixtures, for example, for 25% RAR the higher air voids was 22.625% for 5gyrations and 10.057% for 80 gyrations which is considerable.

While the trend was not observed for 15, 20 and 20% of RAR mixtures, the results showed the effect of viscosity of these ;mixtures on their compactability by showing less densities and higher air voids which is expected as these mixtures need higher compaction temperatures above 180°C. At 80 gyrations, the 25, 20 and 15% RAR have the lowest densities and highest air voids respectively as shown in the fig 11 which confirms the comments.

5.2. 2Indirect Tensile Stiffness Modulus.

Figure 12 shows the ITSM results for temperature of 15 °C. The results showed that the stiffness modulus apparently increases with the increasing percentage from 10 to 25% RAR. The modified mixture showed an increase of stiffness modulus with highest value for 15% RAR. Meanwhile, this is due to the hardening of the bituminous

binder as RAR percentage increased. For higher contents of RAR typically 25% there is improvements in the stiffness regarding the conventional but lower than 10, 15 and 20% RAR.
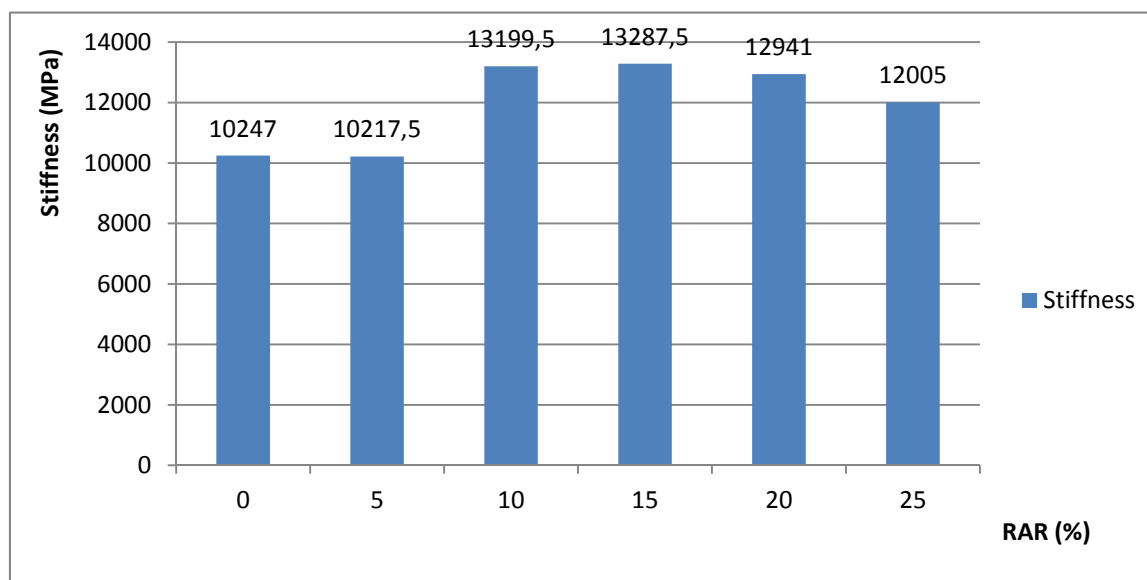

Figure 12: Effect of RAR content on the Stiffness Modulus of bituminous mixtures at 15°C.

Finally, to determine the effect of the reacted and activated rubber on the bearing capacity of the mixes, an indirect tensile stiffness modulus test were performed (see figure 11), the RAR mixes had a higher stiffness modulus value than the reference mix. In fact, this may even be dangerous because an excessive increase in mix stiffness can cause crack reflection in the pavement.

The results also showed that the addition of RAR increases the stiffness of the mixtures, this is converged with physical results of the modified binders especially the penetration, ductility and softening point. That means that RAR modified mixtures would have better rutting resistance and bleeding.

The use of this technique also reduced bitumen penetration, which hardened the mix and increased the stiffness modulus. Nonetheless, it should be underlined that an overly stiff mix can cause the road surface to crack. Because the pavement is not as elastic which is not the case, crack propagation energy is dissipated to a much lesser extent. It was observed that in this climate (15°C), the stiffness modulus of the mix increased. Even though the bitumen is slightly harder (with lower penetration), the elastic rubber particles dissipate the energy applied by traffic loads. Consequently, it had a lower stiffness response (and thus a better performance under temperature-induced stresses and strains).

5.2.3 Cracking Resistance

5.2.3.1 Tensile Forces

Figure 13 shows the difference in behavior between tested mixtures. The initial increased slope of the load-displacement curve represents the stiffness while the rapidly dropping post-peak curve provides a sense of the brittleness of the binder [13]. Thus, it can be observed that the 15 RAR modified binder reflects the higher stiffness and brittleness at a test temperature of 25°C. The figure also showed that 15 % of RAR the peak force was increased considerably, therefore for 20 and 25 % of RAR this force was decreased by much of 50% and 60% respectively because of the such stiffness that they have reached.
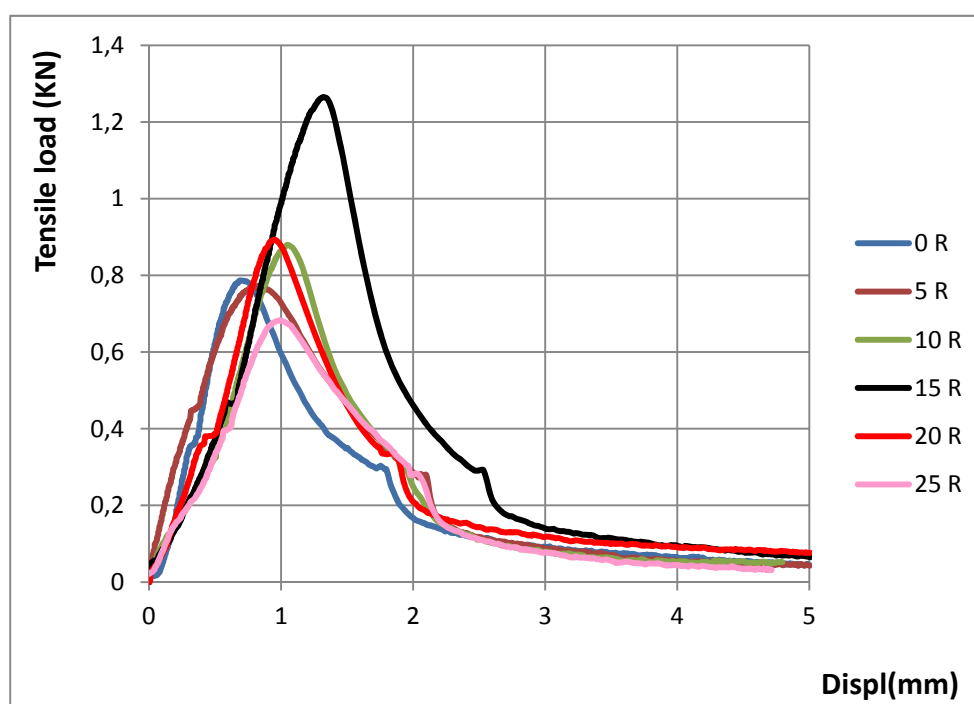
Figure 13: Load-displacement curve at a test temperature of 25°C

Based on this output curve, the parameters involved in the cracking process are obtained. The mean values for fracture energy, tensile stiffness index, toughness index and displacement at 50% post-peak load were obtained from three individual results.

The maximum tensile load was recorded for 15% of RAR which is expected returning to the hard bitumen used (35/50) and considerable decrease in these tensile forces for higher contents of RAR.

5.2.3.2 Fracture energy (Gf)

Figure 14 illustrates the change in fracture energy, which represents the work required for crack initiation, with RAR content for all the tested mixtures: conventional and RAR-MB. The fracture energy clearly varies on the basis of the content of RAR incorporated in the binder.
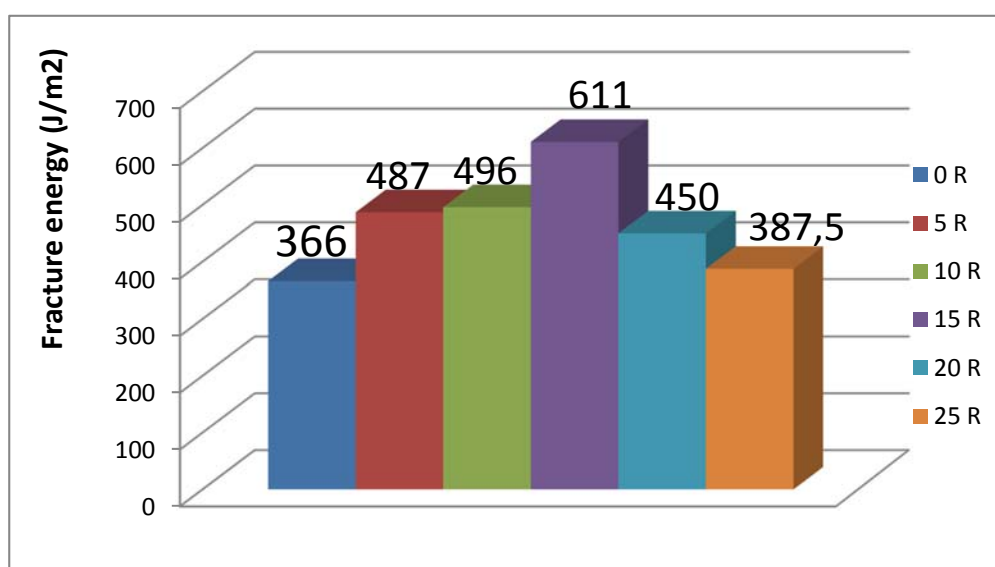

Figure 14: Fracture energy versus RAR content at 25°C

It is observed that asphalt binders reach a maximum of the fracture energy at 15 of RAR. An increase is observed in the fracture energy as RAR content increase for 5, 10 and 15% because these modified binders have reached a better stiffness with low decrease in ductility, this stiffness increased considerably for 20 and 25% of RAR in such a way the binder became stiffer and it lost of ductility which results in lowest fracture energy. The high stiffness and loss of ductility are the two reasons that make the 20 and 25 RAR modified binders more susceptible to thermal cracking.

5.2.3.3 Displacement at 50% post-peak load

The displacement at 50% post-peak load (d0.5PostFmax) has been considered as a parameter directly related to the ductility of the mixture, since it allows evaluating the type of fracture [22], fig15 showed an increase in max load for 10, 15 and 20% RAR because of the stiffening of the binder after modification while keeping some ductility
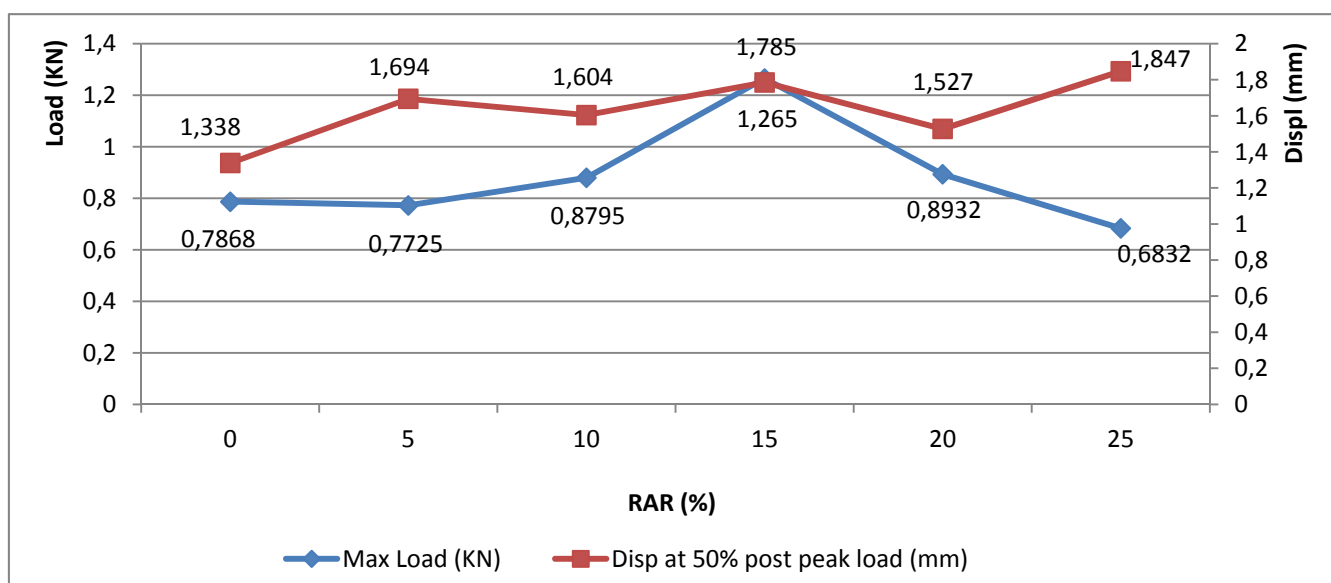
Figure 15: Max load and displ at 50% post peak load versus RAR content

From 15% RAR, the max load was still decreasing until it got the lowest value for 25% RAR, this is expected due to the increasing in consistence of the binder for all RAR percentages, displacement at 50% post peak load is increasing which means a decrease in ductility, this hypothesis is confirmed with previous results on binders for ductility test, it should be mentioned that high max load values and low displacements at 50% post peak load did not mean better performance.

5.2.3.4 Tensile stiffness index (IRT)

The tensile stiffness index assesses the tested specimen modulus or the stiffness of the mixture. Tensile stiffness index values strongly decrease with increasing of RAR content for all asphalt binders. The obtained results are clear not converged with ITSM previous results (**Figure 16**).
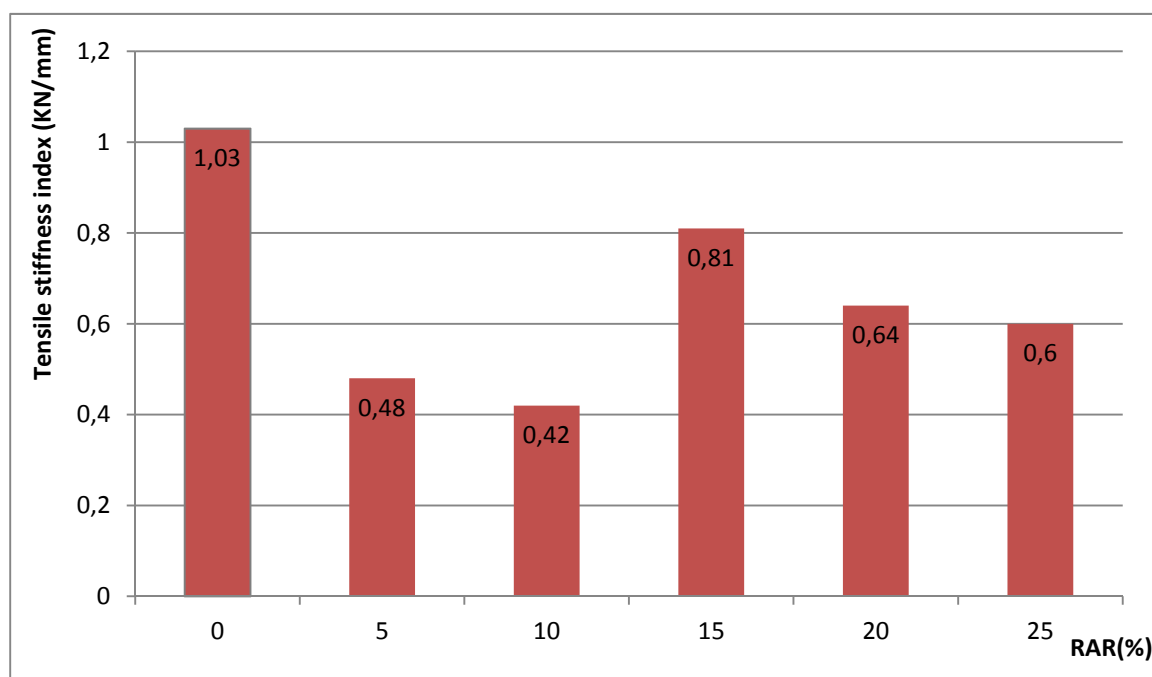
Figure 16: Tensile stiffness index versus RAR content at 25°C

The same trend is observed for all the tested mixtures. The results don't coincide with penetration grade tests as it indicates the increase of consistency with RAR content increase except for 25% of RAR which shows a decrease in the stiffness for non-explanation.

5.2.3.5 Toughness index (TI)

The toughness index gives a measure of the ability of the binder to resist cracking fracture after reaching maximum resistance. In other words, it assesses whether the type of fracture is more or less ductile.

Indeed, the toughness index is defined as the fracture energy after achieving the peak load weighted by a post-peak displacement. For this reason, the obtained patterns are consistent with the energy fracture patterns.
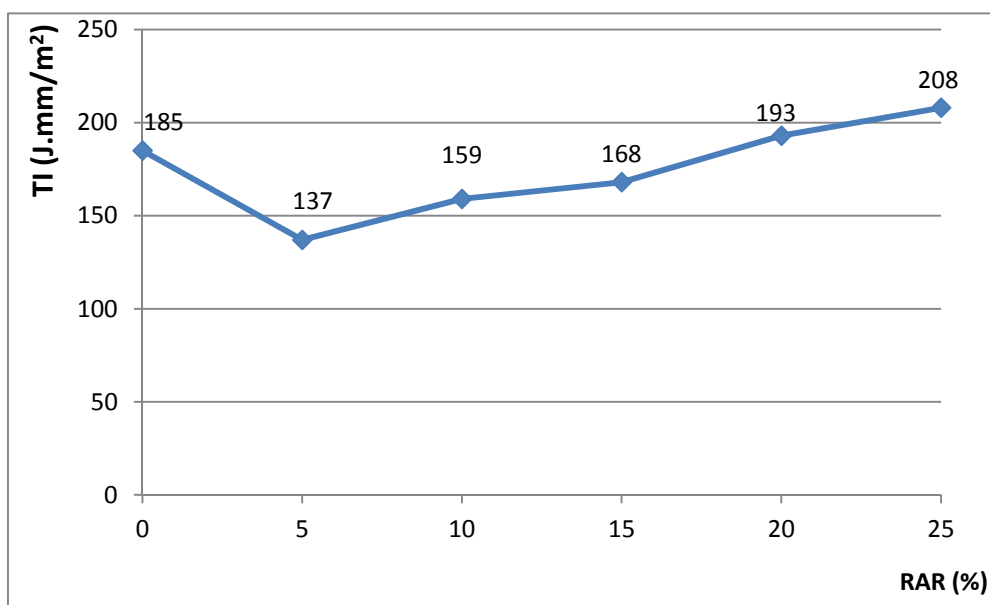
Figure 17: Toughness index versus RAR content at 25°C

Results indicate that high penetration binders (low RAR content) become tougher and more ductile at intermediate temperatures, although at 25°C the toughness index is not highest for 05 RAR content due to the hardening process that leads to a reduction in binder ductility that leads to a brittleness fracture. Where the lowest value of TI was recorded to 05% of RAR modified mixture (**fig 17**).

Conclusion

From this modest research, it can be said that the reacted and activated rubber (RAR) as an alternative solution to enhance the mechanical performance of bituminous mixtures by modifying the base bitumen and gain high mechanical performance over conventional bituminous mixtures, incorporating the RAR through dry process in our road pavements participates in recycling end of life tires from landfill and develops a sustainable solutions to environment by find a practical ways to deal with end of life tires pollution problem.

The main conclusions and findings that can be warranted based on the analysis presented in this paper are as follows:

1. The modification of bitumens by reacted and activated rubber can enhance the physical and mechanical properties of binders and mixtures.
2. The modification by reacted and activated rubber enhances the physical properties of the binders by decreasing its penetration and increasing softening point, it also enhances the elastic properties by increasing the elastic recovery.

3. The modification by reacted and activated rubber affects the ductility of the binder considerably by decreasing this ductility at lowest and highest contents of RAR.
4. The modification by reacted and activated rubber affects the compactability of mixtures. Especially for high RAR contents while no effects have been seen for lower RAR contents.
5. The Stiffness of the RAR mixtures is increased above the conventional; this is due to the increase in consistency of RAR modified bitumens as showed by Penetration and softening point results.
6. The RAR modified mixtures increase the tensile forces of binders which are translated to better cracking resistance of bituminous mixtures.
7. From the results of Fénix test, the RAR modified mixtures increase the fracture energy of binders which are translated to better cracking resistance of bituminous mixtures.
8. 15% RAR is the most suitable content for this hard bitumen returning to previous results.

Acknowledgments

References

[1] Jorge B .Sousa, Andrey .V, Geoffrey M. Rowe, and Llan Ishai, "Reacted and activated rubber, Elastomeric asphalt extender", Transportation Research Record, Journal of the transportation research board, No 2371, Washington D.C; 2013, pp 32-40.

[2] Baya T L. Purnomo, Latif B . Superman, Agus T. Mulyono,"Laboratory Study of the use of additional reacted and activated rubber (RAR) materials on asphalt concrete wearing course(AC-WC) mix", Inter . Journ of multidiscipline Science (IJ-MDS), 2019, pp10-18

[3] Sampat . K, Gourab . Saha, Krishna P. Biligiri, Jorge B. Sousa, "Performance characterization of reacted and activated rubber modified dense graded asphalt mixtures " Conference paper, January 2017.

[4] Sampat . K, K . P . Biligiri, and Jorge B Sousa." Advanced Rheological characterization of reacted and activated rubber modified asphalt binders". Constr and Build materials, Vol 122, 2016, PP 12-22.

[5] Kedarisetty .S, "Performance characterization of reacted and activated rubber (RAR) modified dense graded asphalt mixtures", master of technology thesis, Indian Institue of technology Karagpur , India, May 2016.

[6] L. Ishai, G. Svechinsky, Jorge. B. Sousa," Introducing an activated mineral as innovative binder-stabilizer for SMA paving mixtures " Compendium, International road congress on innovation in road infrastructures, International road federation- IRF, Moscow, Russia, 2011.

[7] Jorge B. Sousa, A. Vorobien, L. Ishai, G. Svechinsky," Elastomeric asphalt extender – A new frontier on asphalt rubber mixes ", in 5th international asphalt rubber conference, Munich, Germany, Oct 2012.

[8] EN 1426:2015, Bitumen and bituminous binders- determination of needle penetration.

[9] EN 1427:2015, Bitumen and bituminous binders- determination of softening point- ring and ball method.

[10] ASTM D113-07: Standard test method for ductility of asphalt materials.

[11] EN 13398: Bitumen and bituminous binders: determination of the elastic recovery of modified bitumens.

[12] ASTM C127-15: Standard test method for relative density (specific gravity) and absorbtion of coarse aggregates.

[13] ASTM C128-15: Standard test method for relative density (specific gravity) and absorbtion of fine aggregates.

[14] EN933-1:2012: Tests for geometrical properties of aggregates, determination of particle size distribution . sieving method

[15] EN933-8:2012: Tests for geometrical properties of aggregates, part 8: assesment of fines-sand equivalent test.

[16] EN933-9:2012: Tests for geometrical properties of aggregates, part 9: assesment of fines-methylene bleu test.

[17] EN1097-2:2010: Tests for mechanical and physical properties of aggregates, methods for the determination of resistance to fragmentation.

[18] EN1097-1:2010: Tests for mechanical and physical properties of aggregates, methods for the determination of resistance to wear (Micro-deval).

[19] EN12697-31:2007: Bituminous mixtures test methods for hot mix asphalt, Specimen preparationby gyratory compaction.

[20] EN12697-26:2007: Bituminous mixtures test methods for hot mix asphalt, Stiffness.

[21] Félix Pérez-Jiménez and al, 'Fenix Test, development of a New Test Procedure for Evaluating Cracking Resistance in Bituminous Mixtures', *Transportation Research Record: Journal of the Transportation Research Board*, pp 36-44, 2010.

[22] Livia Garcia-Gil, Rodrigo Miro, Félix. E. Pérez-Jiménez, "New approach to characterize cracking resistance of asphalt binders, Constru. Build. Mater 166 (2018) 50-58.

[23] X. Li, M. Marastneau, "Cohesive modeling of fracture in asphalt mixtures at low temperatures", Int. Journ. Fract. 2005.

[24] J. Zhang, A.N. Faruk, P. Karki, I. Holleran, X. Hu, L. Walubita, Relating asphalt binder elastic recovery properties to HMA cracking and fracture properties, Constr. Build. Mater. 121 (2016) 236–245.

[25] R. Velasquez, H. Tabatabaee, H. Bahia, Low temperature cracking characterization of asphalt binders by means of the single-edge notch bending (SENB) test, J. Assoc. Asphalt Paving Technol. (2011)

[26] J. Liu, S. Zhao, L. Li, P. Li, S. Saboundijan, Low temperature cracking analysis of asphalt binders and mixtures, Cold Reg. Sci. Technol. 141 (2017) 78–85.
[27] U. Isacsson, H. Zeng, Cracking of asphalt at low temperature as related to bitumen rheology, J. Mater. Sci. 33 (1998) 1265–2170.

[28] Xiao F., Amirkhanian S.N. and Juang H.C. (2009) " Prediction of Fatigue Life of Rubberized Asphalt Concrete Mixtures Containing Reclaimed Asphalt Pavement Using Artificial Neural Networks" Journal of Materials in Civil Engineering, Vol. 21, No. 6, pp.253-261, 2009

[29] Daniel, J. S., and Kim, R. Y. (2001) "Laboratory Evaluation of Fatigue Damage and Healing of Asphalt Mixtures." Journal of Materials in Civil Engineering, Vol. 13, 434-440.

[30] Xiao F. and Amirkhanian S.N. (2009 " Asphalt Binder Rheology Sensitivity Investigation on Resilient Modulus of Rubberized Mixtures Using Artificial Neural Network Approach" Journal of Testing and Evaluation (ASTM), Vol. 37, No.2, pp. 129-138, 2009.

Sistem de Securitate pentru Zonele de Acces din Instalațiile Electrice de Distribuție

Security System for Access Areas in Electrical Distribution Installations

Cristina Gabriela Sărăcin[1], Cornel-Ovidiu Ivan[1]

[1]Universitatea Polithnica din București, România
Splaiul Independenței Nr.313
E-mail: cristina.saracin@upb.ro, icornel14@yahoo.com

Rezumat.– *Această lucrare prezintă o soluție viabilă pentru asigurarea securității instalațiilor fixe de alimentare ale sistemului de distribuție electrică. Transmisia energiei electrice către consumatori casnici sau industriali se face prin rețele locale private și prin rețeaua publică. În aceste condiții, devine posibil accesul persoanelor neautorizate la instalațiile electrice de distribuție. Având în vedere acest aspect, lucrarea pune accentul pe securitatea distribuitorilor de energie electrică și metodele lor de securizare a zonelor de acces în instalațiile de distribuție a energiei electrice. Pentru fiecare zonă din cadrul unei instalații de distribuție electrică este identificat nivelul ei de accesibilitate rezultat din gradul de vulnerabilitate. Având în vedere acest aspect, trebuie luate măsuri de securizare a stațiilor de distribuție pentru a preveni potențialele consecințe negative asupra sistemului de distribuție a energiei electrice. Securitatea instalațiilor de distribuție electrică în contextul managementului de energie electrică în timp real din cadrul unui dispecerat energetic, conduce la creșterea nivelului de protecție al infrastructurilor critice naționale și europene.*

Cuvinte cheie: instalații electrice de distribuție, securitate zone de acces

Abstract.– *This paper presents a viable solution for ensuring the security of the fixed power supply installations of the electrical distribution system. The transmission of electricity to domestic or industrial consumers is done through local private networks and through the public network. Under these conditions, it becomes possible for unauthorized persons to access the electrical distribution installations. Given this aspect, the paper focuses on the security of electricity distributors and their methods of securing access areas in electricity distribution facilities. For each area within an electrical distribution installation, its level of accessibility resulting from the degree of vulnerability is identified. In view of this, measures must be taken to secure the distribution stations in order to prevent potential negative consequences for the electricity distribution system. The security of electricity distribution installations in the context of real-time electricity management within an energy dispatcher, leads to increasing the level of protection of national and European critical infrastructures.*

Key words: electrical distribution installations, security access areas

1. Introducere

Riscul rațional sau acceptat reprezintă modalitatea de acțiune bazată pe perceperea în cunoștință de cauză a gradului de amenințare și de vulnerabilitate. Riscul se minimizează în măsura în care alegerea variantei de contracarare a pericolului se optimizează. Securitatea reprezintă conceptul care poate răspunde dorințelor de siguranță și stabilitate necesare bunei funcționări a sistemelor. [3]

Sistemul de securitate constă în ansamblul de echipamente, dispozitive și subsisteme specifice care asigură protecția instalațiilor electrice de distribuție. Subsistemele specifice, interconectate constructiv și procesual, îndeplinesc următoarele funcții: protecție perimetrală, control acces, detecție și avertizare la efracție, supraveghere prin CCTV, detecție și semnalizare/stingere la incendii, inundații și alte pericole, comunicații de securitate, monitorizare, comandă și control. [4]

Din amenințările uzuale, putem evidenția următoarele: factorul uman, echipamentele electrice, rețeaua de transmisie a informație.

Vulnerabilitățile pot fi datorate următoarelor [5]:
- protecție fizică slabă a obiectivelor;
- sisteme tehnice neperformante (surse de alimentare, unități de procesare, servere de baze de date , software necontrolat , etc);
- protecție informațională inadecvată.

2. Sistemul de control acces al stației de distribuție

Sistemul de control acces monitorizează intrarea în stațiile de distribuție. Scopul acestuia este de a oferi acces rapid persoanelor autorizate, restricționând accesul persoanelor neautorizate. Prima variantă studiată o reprezintă sistemul realizat cu controlere principale și secundare (figura 1).
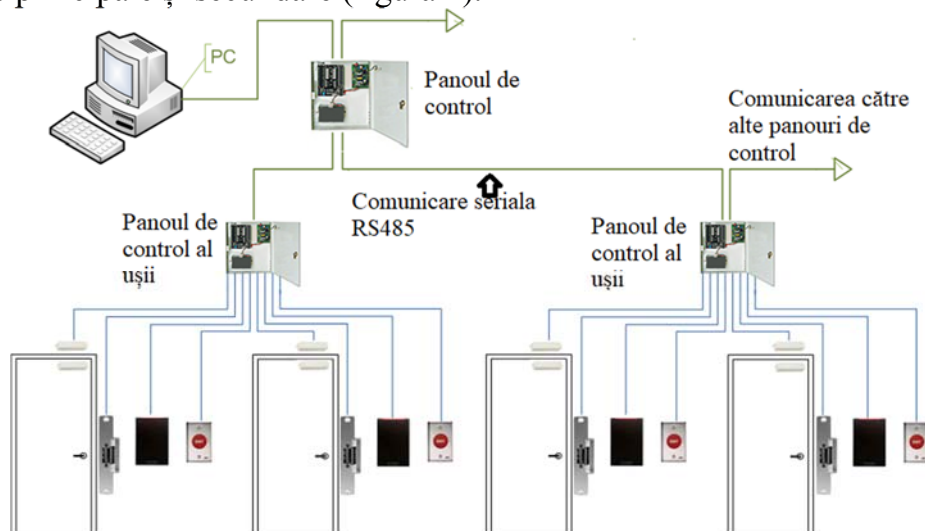

Fig. 1. Schema de conectare a controlerelor principale și secundare

Toate echipamentele pentru uși sunt conectate la controlere secundare (de ușă sau interfețe pentru uși). Controlerele secundare, de obicei, nu iau decizii privind accesul și înaintează toate cererile controlorilor principali. Pentru control acces se utilizează cititorul de identitate. Rolul acestuia este de a căuta într-o bază de date un anumit indicativ. În cazul identificării se acționează electric yala și se permite accesul în cameră.

A doua variantă studiată este compusă din controlere principale seriale și cititoare inteligente (figura 2). Toate echipamentele pentru uși sunt conectate direct la cititoare inteligente sau semi-inteligente. Cititorii de obicei nu iau decizii de acces și înaintează toate cererile către controlorul principal. Doar dacă conexiunea cu controlerul principal nu este disponibilă, cititorii vor utiliza baza lor de date internă pentru a lua decizii de acces și a înregistra evenimente. Cititorul semi-inteligent, care nu are o bază de date și nu poate funcționa fără controlerul principal poate fi utilizat în zone care nu necesită securitate înaltă. Criteriile de risc sunt stabilite în funcție de destinația încăperilor aferente stației de distribuție.
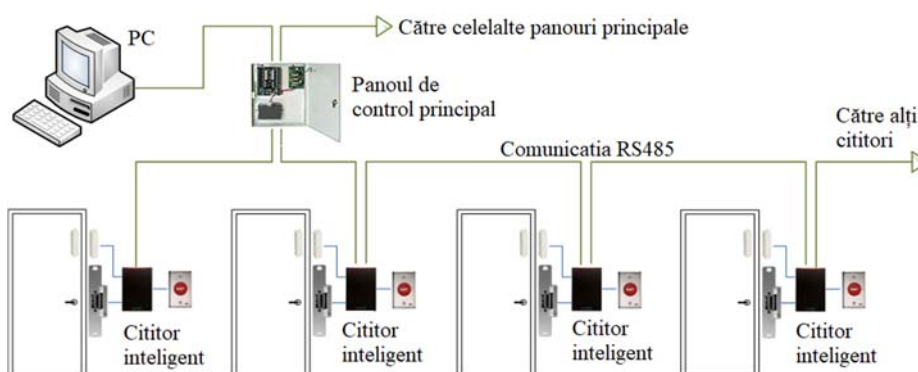

Fig. 2. Schema de conectare a controlerelor principale cu cititori inteligenți

A treia variantă studiată este compusă din controlere seriale cu servere terminale (figura 3).
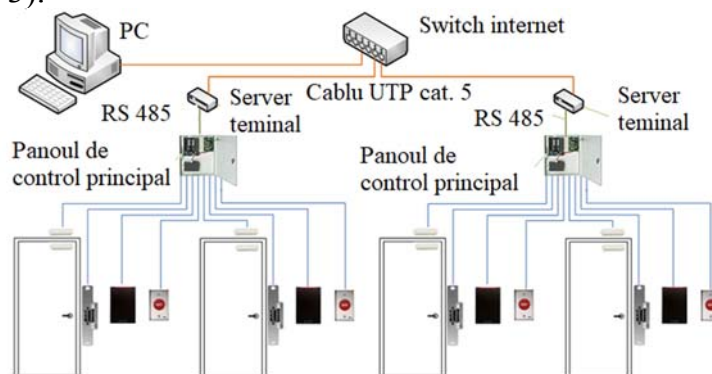

Fig. 3. Schema controlerelor seriale cu servere terminale si panouri ce conțin adrese IP

Avantajele acestui sistem de control acces sunt următoarele:
- utilizează infrastructura de rețea existentă;

- utilizează un număr nelimitat de controlori;
- comunicarea cu controlerele se realizează la viteza rețelei;
- în cazul unei alarme, controlerele pot iniția conexiunea cu PC-ul gazdă.

Orice sistem de control acces prezintă și dezavantaje. Acestea constau în:
- întârzieri în caz de defecțiuni de trafic intens și de echipamente de rețea;
- accesul hackerilor la rețeaua stațiilor electrice;
- distanța maximă de la hub la controler de peste100 de metri.

3. Proiectarea sistemului de control acces

Proiectarea sistemului de control acces implică definirea zonelor pentru care se realizează acest sistem. Arhitectura sistemul (figura 4) a fost creată în programul AUTOCAD 2D.
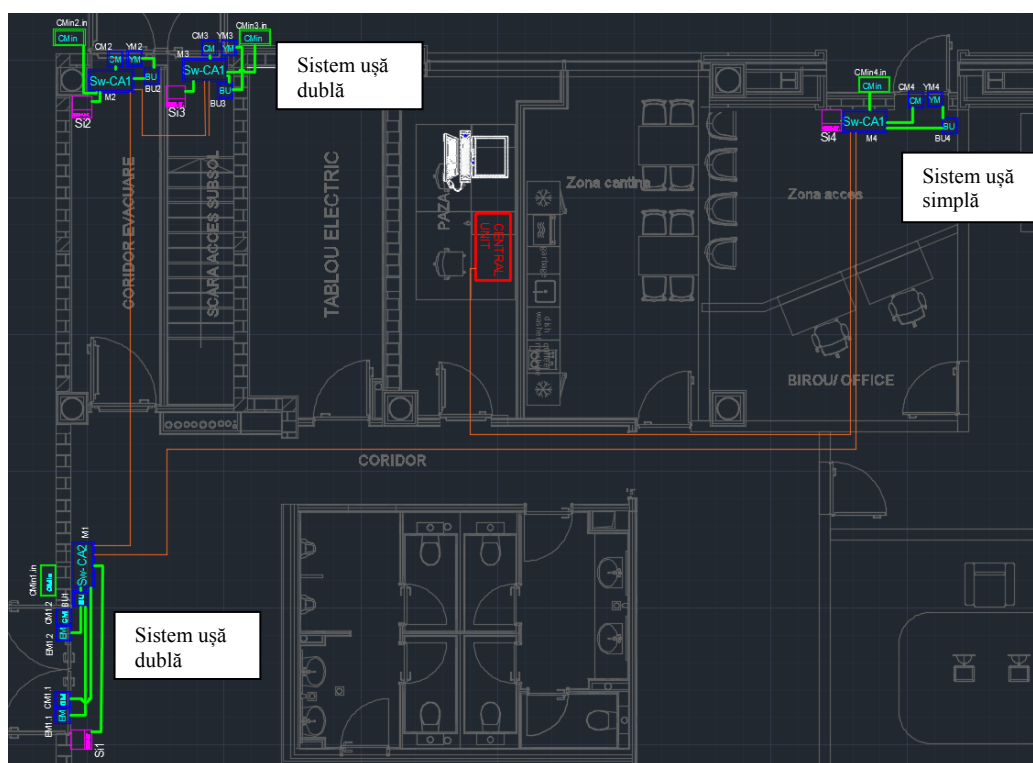

Fig. 4. Integrarea sistemului de control acces

Stația electrică conține o zonă de comandă unde se supraveghează buna desfășurare a procesului de distribuție a energiei electrice. Totodată se mai regăsesc camere tehnice, zone de birou și zone de depozitare. Există trei uși de acces către exterior pentru care se realizează sistemul de control acces.

Filtrele de control acces sunt de tip unidirecțional cu cititoare de carduri prevăzute la intrarea în spațiu, ieșirea realizându-se apăsând butonul de ieșire ce se regăsește pe interiorul fiecărei uși. Ușile vor fi prevăzute și cu o sirenă cuplată la sistemul de control acces pentru a avertiza persoanele din zona atunci când ușa se deschide. Sistemul va fi configurat astfel încât orice utilizare a ușilor să fie

semnalizată. Ușile de evacuare sunt prevăzute cu Panic-bar și vor fi echipate cu yală electromagnetică astfel încât acționarea Panic-bar-ului să întrerupă alimentarea cu energie electrică a yalei electromagnetice.

Modulele de control acces pentru una sau două uși, vor fi prevăzute cu sursă și acumulator de 5Ah inclus și comunicație RS485 cu centrala de control acces. În cazul apariției unui incendiu în această zonă, sistemul de control acces va primi o comandă de la sistemul de detecție incendiu prin care, ușile vor fi deblocate, permițând astfel evacuarea persoanelor în cel mai scurt timp. Această comandă va fi transmisă către sistemul de control acces printr-un releu cu o ieșire integrată în sistemul de detecție incendiu.

4. Sistem de securitate antiefracție și protecție perimetrală

Elementele constitutive ale sistemului de securitate sunt următoarele: senzorii de efracție, centrala, echipamentele periferice ale centralei, dispozitivele de avertizare locală și dispozitivele de comunicare la distanță.

Senzorii preiau o informație de tip stare de alarmă. Centrala procesează informațiile preluate de la senzori în funcție de starea sistemului (activat, dezactivat). Echipamentele periferice ale centralei sunt modulele de expandare și interfețele de comandă. Modulele de expandare au rolul de a extinde numărul de intrări și/sau de ieșiri ale centralei pentru configurarea unor sisteme de capacitate sporită. Interfețele de comandă au rolul de a permite utilizatorilor să comande diferite funcțiuni ale sistemului. Aceste interfețe pot fi contacte cu o cheie specială de securitate, tastaturi sau cititoare de tag-uri de acces, cititoare biometrie, etc.

Dispozitivele de avertizare locală pot fi optice, acustice sau opto-acustice (mixte). Rolul acestor dispozitive este de a semnaliza o stare de alarmă.

Dispozitivele de avertizare la distanță sunt comunicatoare care utilizează diferite canale de comunicație pentru a semnaliza o alarmă la un dispecerat de monitorizare și intervenție.

Pentru stația electrică există următoarele zone:
- instantanee – declanșează instantaneu o alarmă;
- temporizată –activarea generează o temporizare internă a sistemului (zonele de intrare/ieșire respectiv, urmărire);
- de panică-atac la persoană– declanșează o alarmă silențioasă;
- de sabotaj/defecțiune tehnică – sunt zone de 24 de ore utilizate pentru monitorizarea securității sistemului (contactele anti sabotaj ale dispozitivelor).

Realizarea unui sistem de securitate la efracție și control acces este un proces structurat pe mai multe etape și-anume [11,12]:

a) Evaluarea nevoilor obiectivului implică necesitatea de supraveghere (totală sau parțială);

b) Planificarea și proiectarea se realizează prin: selectarea tipurilor de detectoare și poziționarea acestora; partiționarea sistemului de securitate; asigurarea

mijloacelor pentru controlul sistemului şi pentru afişarea indicaţiilor sale; asigurarea surselor de alimentare; realizarea circuitelor.

În ceea ce priveşte unităţile centrale, cele de multiplexare, interfeţele de acces şi interfeţele om–maşină, criteriile sunt următoarele:

a. pentru centrale, multiplexoare şi interfeţe de acces, acestea vor fi amplasate în spaţii protejate şi accesibile numai personalului tehnic de întreţinere. Dacă există camere tehnice dedicate amplasarea elementelor de structură a sistemului antiefracţie va fi făcută în cadrul acestora în măsura în care distanţele maxime specificate pentru dispozitive faţă de unităţile de multiplexare nu sunt depăşite.

b. interfeţe om-maşină – tastaturile de control şi cititoarele de taguri de acces sau identificatoarele biometrice vor fi amplasate ergonomic şi accesibil utilizatorilor. Înălţimea de montaj recomandată este de 1,40 m faţă de pardoseală. O atenţie deosebită se va acorda poziţionării cititoarelor de „taguri" RFID astfel încât acestea să nu interfereze electromagnetic, atât între ele cât şi cu alte echipamente potenţial generatoare de zgomot RF cum ar fi monitoarele TV.

Pentru sistemele de securitate antiefracţie [3,6], afişarea mesajelor generate de sistem se face de regulă prin intermediul tastaturilor. Acestea trebuie amplasate în zone supravegheate (protejate de senzori de mişcare) pentru a preveni tentativele de accesare frauduloasă. Numărul acestor tastaturi depinde de partiţionarea şi funcţionarea sistemului. Unele obiective au prevăzute dispecerate locale de pază la care, chiar dacă sistemul este monitorizabil prin intermediul unui PC, este obligatorie instalarea unei tastaturi de sistem pentru asigurarea funcţionării în caz de avarie electrică. În afară de tastaturi de sistem şi pachete software pentru interfeţele grafice pot fi utile şi panouri sinoptice pentru o mai bună localizare a alarmelor.

Unul din aspectele cele mai importante în asigurarea funcţionării corecte a sistemelor de securitate antiefracţie şi control al accesului îl reprezintă alimentarea cu energie electrică. La stabilirea soluţiei de alimentare trebuie avute în vedere următoarele reguli:

a. toate sursele de alimentare se conectează pe aceeaşi fază printr-o siguranţă dedicată în tabloul general. De preferinţă, în camera tehnică va fi amplasat un al doilea tablou de siguranţe dedicate diferitelor subsisteme de securitate.

b. pot fi luate în considerare diferite modalităţi de asigurare a backup-ului. Pentru sistemele antiefracţie şi control al accesului backup-ul se realizează pe partea de joasă tensiune cu acumulatoare tampon dar, pentru sisteme mari se pot lua în calcul UPS-uri pe alimentarea cu 230V$_{AC}$.

c. dimensionarea raportului secţiune/lungime pentru cablurile de alimentare trebuie atent analizată pentru a păstra tensiunea de alimentare a echipamentelor în limitele impuse de producător. O atenţie deosebită trebuie acordată în cazul alimentării pe sursa de back-up (acumulator) – în cazul acesteia, tensiunea furnizată scade până la 10,8V, valoare la care acumulatorul este considerat descărcat.

Amplasarea modulară a surselor de alimentare pe tronsoane (segmente) de sistem trebuie să ţină cont de încărcarea maximă a fiecărei surse şi de posibilitatea de a asigura încărcarea acumulatoarelor tampon. În consecinţă, calculul energetic va fi efectuat pe fiecare segment de sistem alimentat de o sursă. Se efectuează un calcul

energetic pentru a estima întreg consumul sistemului, după care, în funcție de necesități, acesta va fi segmentat și alimentat din mai multe surse. În cazul utilizării mai multor surse de alimentare, masa întregului sistem va fi comună. Faza va fi separată, astfel fiecare tronson de sistem va fi alimentat dintr-o sursă distinctă (este de preferat evitarea conectării în paralel a surselor chiar dacă echilibrarea tensiunilor se realizează pe rezistența cablurilor de alimentare).

Proiectarea cablajului unui sistem de securitate presupune o înțelegere complexă a fenomenelor electromagnetice cum ar fi: căderile de tensiune pe rezistența electrică a circuitului, cuplajul inductiv, apariția capacităților parazite și efectele negative ale buclelor de masă.

În proiectarea cablajelor, se va urmări respectarea următoarelor reguli:
- separarea traseelor de curenți tari și curenți slabi;
- alegerea tipurilor adecvate de cabluri pentru fiecare tip de semnal în parte: cabluri de semnalizare pentru senzori, contacte, yale electromagnetice etc., cabluri de date (cu impedanța caracteristică standard de 120 ohmi) pentru magistralele de comunicație de tip RS 485 și cabluri cu secțiune corespunzătoare pentru tipurile de magistrale care nu folosesc acest standard;
- se vor evita zonele în care există perturbații electromagnetice puternice (mediu industrial cu mașini electrice sau procese electrochimice), încăperi pentru stații de radio-emisie etc.

Situații grave pot apare datorită căderii unor componente sau întreruperii magistralelor. Se consideră ca fiind prag critic funcțional un defect în urma căruia parametrii funcționali ai sistemului scad la 70,7% din valorile nominale. Totodată există anumite funcționalități critice în utilizarea unui sistem, cum ar fi în cazul control-accesului funcționarea ușii principale de acces într-un obiectiv.

După cum am exemplificat în paragraful de mai sus, pentru zona de acces a stației de distribuție s-au stabilit zonele de risc astfel încât, amplasarea echipamentelor sistemului de efracție să fie amplasate corect. Astfel, pentru ușile ce au rol de acces dinspre exterior se folosesc contacte magnetice pentru a împiedica accesul persoanelor neautorizate. Pentru ca sistemul să fie redundant, fără să apară breșe de securitate, în fiecare zonă de acces se amplasează detectori de mișcare.

Centrala de efracție se va poziționa în zona dispeceratului de pază, pentru a putea monitoriza în timp real. În apropierea centralei de efracție se va amplasa tastatura de armare/dezarmare. Având în vedere programul de lucru al personalului stației se pot separa anumite filtre pentru a se arma la ore diferite pentru a nu primi alarmă falsă. Contactul magnetic se va amplasa pe fiecare ușa care se consideră că ar fi de risc.

4. Concluzii

În aceasta lucrare s-a ales, ca studiu de caz în proiectarea sistemelor de securitate, o stație de distribuție a energiei electrice deoarece aici se regăsesc încăperi cu destinații diferite ce necesită un grad de protecție sporit.

Funcționând în parametrii nominali, cele două sisteme de securitate prezentate, contra incendiu si antiefracție, reduc posibilitatea apariției unui eveniment neplăcut ce poate afecta negativ procesul de distribuție al energiei electrice.

Echipamentele centrale ale celor două sistemelor de securitate, centrala antiincendiu și antiefracție s-au amplasat în camera dispeceratului local, deoarece acestea sunt monitorizate în permanență de un personal calificat, iar în cazul unei alarme de foc sau efracție, acestea vor fi rezolvate în cel mai scurt timp. Având în vedere că sunt distanțe mici de la unitatea centrală până la fiecare echipament de securitate aflat în dotarea stației de distribuție electrică, nu apar probleme datorită căderilor de tensiune.

Sistemul de control acces și cel de securitate antiefracție pot dialoga cu sistemul de detecție al incendiului printr-o interfață comună. În momentul în care este confirmat un incendiu în zona stației de distribuție, centrala sistemului de detecție incendiu transmite un semnal către releul ce este conectat atât la centrala de comunicare a sistemului de efracție cât și la sistemul de control acces, iar acest impuls are rolul de a decupla toate ușile de acces pentru a permite evacuarea personalului în cel mai scurt timp.

Sistemul de control al accesului, pe lângă funcția de bază de a restricționa accesul poate fi utilizat și ca echipament de pontaj, reducând astfel costurile prin achiziționarea de echipamente auxiliare.

Referințe

[1] C. G. Sărăcin, M. Sărăcin, V.V. Golea, „Sisteme de telemăsurare", Editura Matrix ROM, 2004.
[2] C. G. Sărăcin, „Instalații electrice", Editura Matrix ROM, 2009.
[3] Tiberiu Urdăreanu, Gheorghe Ilie, Mircea Blaha: Securitatea Instituțiilor Financiar Bancare, EdituraUTI , 1998
[4] MIL-HDBK-1013: Ghid de proiectare pentru securitatea fizică a obiectivelor
[5] Harold F. T., Mickey K., editors: Information Security Management Handbook
[6] Dr. Ing. Gheorghe Ilie: Securitatea mediului de afaceri, Editura UTI Press, 2006
[7] http://www.unitedtecgroup.com/access-control-systems.html
[8] https://vividcomm.com/2018/04/13/cctv-video-management-systems/
[9] Dr. Ing. Gheorghe Ilie, Ing. Adrian Roșca: Determinarea riscului de securitate; Revista ALARMA,NR. 2/2010 .
[10] Adrian Roșca: Curs pentru ingineri de sisteme de securitate; ARTS: 2009- 2010.
[11] Legea nr.333/2003 privind paza obiectivelor, bunurilor, valorilor și protecția persoanelor, republicată în 2014;
[12] H.G. nr.301/2012 pentru aprobarea Normelor metodologice de aplicare a prevederilor proiectului Legii, modificată și completată de HG nr.1002/2015.
[13]https://www.designingbuildings.co.uk/wiki/Access_control_in_buildings
[14]http://www.rollsoft.ro/sisteme-control-acces-hotelier-biometric/

Materiale noi pentru poduri – sticla celulară

New materials for bridges – foam glass

Iulia Andreea Sîngeorzan

Școala doctorală IOSUD Universitatea Tehnică din Cluj Napoca
Adresa Strada Constantin Daicoviciu nr. 15, Cluj Napoca, Romania
E-mail: iulia13andreea@gmail.com

Rezumat. *Sticla celulară este un material nou, prietenos cu mediul și economic pe termen lung. Este 100% mineral, produs din sticlă reciclată, produsul finit poate fi sub forma de plăci sau granule. Sticla celulară este un material foarte ușor, rezistent la îngheț-dezgheț, nedeformabil, rezistent la compresiune, umiditate, temperaturi extreme, dăunători și foc, și poate fi utilizat și în combinație cu alte materiale precum cimentul, cărămida, betonul. O aplicație încă nouă este în domeniul podurilor, unde oferă o alternativă a betonului de umplutură din trotuare. Principalul avantaj fiind greutatea redusă, care duce la o reducere a incărcării suprastructurii.*

Cuvinte cheie: sticla celulară poduri umplutură

Abstract. Foam glass is a new, environmentally friendly and long-term economic feasible material. It is 100% mineral, made of recycled glass, the finished product can be in the form of plates or granules. Foam glass is a very light material, resistant to frost defrost cycle, non-deformable; resistant to compression, humidity, extreme temperatures, pests and fire and can be used in combination with other materials such as cement, brick, concrete. A still new application is in the field of bridges, where it offers an alternative to concrete filling in sidewalks. The main advantage is the low weight, which leads to a reduction in the load of the superstructure.

Key words: foam glass bridges filling

1. Introduction

Foam glass is a new, environmentally friendly and long-term economic feasible material. It is 100% mineral, made of recycled glass, the finished product can be in the form of plates or granules.

Foam glass is a very light material, resistant to frost defrost cycle, non-deformable; resistant to compression, humidity, extreme temperatures, pests and fire and can be used in combination with other materials such as cement, brick, concrete.

Due to its technical properties, this material is increasingly used in the construction sector. Foam glass is used predominantly in civil construction as a thermal insulator, it can also be used for partial replacement of base layer aggregates, green and circulatory roofs, garden fillings, pipe insulators, as well as in the field of bridges as fillers.

A new application is in the field of bridges, where it offers an alternative to the concrete filler in the sidewalks. The main advantage is the reduced weight, which leads to a reduction in the load of the superstructure.

2. Content

During the evolution of the construction industry, man has always tried to find new materials, which through their superior properties to replace the old ones or to coexist with them and make the process of execution much faster and easier; execution time and commissioning are two very important elements in the process of constructions, whether it is civil constructions or roads and bridges.

As far as bridge construction is concerned, a material, still new among engineers, has appeared on the market, foam glass, currently used predominantly in the field of civil engineering, especially as an insulator.

Fig. 1 Foam glass

Cell glass or foam glass is an aggregate in the form of granules or plates. It is 100% mineral, produced from recycled glass that is converted into powder with the help of a ball mill, then mixed with an expansion agent and placed in the oven. [1]

Cell glass is made by heating a mixture of crushed or granulated glass and a foaming chemical agent, such as carbon or limestone. Near the melting point of the glass, the foaming agent releases a gas that will produce a foaming effect in the glass. After cooling, the mixture turns into a rigid material. [4]

Heating takes place in an electric furnace, which is an advantage because industrial water pollution does not occur, nor do burning emissions, thus protecting the environment. [2]

Cell glass was created from the beginning as an eco-product, 100% recycled glass and with neutral ph: 7. [1] Thus the recycling process goes smoothly and uninterruptedly, starting from glass waste and ending with the finished product. [2]

Fig. 2 Cellular glass manufacturing process [5] [6]

This material is extremely versatile in the construction field, having the following applications:

• Thermo-isolation of foundations, tiles over foundations and floors in houses, office buildings and industrial constructions;

• Thermo-isolation of the foundation at swimming pools;

• Rehabilitation of old and heritage buildings- restoration of floors and thermal insulation over floorboards;

• Support layer for floor heating systems;

• Walkable green roofs;

• Gabion walls. [2]

Another application that this product has, but that does not appear in the lists given by manufacturers because it has a more recent use, is as a filler material for sidewalks on bridges.

Due to the properties that this material has is an alternative to the filler concrete for sidewalks on bridges.

The properties of cell glass and the advantages of its use in the field of bridges

Cell glass is a material that is environmentally friendly and economical in the long run, these being only two of its many qualities. [1]

The first question that will come to the mind of any bridge engineer when he hears about this proposal to replace concrete with cell glass is going to be Why? What does this material promise compared to the classic concrete?

Cell glass has the following characteristics:
- Fire resistance class – A1;
- The density is 150-175 kg/mc;
- The EV2 linear deformation static module has a value >52MPa, depending on the degree of compaction and the thickness of the layer;
- Thermal conductivity coefficient l≤0.086W/mk.[2]

Properties of cell glass:
- Thermo-insulating: The large amount of air enclosed in its pores provides excellent thermal insulation.; [2]
- Dimensionally stable, shape-retaining: Following compaction, the foam glass doesn't shrink, it is shape-retaining. Due to its adequate rigidity no deformation occurs, not even under long-term loading conditions. [2]
- Static stability enhancer: By applications in weak soils the load bearing capacity of these types of soils can be increased. For this reason stone materials for beddings may be partly or entirely replaced during construction, depending on the loads. [2]
- Compression resistant: Granular foam glass of 150-175 kg/m3 bulk density has in itself a modulus of load-bearing capacity of 40-50 MPa at a 1.4 compaction rate. Therefore, it can be used as load bearing thermal insulation. [2]
- Highly lightweight: With a bulk density of merely 150-175 kg/m³ it is a very easy-to-handle product. By contrast, concrete and stone rubbles are about 8 to 15 times heavier than the foam glass granules. [2]
- Time and cost efficient: It reduces execution time, because one layer of incorporated granules replaces both the gravel and the thermal insulation material. This results in less work processes, and lower foundation work costs.[2]
- Frost proof: The foam glass has excellent frost-resistant properties. An easy-to-build, easy-to-handle material that only absorbs a minimum amount of moisture because of its closed-cell structure. [2]
- Capillary barrier effect: The particle-size distribution and the lack of fine material particles ensures the capillary break effect. It's non-absorbent and non-swelling because of its closed-cell structure. [2]
- Fireproof: The foam glass is resistant to fire. Fire protection classification: A1.[2]
- Sound insulating: The foam glass is an excellent sound-insulating material, therefore it is widely used in the construction of noise barriers and gabion walls. [2]
- Environment friendliness: The foam glass does not contain toxic substances. Thanks to the recycling process involved, the use of glass waste as raw material creates an excellent energy balance. It is harmless to living organisms.[2]

- Inert: It does not undergo any physical, chemical or biological transformations. It is generally resistant to organic solvents, acids and ageing. [2]
- The carrying capacity can be determined with the Lucas plate, a determination that cannot be achieved in the case of other thermal insulation materials.[3]

If we are talking about this material as an alternative to concrete filler material for sidewalks on bridges, the main advantage would be the low weight compared to concrete. Having a density between 150 – 175 kg/mc, cell glass can successfully replace concrete, which has a density almost fourteen times higher, in this way minimizing the loading of the resistance structure.

Another advantage would be compression resistance. The load-bearing capacity module of cellular glass granular material with a volumetric weight of 150-175 kg/mc is 40-50 Mpa [1], this ensuring the safe use of sidewalks.

Based on laboratory and in situ tests, the typical E2 value of the load-bearing capacity module of the cell glass granule material with a volumetric weight of 150-175 kg/m3 compacted at a rate of 1.40 was determined and the result of E2=40-50 MPa was obtained. [1]

Considering pipes and/or cable networks are placed in the filling of the sidewalks on bridges, the fact that it is a thermal insulating material is an advantage, as it provides additional thermal insulation, especially of water pipes.

Cell glass is inert, does not change its volume and does not deform, thus the risks of degradation of the filler layer are eliminated throughout the life of the construction.

Another major advantage is the commissioning, which is done very easily and quickly and there is no need for a large amount of labor, thus greatly lowering the price of workmanship.

Installation of cellular glass as a filling material on sidewalk bridges

In order to better highlight the implementation process of this material, a bridge was taken as an example where this material was chosen.

The process of putting the material into operation starts right from the transport, because it is important that the material is transported properly, so that its properties are not affected. According to the manufacturers, cellular glass can be transported in bulk, without special conditions, or in bags, called big bags. The last mode of transportation makes installation much easier.

Fig. 3 Mode of transport [7] [8]

Once the material has been transported to the installation site, the process is started by laying it over the concrete in the overconcrete plate and any existing water pipes and networks.

Depending on the mode of transport, the material can be unloaded directly from the bags or with the front loader, when it is transported in bulk.

Fig. 4 Spreading cellular glass from Big Bag

The material is bedded in layers of maximum 20 cm and level the surface of the layer, the simplest method is to rake the surface. [3]

After leveling the cell glass layer, you proceed to compaction of each layer with the vibrating plate (50-100 kg), the recommended degree of compaction being 1: 1.3. The cellular glass can also be compacted with a drum compactor when talking about a

larger area. But given that the width of the sidewalks is small, the best option is the vibrating plate.

Fig. 5 Compaction of cell glass with vibrating plate on sidewalks

A layer of concrete with a thickness of 10 cm and a layer of asphalt mixture of 4 cm are poured over the layer of compacted cellular glass.

Before pouring the concrete, the surface of cellular glass granules is covered for separation with polyethylene foil with overlaps of 20 cm. This polyethylene foil has the role of capturing cement milk after which you continue with pouring the concrete.

The concrete layer, 10 cm thick, can be poorly reinforced. At this bridge it was reinforced with welded mesh with a diameter of 8 mm. After pouring and hardening of the concrete, the asphalt mixture can be poured as a last step before putting the sidewalks into operation.

Fig. 6 Laying polyethylene foil and reinforcing with welded mesh

3. Conclusions

Cellular glass is a modern material which incorporates a number of superior and highly sought properties in building materials and which can successfully replace the classic materials, in this case concrete. This material comes as an alternative to the concrete filling of bridge sidewalks, where a lighter material is preferable, so as not to unnecessarily load the superstructure. Cellular glass is a material increasingly appreciated by engineers around the world, and its applications in civil engineering, from houses to bridges, prove this more and more, and the fact that it does not pollute makes it all the more appreciated.

Reference:

[1] www.casebune.ro – "Ce este izolația din spumă de sticlă?", Camelia Crapatureanu

[2] www.energocell.hu.ro – Sticla celulară

[3] Energocell – documente de calitate pentru podul din exemplul dat

[4] www.misiuneacasa.ro – "Ce este sticla celulară și la ce se folosește?"

[5] www.ecoremat.ro – Reciclare și colectare sticla București

[6] www.pixabay.com – Rupt de sticlă spartă

[7] www.heinze.de - GEOCELL Schaumglas

[8] www.casacusoare.ro

Analiza comparativă a influenței principalilor parametri asupra eficientizării stingerii cu apă a incendiilor

Comparative analysis of the main parameters influence on the efficiency of fire extinguishing using water

Alexandru-Florin CHIOJDOIU[1], Ion ANGHEL[2], Valeriu Nicolae PANAITESCU[3]

DOI: 10.37789/rjce.2021.12.2.11

[1]Universitatea Politehnica din București, România
București, sector 6, Splaiul Independenței, nr. 313
Inspectoratul pentru situații de urgență "Dealul Spirii" București-Ilfov
București, sector 5, Calea 13 Septembrie, nr.135
alex.floryn@yahoo.com

[2]Academia de Politie "Alexandru Ioan Cuza" – Facultatea de Pompieri
București, sector 2, Șoseaua Morarilor, nr.3, România
ion_anghel2003@yahoo.com

[3] Universitatea Politehnica din București, România
București, sector 6, Splaiul Independenței, nr. 313
Universitatea Politehnica București
e-mail: valeriu.panaitescu@yahoo.com

Rezumat. În acest studiu este subliniată importanța conceptului de eficiență a stingerii incendiilor folosind apă. Astfel, sunt prezentate mecanismele generale de stingere a incendiilor, manual, folosind țevile de refulare, și automat, folosind instalațiile fixe de stingere cu sprinklere, respectiv cu ceață de apă. Este realizată o analiză comparativă a influenței principalelor caracteristici ale jetului de apă obținut prin utilizarea țevilor de refulare și a instalațiilor fixe asupra eficienței stingerii incendiilor, și anume, a distribuției dimensiunii picăturilor de apă, a densității fluxului de apă refulat și a impulsului jetului. De asemenea, este prezentată și influența altor parametri asupra stingerii manuale și automate a incendiilor, precum dimensiunea picăturilor de apă, tehnicile de manevrare a țevilor de refulare, viteza ventilației longitudinale și debitul de refulare.

Cuvinte cheie: eficiența stingerii incendiilor, dimensiunea picăturilor de apă, sprinklere, ceață de apă

Abstract. This study highlights the importance of the concept of firefighting efficiency using water. Thus, are presented the general mechanisms of water for firefighting, manually, using nozzles, and automatically, using fixed system of sprinklers and water mist. A comparative analysis of the influence of the main characteristics of the water jet obtained by the use of nozzles and fixed installations on fire-extinguishing efficiency is carried out, such as the drop size distribution, the flux density and the spray momentum. Also is shown the influence of other parameters on manual and automatic fire

extinguishing, such as the size of water droplets, discharge nozzle techniques, longitudinal ventilation speed, and flow rate.

Key words: efficiency of firefighting, water droplet dimension, sprinklers, water mist

1. Introducere

Apa este cel mai important agent utilizat la scară largă pentru stingerea incendiilor, putând fi folosită atât în stare solidă, cât și în stare lichidă sau gazoasă [1]. Importanța apei ca agent principal de stingere a incendiilor este dată, în primul rând, de principalele proprietăți ale acesteia, și anume, dilatarea volumică, căldura specifică, respectiv căldura latentă de vaporizare [2].

Dilatarea volumică presupune mărirea volumului apei prin transformarea acesteia în aburi, fenomen determinat de creșterea temperaturii apei ca urmare a absorbției energiei termice degajate de incendiu. De asemenea, odată cu creșterea temperaturii aburilor, are loc o creștere direct proporțională a volumului acestora. Această teorie poate fi explicată prin legile gazelor și prin modul în care acestea pot fi integrate în legea gazului ideal, conform figurii 1 [3].
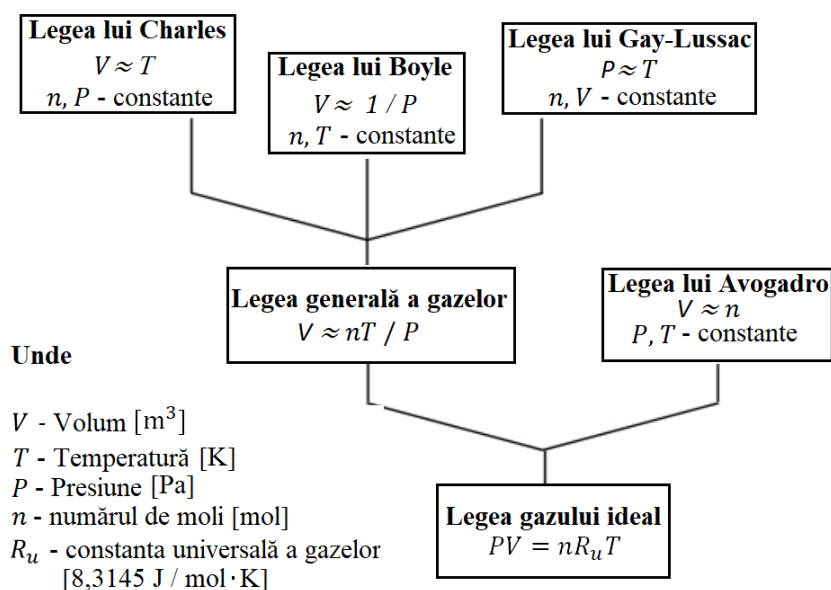
Figura 1 Integrarea legilor gazelor în Legea gazului ideal [3]

Utilizând legea gazelor ideale, se poate determina de câte ori se mărește volumul apei transformată în aburi la temperatura de 100 °C, ținând cont de valorile următorilor parametri: masa moleculară a apei $18 \cdot 10^{-3}$ kg/mol; punctul de fierbere al apei la presiunea atmosferică: 100 °C (373,15 K); densitatea apei, $\rho_{apă}$, la 20 °C (293,15 K): 10^3 kg/m³; presiunea atmosferică: 101325 Pa; constanta universală a gazelor (R_u): 8,3145 J/molK. Volumul unui mol de aburi se poate calcula folosind legea gazului ideal,

$$V = R_u \left(\frac{nT}{P}\right) = 8,3145 \left(\frac{1 \cdot 373,15}{101325}\right) = 0,0306 \text{ m}^3. \tag{1}$$

Densitatea aburilor la temperatura de 100 ℃ este dată de raportul dintre masa molară a vaporilor de apă, H₂O, 2×1+16 =18, și volumul unui mol de aburi,

$$\rho_{aburi} = \frac{18 \cdot 10^{-3}}{0,0306} = 588,2 \cdot 10^{-3} \text{ kg/m}^3. \tag{2}$$

Raportul dintre densitatea apei și densitatea aburilor arată de câte ori se mărește volumul apei atunci când aceasta se transformă în aburi,

$$\frac{\rho_{apă}}{\rho_{aburi}} = \frac{10^3}{588,2 \cdot 10^{-3}} = 1700,10. \tag{3}$$

Astfel, dilatarea volumică a apei poate conduce la stingerea incendiilor prin reducerea concentrației de oxigen a noului amestec format de aer-aburi.

Căldura specifică a apei, reprezintă cantitatea de energie pe care 1 kg de apă o poate absorbi de la incendiu pentru a crește temperatura acesteia cu 1 ℃, având valoarea de 4,2 kJ/kg.

Căldura latentă de vaporizare reprezintă cantitatea de energie necesară transformării unui 1 kg de apă în aburi la temperatura de 100 ℃, având valoarea de 2260 kJ/kg. Ținând cont de faptul că fumul are valoarea căldurii specifice de 1 kJ/kg, se constată astfel că apa este capabilă să absoarbă o cantitate foarte mare de energie termică de la incendiu [3].

Conceptul de eficiență a stingerii incendiilor constă în faptul că, așa cum procentul care definește eficiența procesului de absorbție a căldurii de către apă nu poate atinge valoarea de 100 %, în același mod majoritatea clădirilor sau a încăperilor în care se manifestă incendiul nu pot absorbi 100 % din fluxul termic degajat de incendiu. Astfel, se utilizează coeficientul de absorbție a căldurii degajate de incendiu de către apă, fiind suficientă pentru stingerea unui incendiu o absorbție cuprinsă în intervalul 30 % - 60 % din căldura totală degajată. De asemenea, se folosește coeficientul de eficiență a producerii căldurii de către un incendiu, acesta luând valori cuprinse în intervalul 10 % - 50 % din valoarea totală degajată de incendiu. Eficientizarea stingerii incendiilor presupune: utilizarea unei cantități de apă cât mai mici în scopul reducerii costurilor și a eventualelor pagube provocate clădirilor de acțiunea apei utilizate în exces; reducerea timpului de stingere a incendiului, în scopul salvării vieții oamenilor și animalelor, al protecției mediului, precum și al limitării producerii pagubelor [4].

2. Mecanismele de stingere ale apei refulate prin intermediul țevilor

În funcție de zonele din interiorul unei încăperi în care picăturile de apă se pot vaporiza, există cinci metode principale de a acționa împotriva incendiului, conform figurii 2: refularea picăturilor de apă asupra flăcărilor, respectiv asupra stratului de fum și gaze fierbinți, crearea unei atmosfere inerte prin producerea de aburi în urma vaporizării apei refulate asupra suprafețelor fierbinți, răcirea suprafeței materialelor combustibile care ard, ecranarea suprafeței materialelor combustibile neimplicate încă în procesul de ardere.
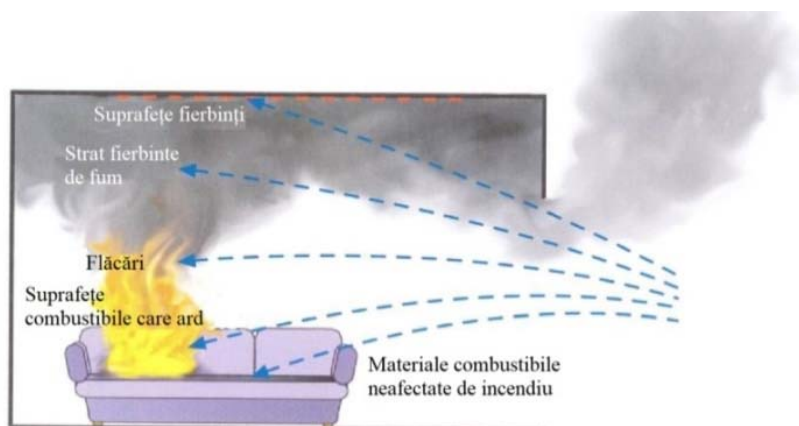
Figura 2 Zonele dintr-un compartiment de incendiu în care picăturile de apă se pot vaporiza [5]

În urma refulării apei asupra unui incendiu care se manifestă într-o încăpere, apa poate produce o serie de efecte [6] asupra acestuia, prezentate în figura 3, precum absorbția de căldură, reducerea concentrației de oxigen, efectul de răcire / ecranarea suprafeței, reducerea radiației termice, respectiv efectul de suflare.
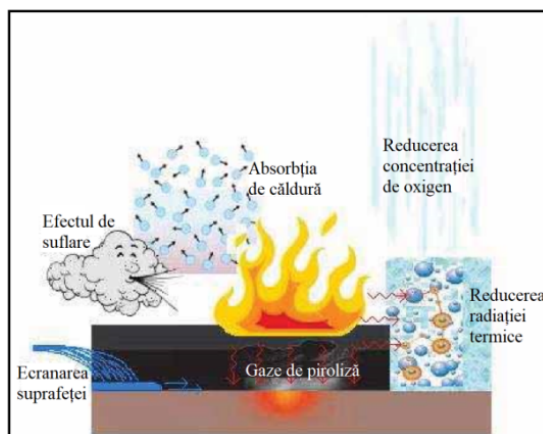

Figura 3 Efectele apei asupra incendiului [6]

Principalul efect pe care apa îl produce asupra unui incendiu este reprezentat de absorbția de căldură. Ținând cont de faptul că arderea este o reacție chimică exotermă, prin refularea apei reci, are loc absorbția energiei termice de către apă, ceea ce conduce la încălzirea acesteia. Arderea este o reacție chimică redox care necesită, pe lângă combustibil și o cantitate de energie suficientă pentru a susține arderea, prezența unui oxidant, și anume a oxigenului. Astfel, ținând cont de faptul că oxigenul se găsește în aer în proporție de 21 %, s-a constatat că, prin reducerea concentrației acestuia sub valoarea de 12 %, se încheie reacția în lanț generată de ardere, ceea ce conduce la stingerea incendiului. Efectul de răcire / ecranarea suprafeței presupune acțiunea directă a apei asupra materialului combustibil. Astfel, prin acoperirea eficientă a suprafețelor materialelor combustibile care ard, are loc răcirea acestora, împiedicarea producerii gazelor de piroliză și implicit stingerea incendiului. Reducerea radiației termice se poate produce, de asemenea, în urma refulării apei supra

incendiului, fiind dependentă de modul de distribuție al apei, dimensiunea picăturilor și modalitatea de stingere a incendiului. În situația în care apa este refulată sub formă de ceață de apă, în funcție de grosimea stratului format, radiația termică poate fi redusă sau blocată în întregime. Efectul de suflare constă în faptul că fluxul de aer antrenat în urma refulării jetului întrerupe continuitatea alimentării flăcării cu gazele de piroliză și a flăcării propriu-zise. Astfel, flăcările se sting deoarece, deși există o cantitate de energie suficientă întreținerii arderii, aceasta nu se află în același loc în care se găsește combustibilul [6].

Pentru ca apa să absoarbă o cantitate de energie cât mai mare este necesar ca picăturile de apă să rămână cât mai mult timp suspendate în aer. Așa cum se poate observa în figura 4, apa poate absorbi energie termică atât de la fum și gaze fierbinți, cât și de la suprafețele fierbinți ale încăperii. Ecuația care descrie echilibrul energetic
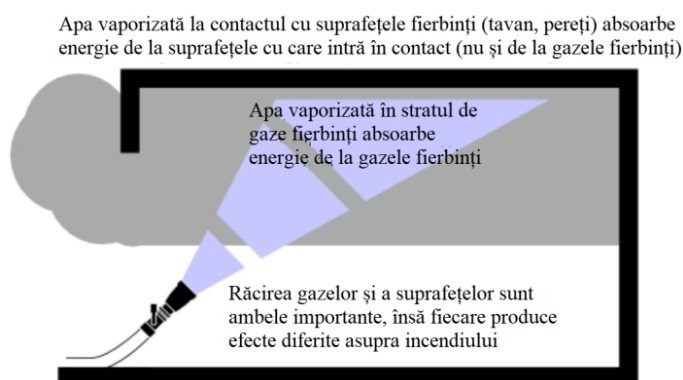
Figura 4 Răcirea gazelor și a suprafețelor fierbinți [7]

dintre gazele fierbinți aflate în stratul superior și apa refulată pentru răcire este:

$$\text{n}_1 C_{p,g}(T_{u1} - T_{u2}) = (\text{n}_2 - \text{n}_1)\left(\text{b}\left(C_{p,w}(373{,}15 - T_{w1}) + L_{Vw}\right) + C_{p,st}(T_{u2} - 373{,}15)\right) \tag{4}$$

unde

$C_{p,g}$ este căldura specifică a gazelor rezultate în urma incendiului/fumului (aproximativ egală cu cea a aerului, 33,2 J/mol K la 1000 K);

$C_{p,st}$ – căldura specifică a aburilor (41,2 J/mol K la 1000 K);

$C_{p,w}$ – căldura specifică a apei (76.663 J/mol K la 215,15 K);

L_{Vw} – căldura latentă de vaporizare a apei, 40680 J/mol;

T_u – temperatura stratului superior [K];

T_w – temperatura apei [K];

n – numărul de molecule;

b – procentul de apă care se vaporizează în stratul superior de fum și gaze fierbinți;

Subscript 1 – se referă la condițiile inițiale;

Subscript 2 – se referă la condițiile ulterioare după refularea apei;

Termenul din stânga al ecuației, reprezintă energia care trebuie transferată de la gazele fierbinți din stratul superior în scopul reducerii temperaturii acestora. Termenul din dreapta al ecuației, reprezintă energia care trebuie transferată apei refulate pentru a

crește temperatura apei, sub formă de aburi, cu aceeași valoare cu care scade temperatura stratului superior de fum și gaze fierbinți [7].

3. Mecanismele de stingere ale apei prin utilizarea instalației cu sprinklere

Unul dintre cele mai eficiente moduri de stingere a incendiilor în urma utilizării instalației cu sprinklere este reprezentat de efectele de răcire produse. Producerea unor picături de apă de dimensiuni mici produce o răcire semnificativă, ceea ce conduce la reducerea feedback-ului radiativ către foc sub nivelul necesar susținerii procesului de ardere [8]. Un alt mod de stingere a incendiilor este reprezentat de efectul de „înăbușire". Acesta constă în evaporarea picăturilor de apă, ceea ce conduce la mărirea volumului de apă de circa 1700 de ori prin transformarea acesteia în aburi, rezultând scăderea concentrației de oxigen a amestecului nou format de aer și aburi. Cele două moduri de stingere a incendiilor au o serie de limitări, principalul aspect fiind reprezentat de faptul că acestea sunt eficiente în situația în care incendiul se manifestă într-o încăpere închisă, neventilată [9]. Cea mai mare eficiență a stingerii incendiilor se obține în cazul încăperilor mici, prin obținerea efectului de „înăbușire" a incendiului, deoarece aproape toate picăturile de apă se pot vaporiza fie la contactul cu flăcările, fie la contactul cu suprafețele fierbinți ale încăperii [10]. În cazul manifestării unui incendiu de amploare într-o încăpere mare, deschisă sau bine-ventilată, se pot crea curenți de aer care îndepărtează picăturile mici de apă făcându-le ineficiente pentru stingerea incendiului.
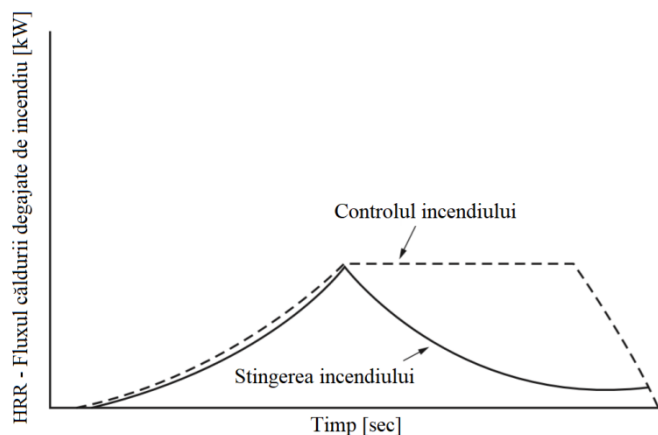

Figura 5 Variația în timp a HRR necesară realizării controlului, respectiv stingerii incendiului [8]

În figura 5 este reprezentată evoluția în timp a HRR (eng: heat release rate), fluxului căldurii degajate de incendiu, caracteristică realizării controlului asupra incendiului, respectiv stingerii acestuia. Controlul incendiului presupune limitarea dimensiunii incendiului prin reducerea fluxului căldurii degajate și refularea apei asupra materialelor combustibile aflate în apropiere, neimplicate încă în procesul de ardere. Stingerea incendiului presupune reducerea fluxului căldurii degajate de incendiu până în punctul în care creșterea din nou în intensitate a incendiului nu mai

este posibilă ca urmare a refulării apei, prin flăcări, către suprafața materialelor combustibile care ard.

4. Mecanismele de stingere a incendiilor folosind instalația cu ceață de apă

Modul de acțiune al sistemelor cu ceață de apă folosite pentru suprimarea unui incendiu este prezentat în figura 6 și constă în trei mecanisme de stingere primare și două mecanisme de stingere secundare [8]. Mecanismele de stingere primare sunt reprezentate de absorbția de căldură, scăderea concentrației de oxigen și blocarea radiației termice. Mecanismele secundare care intervin în stingerea incendiilor sunt diluarea amestecului de aer și vapori ai materialelor combustibile care ard, respectiv efectele cinetice, însă este dificil de cuantificat importanța acestora.
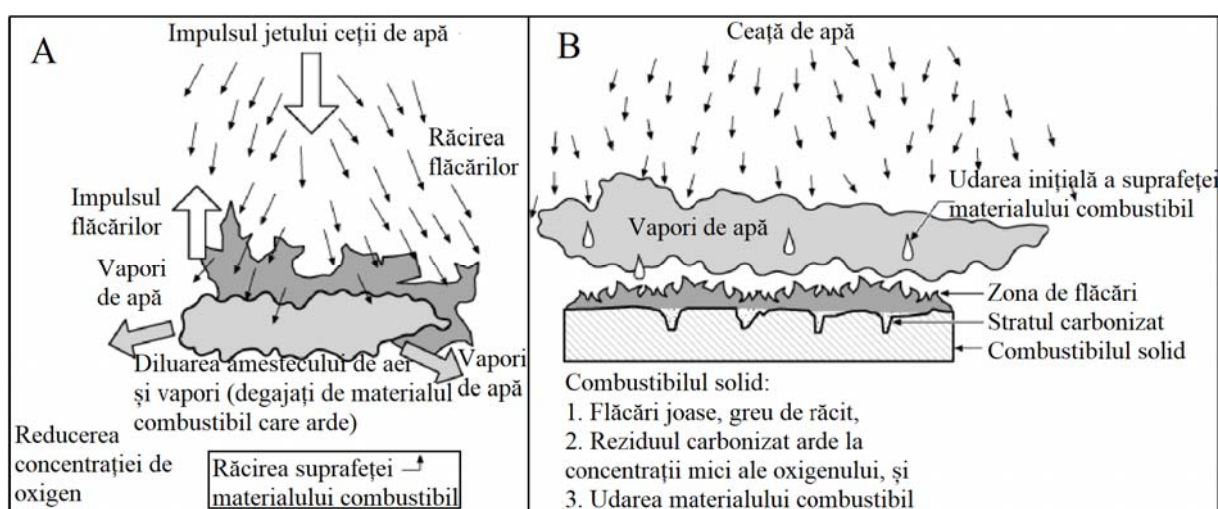
Figura 6 Mecanismele stingerii cu ceață de apă a unei tăvi cu combustibil lichid (A) și asupra unui combustibil solid caracterizat de un strat de reziduu carbonizat și degajări de flăcări (B) [8]

Absorbția căldurii, denumită și răcire, presupune faptul că, atunci când ceața de apă este refulată asupra incendiului, căldura este absorbită în trei zone, astfel: de la gazele fierbinți și de la flăcări, de la materialele combustibile care ard, respectiv de la obiectele și suprafețele aflate în apropierea incendiului. Dacă este absorbită o cantitate suficientă de căldură, temperatura fazei gazoase a flăcărilor poate fi scăzută sub valoarea critică necesară susținerii reacției de combustie, cca 1327 ℃ [11], și astfel flăcările sunt stinse. Conform unor studii efectuate [12], cantitatea „suficientă" de căldură absorbită necesară opririi procesului de ardere variază între 30 % și 60 % din căldura totală degajată de incendiu. Incendiile care se manifestă la lichide combustibile al căror punct de aprindere este peste temperatura ambientală, pot fi stinse relativ ușor prin răcirea flăcărilor și reducerea emisiei radiației termice către suprafața combustibilului. Incendiile care se manifestă la lichide combustibile ale căror puncte de aprindere sunt sub temperatura normală ambientală, sunt mult mai greu de stins deoarece temperaturile nu pot fi reduse suficient de mult pentru a contracta amestecul de aer și vapori situat deasupra suprafeței combustibilului sub limita joasă de

inflamabilitate a acestuia [13]. Răcirea flăcărilor materialelor combustibile solide care ard reduce, de asemenea, fluxul termic radiativ către suprafața materialului combustibil și rata pirolizei materialului combustibil. Așa cum se poate observa în figura 4 B, reacția de ardere are loc în interiorul zonei poroase bogate în carbon care se formează la suprafața materialului combustibil [11].

Reducerea concentrației de oxigen, are un rol mai important decât răcirea flăcărilor [14]. Ținând cont de faptul că volumul apei rezultat în urma vaporizării la 100 °C se mărește de cca 1600 – 1700 de ori, refularea ceții de apă sub forma unor picături mici în interiorul unui compartiment de incendiu cu temperaturi ridicate conduce la vaporizarea rapidă a apei, dilatarea volumului acesteia și dislocarea aerului de către aburi. Testele [12], [9], [14], [15] efectuate în special asupra combustibililor lichizi confirmă faptul că reducerea concentrației de oxigen este principalul mecanism prin care ceața de apă produce stingerea flăcărilor atât în interiorul încăperilor cât și în aer liber, prin intermediul unei concentrații mari de vapori de apă. Concentrația vaporilor de apă la nivelul suprafeței materialului combustibil care arde poate fi făcută fie prin acoperirea incendiului care se manifestă în interiorul unei încăperi, fie prin direcționarea și aplicarea jetului cu suficientă forță, valoarea ridicată a impulsului jetului împingând vaporii de apă la nivelul suprafeței combustibilului. În general, gazele și vaporii inflamabili degajați prin arderea hidrocarburilor încetează să mai ardă la concentrații ale oxigenului sub 13 %, în timp ce materialele solide combustibile caracterizate prin reziduu carbonizat pot arde până la concentrații ale oxigenului de 7 % [11].

Blocarea radiației termice constă în oprirea propagării incendiului către materialele combustibile neafectate încă de incendiu și reducerea procesului de piroliză. Studiile teoretice [16], [17] au arătat că reducerea radiației termice este influențată de diametrul și de densitatea masică a picăturilor. Astfel, pe măsură ce concentrația picăturilor cu diametrul mai mic de 50 μm crește, se mărește și gradul reducerii radiației termice. De asemenea, considerațiile teoretice [18] sugerează faptul că ceața de apă, respectiv aburii care pătrund în spațiul dintre flăcări și suprafața materialului combustibil reduce fluxul termic radiativ către suprafața materialului.

Diluarea amestecului de vapori combustibili și aer constă în faptul că aerul, respectiv vaporii de apă antrenați de jetul de ceață de apă pot dilua amestecul aer-vapori degajați de materialele combustibile care ard, sub limita inferioară a inflamabilității. Diluarea amestecului de aer și vapori combustibili este considerat un mecanism de stingere secundar, deoarece este foarte greu de realizat stingerea incendiului doar prin aplicarea acestui mecanism. Amestecul realizat la nivelul materialelor combustibile care ard este deseori turbulent și neuniform, fiind foarte probabil să existe întotdeauna anumite zone de aer și vapori combustibili aflate în intervalul de inflamabilitate.

Efectele cinetice ale ceții de apă asupra flăcărilor constau în faptul că, uneori, arderea unui lichid combustibil se intensifică în urma refulării ceții de apă în primele secunde, rata de ardere mărindu-se pentru anumite perioade de timp. Intensificarea temporară a arderii este atribuită, conform concluziilor obținute în urma efectuării mai

multor teste [19], [20], efectului picăturilor de apă care lovesc suprafața materialului combustibil, determinând creșterea ratei de producere a vaporilor combustibili. Au fost efectuate teste în scopul analizării evoluției în timp a HRR, conform figurii 7, în urma stingerii heptanului și ulterior motorinei, care ardeau în tăvi, dispuse în aer liber.
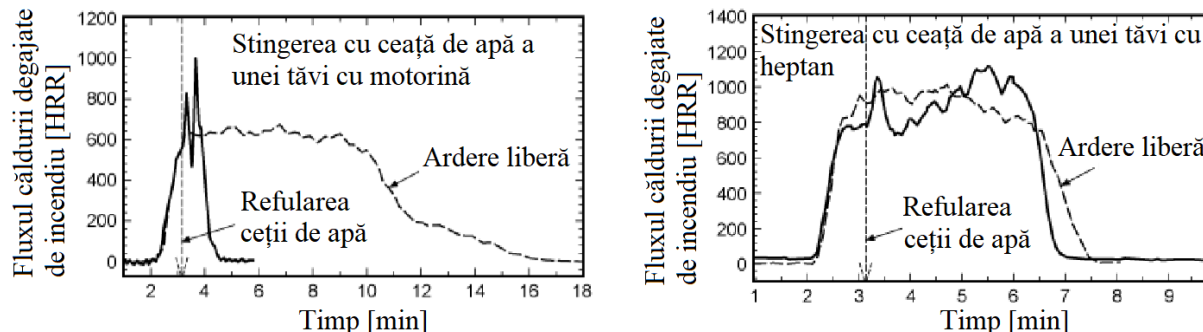

Figura 7 Evoluția în timp a HRR în cazul stingerii unor tăvi cu motorină și heptan folosind ceață de apă [8]

Spre deosebire de cazul stingerii motorinei, unde se constată o creștere pentru scurt timp a HRR urmată de stingerea completă în următoarele 60 sec, în situația stingerii heptanului, are loc, de asemenea, o creștere pentru scurt timp a HRR urmată de o stingere parțială și apoi de o creștere continuă a ratei de ardere a heptanului. Jetul de ceață de apă nu a reușit să stingă focul, iar flăcările turbulente au continuat până când combustibilul a fost consumat.

5. Influența principalelor caracteristici ale jetului apei refulate în urma utilizării țevilor de refulare și a instalațiilor fixe asupra eficienței stingerii incendiilor

Stingerea incendiilor poate fi realizată fie manual, prin utilizarea țevilor de refulare, fie automat, prin utilizarea unor instalații fixe de stingere, precum instalația de sprinklere sau instalația de ceață de apă. Dintre caracteristicile principale ale jetului apei refulate care influențează în mod direct eficiența stingerii incendiilor pot fi enumerate următoarele: distribuția dimensiunii picăturilor de apă; densitatea fluxului de apă – raportul dintre masa picăturilor de apă suspendate și unitatea volumului încăperii; impulsul jetului – viteza cu care apa este refulată către baza focarului de incendiu.

5.1. Influența distribuției dimensiunii picăturilor de apă asupra stingerii incendiilor

Distribuția dimensiunii picăturilor de apă este una dintre principalele caracteristici ale jetului refulat, cu impact direct asupra eficienței stingerii incendiilor, deoarece, cu cât suprafața picăturii este mai mică, cu atât cantitatea de căldură absorbită va fi mai mare. Astfel, cu cât numărul picăturilor cu dimensiune mică este mai mare, cu atât eficiența stingerii va fi mai ridicată. Distribuția dimensiunii picăturilor se referă la intervalul dimensiunilor picăturilor conținute într-un jet de apă

sau de ceață de apă, fiind dependentă de locația picăturilor în interiorul jetului, în centru sau către marginile exterioare, respectiv de timp.

În cazul unei refulări continue, distribuția dimensiunii picăturilor de apă este influențată de distanța față de duza / țeava de refulare, putând avea loc coliziunea picăturilor cu alte picături sau cu suprafețele încăperii. În cazul unei refulări de scurtă durată, distribuția dimensiunii picăturilor măsurată într-o anumită zonă este influențată de timp, datorită faptului că picăturile cu dimensiuni mai mari se deplasează rapid, părăsind zona respectivă, rămânând astfel picături cu dimensiuni mici, caracterizate de viteză mică de deplasare.

A fost realizată o clasificare a sistemelor de ceață de apă în funcție de distribuția dimensiunii picăturilor de apă, dimensiunea fiind reprezentată de diametrul mediu volumic al acestora [21]. Diametrul mediu volumic reprezintă diametrul unei picături de apă care are același volum cu media volumului tuturor picăturilor. Astfel, în cazul clasei I, 90 % din totalul picăturilor au diametrul mediu volumic mai mic de 200 μm, în cazul clasei a II-a, 90 % din totalul picăturilor au diametrul mediu volumic cuprins în intervalul 200 μm – 400 μm, iar în cazul clasei a III-a, 90 % din totalul picăturilor au diametrul mediu volumic cuprins în intervalul 400 μm – 1000 μm. Un număr mare de țevi de refulare și sprinklere au diametrul mediu volumic al picăturilor de apă mai mare de 400 μm [5].
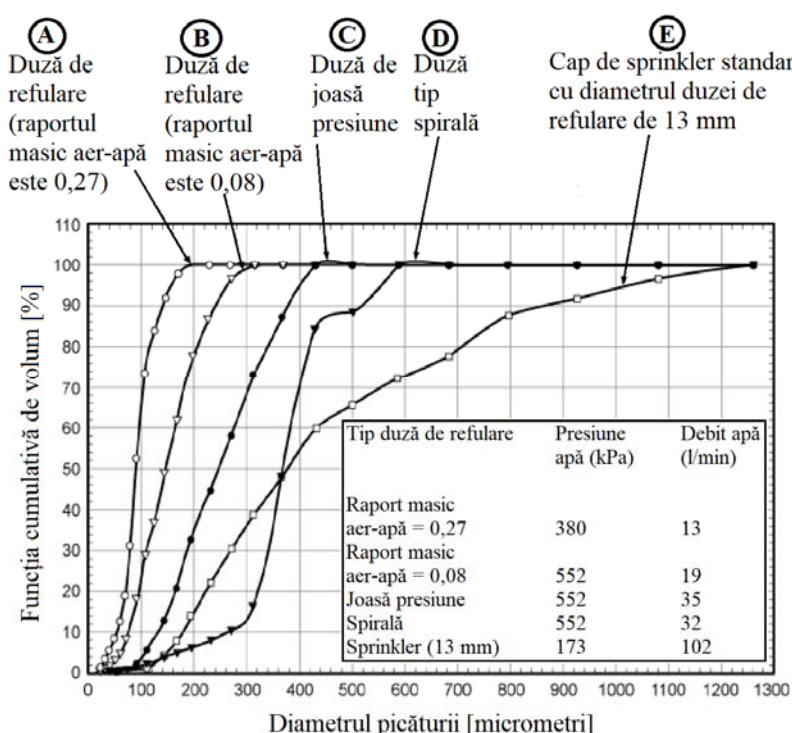
Figura 8 Variația funcției cumulative de volum a picăturilor de apă în funcție de diametrul acestora, pentru diferite duze de refulare a instalației cu ceață de apă, A, B, C, D, respectiv cu sprinklere E [8]

În figura 8 este analizată variația funcției (probabilității) cumulative a volumului picăturilor de apă cu diametrul acestora, în cazul utilizării unor duze de refulare diferite, caracteristice instalației cu ceață de apă și sprinklere. Funcția

cumulativă de volum reprezintă probabilitatea ca diametrul mediu de volum al picăturilor de apă refulate să fie mai mic sau egal cu o valoare dată. De exemplu, în cazul instalației cu sprinklere, există o probabilitate de 10 % ca diametrul mediu de volum al picăturilor să fie mai mic de cca 200 μm. Astfel, s-a realizat o analiză comparativă a distribuției dimensiunii picăturilor măsurate la o distanță de 0,9 m de duză, presiunea de refulare fiind mai mică de 11,9 bar.

5.2. Densitatea fluxului apei refulate necesară stingerii incendiilor

Densitatea fluxului apei refulate reprezintă o caracteristică importantă în ceea ce privește stingerea incendiilor, fiind exprimată fie în l/min · m², fie în l/min · m³.

În cazul stingerii manuale a incendiilor folosind țevile de refulare, în vederea eficientizării acțiunii de stingere, este necesară o distribuție uniformă a apei. Distribuția apei, denumită și densitatea fluxului apei refulate, poate fi determinată folosind testul standard SS 3500, 1987. Proporția zonei în care nu a fost refulată apă nu trebuie să fie foarte mare. De asemenea, valoarea maximă a densității fluxului apei refulate nu trebuie să foarte mare comparativ cu valoarea medie. În cadrul unui studiu efectuat pentru a observa influența țevilor de refulare asupra răcirii gazelor de ardere, se analizează fluxul densității apei refulate prin intermediul a două țevi de refulare diferite, analiza comparativă fiind prezentată în figura 9.
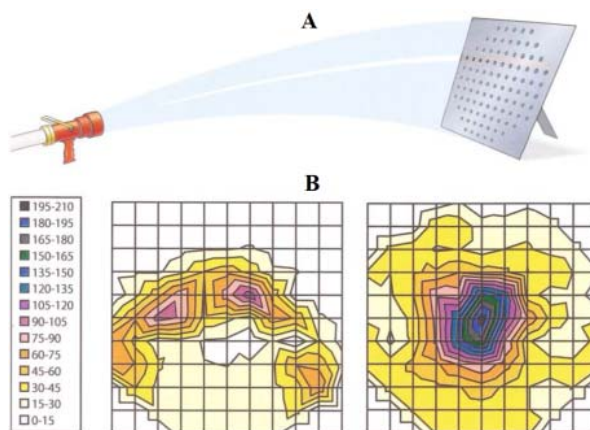
Figura 9 Densitatea fluxului apei refulate: mod de determinare folosind testul standard SS 3500, 1987 (A); analiză comparativă în urma folosirii a două țevi de refulare diferite (B) [5]

În figura 10 este prezentată variația densității fluxului apei refulate în funcție de distanța dintre țeava de refulare și zona în care se manifestă incendiul, pentru diferite valori ale debitului și presiunii, unghiul conic al jetului fiind de 30 ° [5].
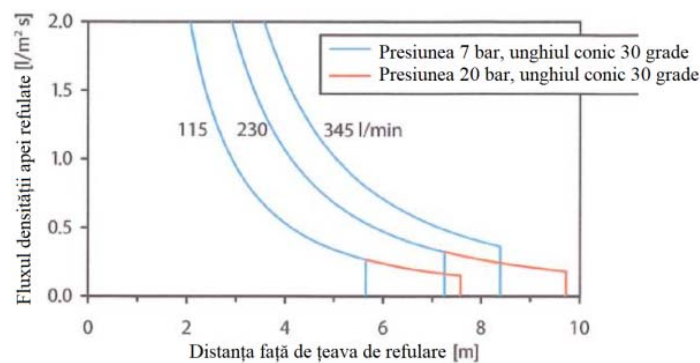
Figura 10 Variația fluxului densității apei refulate cu distanța dintre țeava de refulare și zona în care se manifestă incendiul, pentru valori diferite ale debitului și presiunii [5]

Fiecare țeavă de refulare are o distanță normată față de incendiu la care poate fi folosită, în funcție de traiectoria jetului și distribuția dimensiunilor picăturilor. Dacă țeava de refulare se află la distanță mare față de incendiu, este nevoie de o traiectorie mai mare, motiv pentru care modelul jetului va fi modificat. În cazul unui jet având forma ideală a unui con, gravitația fiind neglijată, valoarea medie a fluxului densității apei refulate [l/m^{2}s] poate fi estimată astfel:

$$q''_{medie} = \frac{q}{\pi(l \tan(\propto/2))^2}$$ (5)

unde

q''_{medie} este valoarea medie a densității fluxului apei refulate [l/m^{2}s];

q – debitul apei refulate [l/s];

l – distanța țevii de refulare față de zona în care se manifestă incendiul [m];

$\propto$ - unghiul conic al jetului [°].

Astfel, se constată că valoarea densității medii a fluxului apei refulate este invers proporțională cu pătratul distanței țevii de refulare față de incendiu. Când această distanță este mică, densitatea fluxului apei refulate este de câteva ori mai mare decât valoarea necesară stingerii incendiului. Cu cât jetul este mai compact, cu atât mai mare este densitatea fluxului și mai mică suprafața acoperită de apa refulată. Dacă distanța dintre țeava de refulare și incendiu este mare, este necesară utilizarea unui debit mare și a unui unghi conic al jetului mic pentru ca apa să fie refulată acolo unde se dorește. Astfel, valoarea medie a densității fluxului apei refulate este mare acolo unde jetul lovește focul, fiind nevoie ca jetul să fie mutat energic pentru a acoperi o suprafață cât mai mare [5].

Stingerea automată a incendiilor prin utilizarea instalației de sprinklere presupune faptul că, odată cu creșterea densității fluxului apei refulate, exprimată în l/min · m^3, sau în l/min · m^2, peste valoarea critică, timpul necesar pentru controlul sau stingerea incendiului scade rapid. În figura 11 este prezentat faptul că, prin creșterea valorii densității fluxului apei refulate, se reduce timpul necesar stingerii incendiului [10].
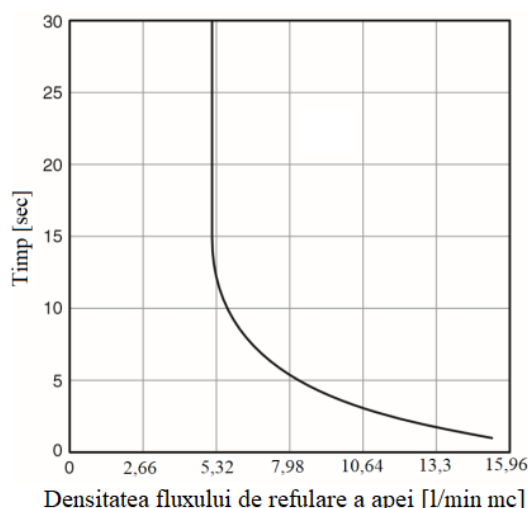
Figura 11 Corelația dintre densitatea fluxului de refulare a apei și
timpul necesar stingerii incendiului [10]

Densitatea fluxului apei refulate este direct proporțională cu gradul riscului de incendiu al clădirilor cu diferite destinații. Astfel, există cinci clase principale de risc de incendiu, și anume, risc scăzut, risc moderat 1, risc moderat 2, risc ridicat 1 și risc ridicat 2. *Riscul scăzut* este caracteristic clădirilor cu destinația de biserică, club, educație, spital, adăpost de animale, muzeu, birou, clădiri instituționale, clădiri rezidențiale, mansarde/poduri neutilizate – cantitatea și gradul de combustibilitate al materialelor este mic, incendiile având valori ale fluxului căldurii degajate scăzute. *Riscul moderat 1* este specific clădirilor cu destinația de zone de showroom-uri auto, brutării, baruri, realizarea produselor lactate, a produselor electronice, a sticlei, spălătorii - gradul de combustibilitate este scăzut, există cantități moderate de materiale combustibile, depozitarea pe verticală nu depășește 2,4 m, fluxul căldurii degajate de incendiu fiind moderat. *Riscul moderat 2* este specific clădirilor cu destinația de hambare și grajduri, distilerii, uscătorii, librării, service-uri auto, industria chimică - cantitatea și gradul de combustibilitate al materialelor este moderat, depozitarea în plan vertical a materialelor cu un flux al căldurii degajate moderat nu depășește 3,6 m, iar a materialelor cu un flux al căldurii degajate mare nu depășește 2,4 m. *Riscul ridicat 1* este specific clădirilor cu destinația de hangare de aeronave, prelucrarea PAL-ului, textile, tapițerii, sală gatere - cantitatea și gradul de combustibilitate al materialelor este foarte ridicat, fiind prezente praful, scamele sau ale materiale care conduc la o dezvoltare rapidă a incendiilor, cu valori ridicate ale fluxului căldurii degajate, în absența sau în prezența unei mici cantități de lichide inflamabile. *Riscul ridicat 2* este specific clădirilor cu destinația de prelucrare a materialelor plastice, parcări auto prevăzute cu lifturi, depozitarea lichidelor inflamabile – cantitatea de lichide combustibile sau inflamabile este de la moderată la însemnată [8], [22]. Conform figurii 12 se constată că, odată cu creșterea suprafeței încăperii și a gradului riscului de incendiu este necesară utilizarea unor valori mai mari ale densității fluxului apei refulate pentru stingerea incendiului.
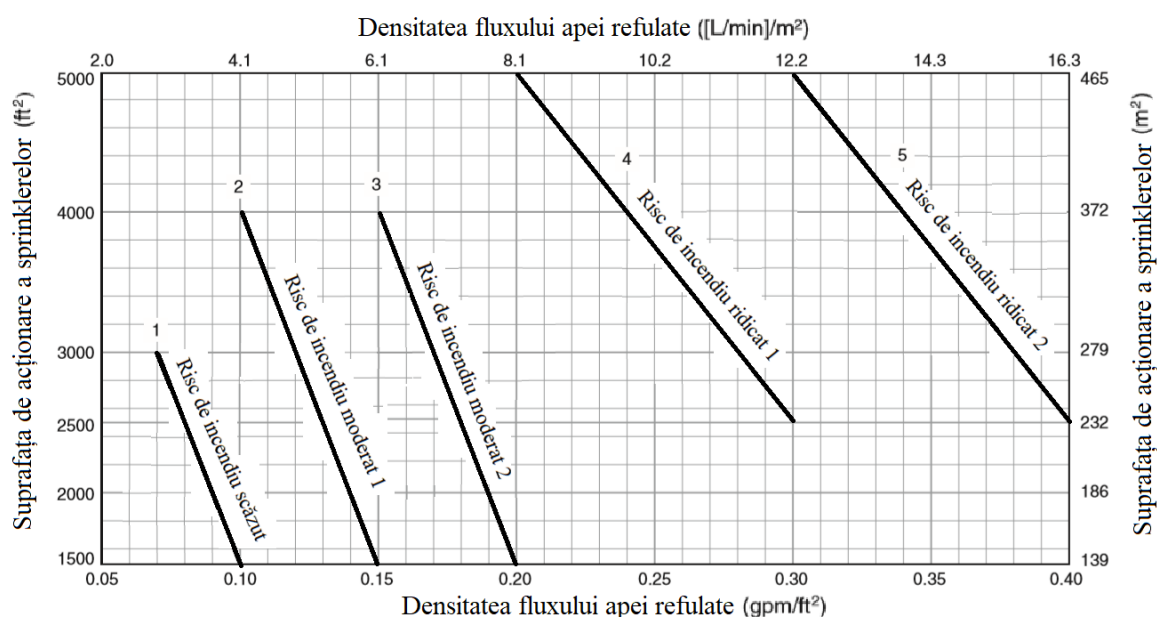
Figura 12 Variația densității de refulare a apei în funcție de suprafața încăperii, pentru tipurile de riscuri de incendiu asociate clădirilor cu diferite destinații [8]

Stingerea automată a incendiilor prin utilizarea instalației de ceață de apă este caracterizată de o densitate neuniformă a fluxului ceții de apă pulverizate. Astfel, în situația utilizării a două duze de refulare situate la 3 m deasupra podelei, la o distanță de 2 m între ele, pentru stingerea unei tăvi cu motorină și a unei tăvi cu heptan, valoarea densității fluxului de apă a variat de la 17,2 l/min · m² sub duza de refulare, la 3 l/min · m² la marginile exterioare, respectiv la 6,6 l/min · m² la mijlocul distanței dintre cele două duze, așa cum se poate observa în figura 13.
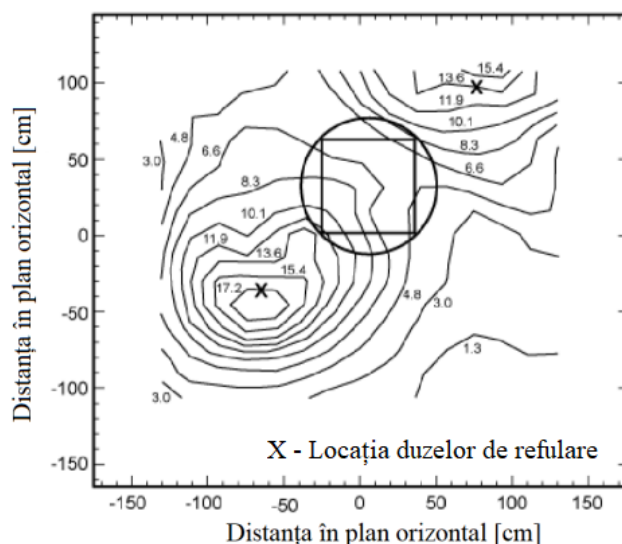
Figura 13 Influența distanței față de duza de refulare asupra densității fluxului apei refulate [8]

În situația în care cele două tăvi cu combustibil au fost plasate sub duzele de refulare, stingerea s-a realizat în mai puțin de 10 secunde. În situația în care tăvile cu

combustibil au fost plasate la mijlocul distanței dintre cele două duze de refulare, stingerea motorinei s-a realizat într-un timp mai mare, iar în cazul heptanului stingerea nu s-a realizat. Astfel, cu cât densitatea fluxului apei refulate este mai mare, cu atât timpul necesar stingerii incendiului este mai mic. Majoritatea duzelor concentrează un mare procent din jetul ceții de apă în centrul conului de refulare deoarece se creează o presiune negativă în interiorul conului ceea ce conduce la atragerea picăturilor refulate către marginile exterioare spre interior [8].

5.3. Influența impulsului generat de apa pulverizată asupra stingerii incendiului

Impulsul jetului de apă refulat reprezintă un parametru important în ceea ce privește eficiența stingerii incendiilor, fiind influențat de trei factori: viteza de deplasare a picăturilor de apă ce compun jetul, direcția acestuia față de flăcări, respectiv masa picăturilor de apă refulate în interiorul flăcărilor sau pe suprafața materialelor care ard. Cu cât se poate exercita un control mai mare asupra impulsul jetului, cu atât mai mare va fi capacitatea de a controla volumul total de apă și timpul necesar stingerii incendiului, precum și pagubele produse de acțiunea apei asupra proprietăților afectate de incendiu și / sau asupra celor adiacente.

În urma utilizării țevilor de refulare, prin folosirea unui jet pulverizat, având unghiul conic mai mare de 50° și dimensiuni mai mici ale picăturilor de apă decât în cazul jetului compact, impulsul jetului este transferat aerului pe o distanță de câțiva metri față de țeavă. Astfel, cantitatea de aer antrenată de jetul de apă poate conduce la stingerea incendiului prin întreruperea continuității alimentării flăcării cu gazele de piroliză și a flăcării propriu-zise. De asemenea, cu cât viteza picăturilor la ieșirea din țeavă este mai mare, cu atât acestea se deplasează pe o distanță mai mare, chiar dacă au dimensiunea mai mică.
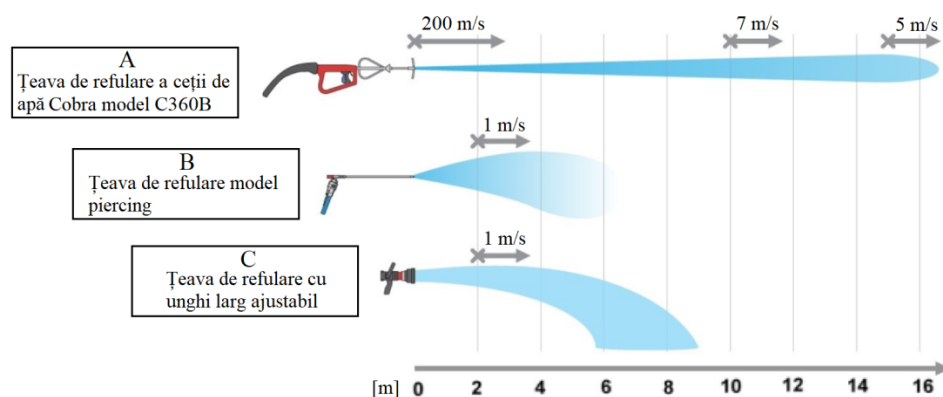

Figura 14 Analiza comparativă variației distanței de deplasare a picăturilor de apă în funcție de viteza acestora la ieșirea din țeavă, pentru diferite tipuri de țevi de refulare[23]

Conform figurii 14, țeava de refulare tip A produce ceață de apă, picăturile având viteza de 200 m/s la ieșirea din țeavă, iar țeava de refulare tip B, utilizată în special pentru a trece prin pereții și podelele clădirilor, respectiv tip C au viteza

picăturilor la ieşirea din ţeavă de 1 m/s. Cele trei ţevi au dimensiunea picăturilor mai mică de 200 μm, 700 μm, respectiv 900 μm, în timp ce distanţa de deplasare a picăturilor de apă este de minim 16 m, 6 m, respectiv 9 m. Cu cât distanţa de deplasare a picăturilor este mai mare, cu atât acestea vor absorbi o cantitate mai mare de căldură de la incendiu. Folosind programul de simulare Fire Dynamic Simulator [25], a fost efectuată o analiză comparativă privind eficienţa stingerii în urma utilizării ţevii de stingere folosind hidro-perforarea şi a unui sistem joasă presiune (presiune mai mică de 20 bar), caracteristicile jetului în cazul celor două sisteme fiind: debitul, 60 l/min, respectiv 100 l/min, viteza iniţială a picăturilor, 220 m/s, respectiv 65 m/s şi diametrul mediu Sauter, 162 μm, respectiv 1000 μm. O valoare mai mare a impulsului picăturilor creşte gradul de amestecare al gazelor ceea ce conduce la omogenizarea temperaturii şi implicit la creşterea valorii acesteia în apropierea picăturilor, rezultând mărirea vitezei răcirii gazelor şi a vaporizării picăturilor.

În cazul instalaţiei fixe de sprinklere, în momentul acţionării acesteia, cantitatea picăturilor de apă care trec prin flăcări şi ajung pe suprafaţa materialelor care ard este influenţată de impulsul jetului. Aceasta poate fi fie calculată, în baza datelor referitoare la fluxul căldurii degajate în zona tavanului, distribuţia unghiulară a picăturilor de apă, fluxul apei refulate şi viteza picăturilor de apă în zona duzei, fie măsurată, aşa cum se poate observa în figura 15.

Figura 15 Instalaţie de măsurare a cantităţii picăturilor de apă care trec prin flăcări şi ajung pe suprafaţa materialelor care ard [8]

Sprinklerele care au dimensiuni mai mari ale duzelor de refulare produc picături de apă cu dimensiuni mai mari, caracterizate printr-un impuls al picăturii mai mare. Astfel, valoarea ridicată a masei picăturii coroborată cu valoarea ridicată a vitezei acesteia conduc la obţinerea unui impuls al jetului de apă suficient de mare cât să pătrundă prin flăcări şi să ajungă pe suprafaţa materialelor care ard.

În ceea ce priveşte instalaţiile fixe de stingere cu ceaţă de apă, influenţa asupra impulsului jetului este dată nu doar de caracteristicile duzei de refulare, ci şi de modul în care duzele pot fi amplasate pentru a acoperi cât mai bine zona afectată de incendiu. Astfel, în situaţia în care se foloseşte o duză cu un unghi mare de deschidere al jetului, aceasta este mai puţin eficientă, deoarece este acoperită o zonă mai mică decât situaţia în care se folosesc mai multe duze cu unghi mic de deschidere al jetului, obţinându-se astfel o distribuţie liniară, pe o suprafaţă mai mare.

Analiza comparativă a influenței principalilor parametri asupra eficientizării stingerii cu apă a incendiilor
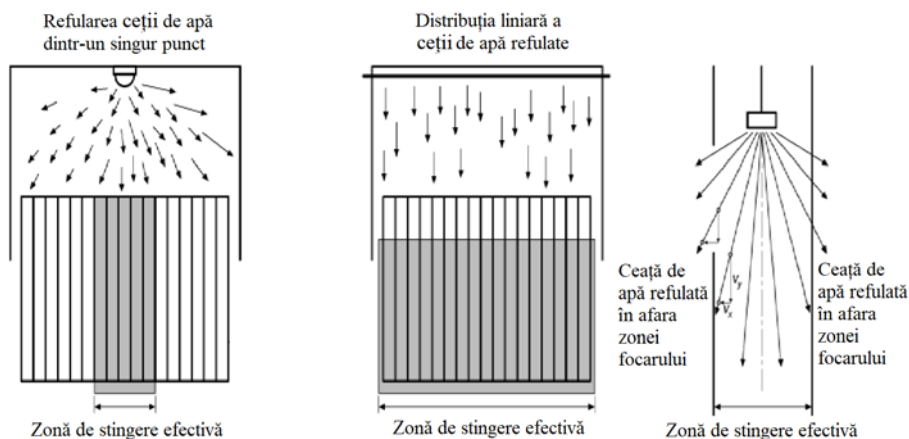

Figura 16 Reprezentarea comparativă a zonelor de stingere eficiente în cazul utilizării uneia sau mai multor duze de refulare [8]

Conform figurii 16, controlul direcției de refulare sau al impulsului jetului poate fi mai important decât distribuția dimensiunii picăturilor de apă sau debitul masic al acestuia [8]. Astfel, în cazul utilizării unei singure duze de refulare, zona efectivă de stingere este mai mică decât în cazul utilizării mai multor duze, în acest caz, distribuția ceții de apă fiind liniară.

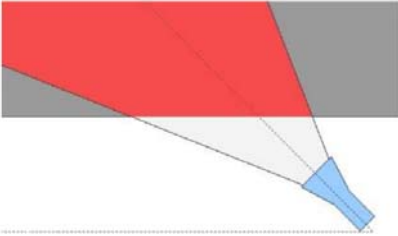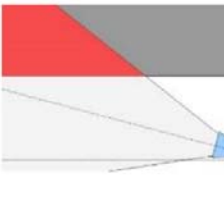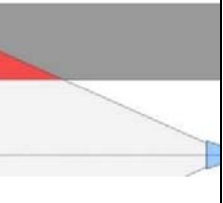## 6. Influența altor parametri asupra eficienței stingerii incendiilor

Dimensiunea picăturilor apei refulate este un parametru deosebit de important. Este necesar ca picăturile de apă să poată să pătrundă prin flăcări și să ajungă pe suprafața materialului fierbinte care arde, în vederea răcirii acestuia și întreruperii procesului de ardere. Cu cât dimensiunea picăturilor de apă este mai mică, cu atât cantitatea de energie termică absorbită de la incendiu este mai mare, fiind astfel utilizat un volum mai mic de apă. Conform unui studiu efectuat [25], absorbția a 30 % până la 60 % din energia termică totală degajată de un incendiu poate fi suficientă pentru stingerea acestuia. În urma unor calcule efectuate [8] s-a constatat că diametrul optim al unei picături de apă se află în intervalul 0,3 mm – 1 mm. Astfel, nivelul cel mai ridicat al eficienței stingerii se obține în situația în care picăturile sunt destul de uniforme în dimensiune.

De asemenea, tehnica de refulare reprezentată de modul de manevrare al țevii de refulare, de unghiul conic al jetului și unghiul de înclinare al țevii față de planul orizontal, au o mare importanță asupra eficienței răcirii stratului de fum și gaze fierbinți, așa cum se poate observa în tabelul 1. Prin răcirea gazelor fierbinți se realizează reducerea temperaturii în interiorul încăperii în scopul pătrunderii cât mai rapide a echipajelor de intervenție și a refulării apei direct asupra focarului. Dacă țeava este orientată astfel încât picăturile de apă lovesc rapid tavanul, efectul de răcire va fi diminuat. Cu cât traiectoria picăturilor de apă este mai mare în interiorul stratului de fum, cu atât efectul de răcire va fi mai mare.

Tabel 1

Influența unor parametri diferiți asupra eficienței răcirii fumului și gazelor fierbinți prin refularea apei sub formă de impulsuri scurte [26]

Criteriile de răcire ale stratului de fum și gaze fierbinți prin refularea apei sub formă de impulsuri scurte	Gradul de eficiența a apei de răcire a fumului și gazelor fierbinți (procentul de transformare a apei din stare lichidă în stare gazoasă)			
	Eficient Peste 75 %	Adecvat Între 75 % și 50 %	Ineficient Între 50 % și 25 %	Mediocru Sub 25 %
Diametrul mediu al picăturii [mm]	0,3 mm	0,2 mm sau 0,4 mm	0,1 mm sau 0,5 mm	< 0,1 mm sau > decât 0,5 mm
Unghiul conic al jetului	45 °	30 °	90 °	120 °
Înclinarea țevii de refulare față de planul orizontal	Peste 45 °		25 °	0 °

Conform tabelului 2, eficientizarea stingerii incendiilor este influențată și de ajutajele țevilor de refulare, utilizarea acestora conducând la obținerea unor valori diferite ale absorbției de căldură.

Tabel 2

Capacitatea de absorbție a căldurii a diferitelor ajutaje [27]

Echipament	Absorbție maximă de căldură [MJ/kg]	Debit masic al apei [kg/s]	Capacitatea absorbției de căldură [MW]
Ajutaj standard (7mm)	2,6	1,3	1,4
Ajutaj standard (14mm)	2,6	4,6	5
Ajutaj standard (22mm)	2,6	9,2	7,2
Ajutaj de capacitate mare	2,6	16,7	13
Lance cu ceață de apă	3,6	1,2	2,6
Ajutaj ce produce ceață de apă	3,6	5	11

Viteza ventilației longitudinale și poziția materialelor combustibile care ard, și anume o stivă de lemne în cazul studiul efectuat [28], față de duza de refulare a unei instalații de stingere cu ceață de apă influențează eficiența stingerii. Astfel, așa cum se poate vedea în figura 18, se poate atinge o viteza a ventilației longitudinale optime pentru stingerea incendiului într-un timp cât mai scurt, însă, după atingerea acestei valori, odată cu creșterea vitezei aerului se mărește și timpul de stingere a incendiului. De asemenea, cu cât distanța dintre stivă și duza de refulare este mai mică, cu atât timpul necesar stingerii este mai mic.

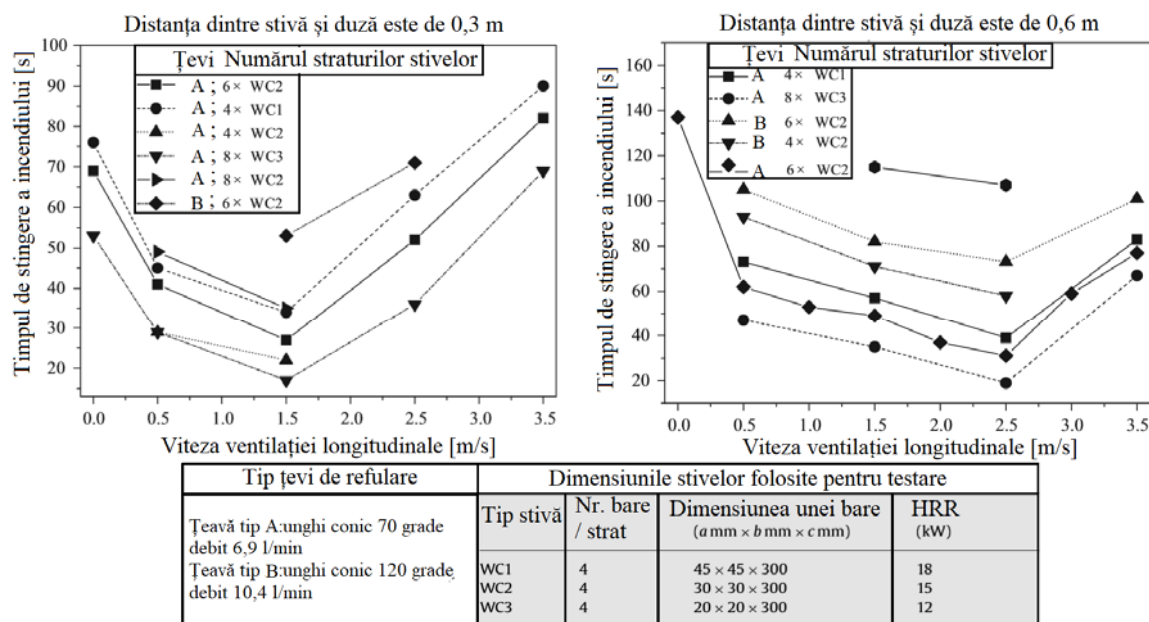| Tip țevi de refulare	Dimensiunile stivelor folosite pentru testare			
	Tip stivă	Nr. bare / strat	Dimensiunea unei bare (a mm × b mm × c mm)	HRR (kW)
Țeavă tip A:unghi conic 70 grade debit 6,9 l/min Țeavă tip B:unghi conic 120 grade debit 10,4 l/min	WC1	4	45 × 45 × 300	18
	WC2	4	30 × 30 × 300	15
	WC3	4	20 × 20 × 300	12

Figura 18 Variația timpului de stingere a incendiului, care se manifestă la trei tipuri diferite de stive, cu viteza longitudinală a vântului, în cazul utilizării a două tipuri de duze de refulare [28]

De asemenea, debitul de refulare are un rol important în eficientizarea stingerii.
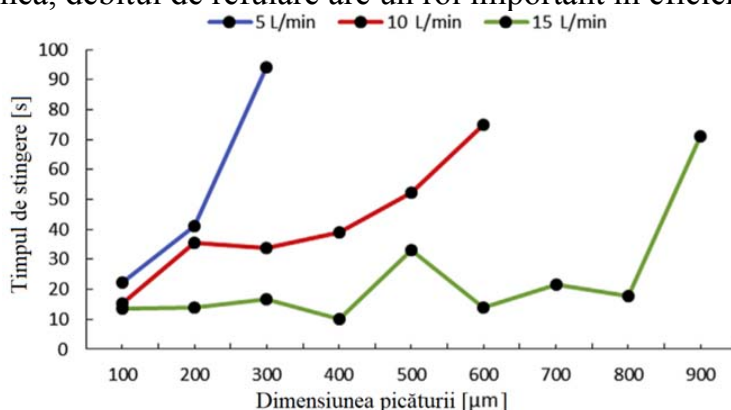

Figura 19 Variația timpului stingerii incendiului în funcție de dimensiunea picăturilor de apă, pentru debite diferite de refulare [29]

Conform figurii 19, cu cât debitul de refulare este mai mare, iar dimensiunea picăturii este mai mică, cu atât timpul necesar stingerii incendiului scade, ceea ce conduce la o creștere a eficienței stingerii incendiilor.

7. Concluzii

Eficiența stingerii incendiilor reprezintă un obiectiv de realizat foarte important, pe de o parte, în vederea reducerii costurilor, iar pe de altă parte, pentru limitarea pagubelor provocate construcțiilor afectate de incendiu sau a celor adiacente acestora, din cauza volumului de apă refulat în exces.

Apa este agentul de stingere a incendiilor utilizat la scara largă. Stingerea incendiilor se poate realiza în diferite moduri, în acest studiu fiind analizată, de exemplu, stingerea manuală, prin utilizarea țevilor de refulare și automată, prin utilizarea instalațiilor fixe de stingere cu sprinklere și ceață de apă. Astfel, în funcție de modul în care se realizează lichidarea incendiilor, apa dezvoltă diferite mecanisme generale de stingere a acestora.

Astfel, în tabelul 3 sunt prezentate mecanismele generale de stingere a incendiilor în urma refulării apei, manual, folosind țevile de refulare și automat, folosind instalațiile fixe de stingere cu sprinklere și ceață de apă.

Tabelul 3

Mecanismele de stingere a incendiilor în urma utilizării apei

Nr. crt.	Modul de stingere a incendiilor		Mecanismele apei de stingere a incendiilor	
1.	Manual	Prin utilizarea țevilor de refulare	Absorbția căldurii degajate de incendiu de către apă	
			Reducerea concentrației de oxigen	
			Efectul de răcire / ecranarea suprafeței	
			Reducerea radiației termice	
			Efectul de suflare	
2.	Automat	Prin utilizarea instalației de sprinklere	Efectul de răcire	
			Efectul de „înăbușire" a incendiului	
3.		Prin utilizarea instalației de ceață de apă	Mecanisme de stingere primare	Absorbția căldurii / Răcire
				Reducerea concentrației de oxigen
				Blocarea radiației termice
			Mecanisme de stingere secundare	Diluarea amestecului de vapori combustibili și aer
				Efectele cinetice ale ceței de apă asupra flăcărilor

În cadrul studiului a fost realizată o analiză comparativă a influenței principalilor trei parametri ai jetului de apă refulat prin utilizarea țevilor, a instalațiilor fixe cu sprinklere și cu ceață de apă, în vederea eficientizării stingerii incendiilor. Primul parametru analizat a fost distribuția dimensiunii picăturilor de apă refulată, constatându-se că, cu cât dimensiunea picăturilor este mai mică, cu atât suprafața acestora, raportată la volum, este mai mare, fiind astfel absorbită o cantitate mai mare de energie termică. Al doilea parametru caracteristic jetului de apă care influențează eficiența stingerii îl constituie densitatea fluxului apei refulate, existând, de exemplu, în cazul instalației de sprinklere, anumite valori utilizate în funcție de tipul riscului de incendiu aferent construcțiilor cu diferite destinații. Astfel, în funcție de dimensiunea

suprafeței încăperii în care se utilizează instalația de sprinklere, densitatea fluxului apei refulate ia valori în intervalul 2,84 – 4,1 $l/min \cdot m^2$ - în cazul riscului de incendiu scăzut, 4,1 – 8,1 $l/min \cdot m^2$ - în cazul riscului de incendiu moderat, 8,1 – 16,3 $l/min \cdot m^2$ - în cazul riscului de incendiu ridicat. Al treilea parametru analizat a fost valoarea impulsului jetului apei refulate. Astfel, în cazul țevilor de refulare, o valoare ridicată a impulsului picăturilor conduce la mărirea vitezei răcirii gazelor de ardere și a vaporizării picăturilor.

De asemenea, este prezentată și importanța altor parametri care influențează în mod direct eficiența stingerii incendiilor, cum ar fi dimensiunea picăturilor de apă, utilizarea tehnicilor de refulare, dimensiunea ajutajelor țevilor, viteza ventilației longitudinale, precum și valoarea debitului de refulare.

Astfel, cu cât picăturile de apă au un grad ridicat de uniformitate și o dimensiune mai mică, diametrul optim aflându-se în intervalul 0,3 mm – 1 mm, cu atât crește eficiența stingerii incendiilor.

Utilizarea tehnicilor de refulare este, de asemenea un parametru foarte important, constatându-se că, prin utilizarea unui unghi conic al jetului apei refulate de 45 ° și a unui unghi de înclinare a țevii față de planul orizontal de peste 45 °, procentul eficienței stingerii este de peste 75 %.

Folosirea țevilor de refulare a apei prevăzute cu ajutaje de dimensiuni mari conduce la creșterea capacității de absorbție de căldură a jetului format.

În cazul utilizării unei anumite viteze a ventilației longitudinale se obține un timp minim de stingere a incendiilor.

De asemenea, reducerea timpului de stingere a incendiilor se mai obține odată cu creșterea valorii debitului de refulare, de la 5 l/min la 15 l/min, concomitent cu refularea unor picături de apă cu dimensiuni cât mai mici, aflate în intervalul 0,1 mm – 0,3 mm.

Referințe

[1] C. R. Barnett, „Water Supply for Fire Fighting Purposes", Proceedings of 50th Jubilee Year Conference, Institution of Fire Engineers, New Zealand Branch, 1979.
[2] C. F. Dale, „Water Supply for Fire Protection", Prentice-Hall Inc., Englewood, Cliffs, NJ, 1981.
[3] http://cfbt-us.com/wordpress/?p=1280, accesat în data de 06.01.2020, ora 21.55.
[4] The Society of Fire Protection Engineers (NZ) Technical Publication - Tp 2004/1, „Calculation Methods for Water Flows Used for Fire Fighting Purposes".
[5] S. Särdqvist, „Water and other extinguishing agents", Karlstad, Sweden: Räddnings Verket, 2002.
[6] J. Gsell, „Assessment of Fire Suppression Capabilities of Water Mist – Fighting Compartment Fires with the Cutting Extinguisher", Pg. Dip. Msc. Fire Safety Engineering, Academic year 2009 / 2010.
[7] http://cfbt-us.com/wordpress/?p=1299, accesat în data de 06.01.2020, ora 22.15.

[8] C. C. Grant, J. R. Hall, R. E. Solomon, „Fire Protection Handbook", Twentieth Edition Volume I, 2008.

[9] M. M. Braidech, J. A. Neale, "The Mechanism of Extinguishment of Fire by Finely Divided Water", NBFU Research Report No. 10, Underwriters Laboratories Inc., Chicago, IL, 1955.

[10] P. Nash, D. J. Rasbash, „The Use of Water in Fire Fighting", F.R. Note No. 202/1955, Fire Research Station, Borehamwood, UK, 1955.

[11] D. Drysdale, „An Introduction to Fire Dynamics", 1st ed., pp. 222-225, John Wiley and Sons, New York, 1985.

[12] R. Wighus, "Extinguishment of Enclosed Gas Fires with Water Spray", Proceedings of the Third International Symposium on Fire Safety Science, The University of Edinburgh, Edinburgh, Scotland, 1991.

[13] A. M. Kanury, „Ignition of Liquid Fuels," The SFPE Handbook of Fire Protection Engineering, 2nd. ed., DiNenno, P.J., et al., National Fire Protection Association, Quincy, MA, 1995.

[14] C. P. Hanauska, G. G. Back, „Halons: Alternative Fire Protection Systems, An Overview of Water Mist Fire Suppression Systems Technology", Hughes Associates, Inc., Columbia, MD, 1993.

[15] J. R. Mawhinney, „Water Mist Fire Suppression Systems for Marine Applications: A Case Study", Proceedings of IMAS 94: Fire Safety on Ships—Developments into the 21st Century, Institute of Marine Engineers, London, UK, May 1994.

[16] A. Coppalle, D. Nedelka, B. Bauer, „Fire Protection: Water Curtains", Fire Safety Journal, 20, 1993, pp. 241-255. 23.

[17] T. E. Ravigururajan, M. P. Beltrav, „A Model for Attenuation of Fire Radiation through Water Droplets", Fire Safety Journal, 15: 2, 1989, pp. 171-181.

[18] A. Jones, G. O. Thomas, „The Action of Water Sprays on Fires and Explosions", Transactions of the Institution of Chemical Engineers, 71: Part B, 41-49, 1993.

[19] J. R. Mawhinney, „Characteristics of Water Mist for Fire Suppression in Enclosures", Proceedings of the Halon Alternatives Technical Working Conference, New Mexico Engineering Research Institute (NMERI), Albuquerque, NM, 1993.

[20] M. A. Kokkala, „Extinction of Liquid Pool Fires with Sprinklers and Water Sprays", Valtion Teknillinen Tutkimuskeskus, Statens Teniska Forskningscentral (Technical Research Centre of Finland), Espoo, Finland, 1989.

[21] NFPA 750, „Water mist fire protection systems", National Fire Protection Association, USA, 2006.

[22]https://www.slideshare.net/bajohnso/basic-guide-to-nfpa-13-occupancy-and-commodity classifications.

[23] http://www.ultrans.ro/produse-pompieri/cold-cut-cobra.html, accesat în data de 04.02.2020 la ora 21.00.

[24] R. Svensson, J. Lindström, R. Ochoterena, M. Försth, „CFD simulations of the Cutting extinguisher,,, Fire Research SP Report 2014:43.

[25] J. R. Mawhinney, B. Z. Dlugogorski, A. K. Kim, „A Closer Look at the Fire Extinguishing Properties of Water Mist", Fire Safety Science—Proceedings of the Fourth International Symposium at the Ottawa Congress Centre, Ottawa, Ontario, Canada, Kashiwagi, T., Ph.D., ed., International Association of Fire Safety Science, p. 51, 1994.

[26] J. McDonough, K. Lambert, „Training with intent – effective hose stream techniques", International Structural Fire Conference, Ryn, 09-10 June 2014.

[27] S. Särdqvist, „An engineering approach to fire-fighting tactics", Department of Fire Safety Engineering, Lund Institute of Technology, Lund University, 1996.

[28] L. Chena, W. Zhub, X. Caia, L. Panc, G. Liaoa, „Experimental study of water mist fire suppression in tunnels under longitudinal ventilation", Building and Environment 44, 446–455, 2009.

[29] Z. Wang, W. Wang, Q. Wang, „Optimization of water mist droplet size by using CFD modeling for fire suppressions", Journal of Loss Prevention in the Process Industries 44, 626-632, 2016.